

MODIFICATION OF A DYNAMIC  
SIMULATION TOOL FOR POWER  
NETWORKS TO ANALYSE AND  
CALIBRATE A RISK-BASED OPF  
APPROACH

eingereichte  
DIPLOMARBEIT

von

Andreas Wank

Lehrstuhl für  
ENERGIEVERSORGUNGSNETZE

Technische Universität München

October 2012

## **Acknowledgement**

The author would like to thank Paul A. Trodden and Professor Ken I. M. McKinnon from the University of Edinburgh for the possibility to work on this project as part of their team. They always offered assistance, support and guidance.

Special thanks also to Dipl.-Ing. Sascha Altschäffl and to Professor Dr.-Ing. R. Witzmann from the Technical University of Munich for their supervision and invaluable assistance.

---

# Contents

<b>List of Figures</b>	<b>iv</b>
<b>List of Tables</b>	<b>vi</b>
<b>1. Introduction</b>	<b>1</b>
<b>2. Power Systems</b>	<b>4</b>
2.1. Power System Components . . . . .	4
2.2. Power Flow . . . . .	7
2.2.1. Derivation of Single Line Equations . . . . .	7
2.2.2. Network Equations and Power Flow Problem Formulation . .	13
2.2.3. Solution Techniques . . . . .	18
<b>3. Power System Analysis Toolbox</b>	<b>20</b>
3.1. Basic Operation and Available Cases . . . . .	21
3.2. Structure and Main Routines . . . . .	23
3.2.1. Standard Power Flow Routine <i>fm_spf</i> . . . . .	24
3.2.2. Time-Domain Simulation Routine <i>fm_int</i> . . . . .	26
3.2.3. Implementation of the State Vectors . . . . .	28
3.3. Extensions to PSAT . . . . .	29
<b>4. Optimization in Power Systems</b>	<b>36</b>
4.1. Optimization Problems . . . . .	37
4.2. Economic Dispatch Calculation (EDC) . . . . .	38
4.3. Optimal Power Flow (OPF) . . . . .	40
4.3.1. Full AC OPF . . . . .	42
4.3.2. Linearized DC OPF . . . . .	43
4.4. Security Constrained OPF (SCOPF) . . . . .	44
4.5. Visualisation . . . . .	46
4.5.1. 3-Bus Model . . . . .	46
4.5.2. EDC . . . . .	48

---

4.5.3. DC and AC OPF . . . . .	48
4.5.4. DC SCOPF . . . . .	50
4.6. Summary . . . . .	53
<b>5. Risk Based Optimal Power Flow (RBOPF)</b>	<b>54</b>
5.1. Concept of Risk and Security . . . . .	54
5.2. Description of RBOPF . . . . .	55
5.3. RBOPF Models . . . . .	59
5.4. Discussion and Comparison to SCOPF . . . . .	64
5.5. Problems with RBOPF . . . . .	67
<b>6. Results</b>	<b>69</b>
6.1. New England 39-bus Network . . . . .	69
6.2. Solving the Optimization Problems . . . . .	71
6.3. The Actual Measure of Risk . . . . .	74
6.3.1. Consequence Trees . . . . .	74
6.3.2. Risk Computation . . . . .	77
6.4. Calibration of the Severity Functions . . . . .	81
6.4.1. Concept . . . . .	81
6.4.2. Example . . . . .	83
<b>7. Summary</b>	<b>87</b>
<b>Bibliography</b>	<b>89</b>
<b>A. 39-bus Network Data</b>	<b>91</b>
A.1. MATPOWER File Header . . . . .	91
A.2. Bus Data . . . . .	92
A.3. Generator Data . . . . .	93
A.4. Load Data . . . . .	96
A.5. Branch Data . . . . .	97
<b>B. Nomenclature</b>	<b>99</b>

## List of Figures

1.1. Coal and Gas Price Development . . . . .	1
2.1. Conceptual design of a generating unit . . . . .	5
2.2. T- and $\pi$ -model of a transmission line . . . . .	8
2.3. Transmission line $\pi$ -model . . . . .	9
2.4. Bus variables . . . . .	14
2.5. 2-bus system and n-bus system . . . . .	14
3.1. PSAT command line output . . . . .	22
3.2. <i>fm_spf</i> flowchart . . . . .	25
3.3. <i>fm_int</i> flowchart . . . . .	27
3.4. Breaking routine stopping criterion . . . . .	31
3.5. Breaking routine – frequency diagram . . . . .	32
3.6. Four islanding types . . . . .	35
4.1. EDC theoretical network topology . . . . .	39
4.2. 3-Bus test network . . . . .	47
4.3. DC OPF solution 1 . . . . .	49
4.4. DC OPF solution 2 . . . . .	49
4.5. AC OPF solution 1 . . . . .	50
4.6. P-SCOPF DC solution . . . . .	51
4.7. C-SCOPF DC solution . . . . .	52
5.1. Severity demonstration example . . . . .	57
5.2. Contingency flows of the SCOPF . . . . .	58
5.3. The severity function . . . . .	60
5.4. Histogram of contingency flows 1 . . . . .	65
5.5. Histogram of contingency flows 2 . . . . .	66
6.1. 39-bus network topology . . . . .	70
6.2. Risk vs. Generation Cost . . . . .	73

6.3. Example of a consequence tree . . . . .	75
6.4. Flow chart of the routine <i>xtree</i> . . . . .	77
6.5. Flow to failure rate dependency . . . . .	78
6.6. Flow to probability dependency . . . . .	79
6.7. Visualisation of the risk computation 1 . . . . .	80
6.8. Visualisation of risk computation 2 . . . . .	81
6.9. Calibration 1 . . . . .	84
6.10. Calibration 2 . . . . .	84
6.11. Calibration loop . . . . .	85
6.12. Calibration 3 . . . . .	86
A.1. Turbine governor schematic . . . . .	94
A.2. Automatic voltage regulator schematic . . . . .	95

## List of Tables

2.1. The different bus types . . . . .	17
3.1. The DAE structure . . . . .	23
3.2. 39-bus models . . . . .	28
3.3. Structure of DAE.y . . . . .	29
3.4. Structure of DAE.x . . . . .	29
4.1. Load data . . . . .	47
4.2. Generator data . . . . .	47
4.3. Branch data . . . . .	47
4.4. EDC optimization problem . . . . .	48
4.5. Constraints of the various models . . . . .	53
4.6. Dispatch of generation of the various models . . . . .	53
5.1. Three RBOPF formulations . . . . .	61
6.1. Comparison of different optimization solutions . . . . .	71
6.2. Comparison of the actual risk of the OPF, SCOPF and RBOPF . . .	72
6.3. Load shedding scheme . . . . .	83
6.4. Settings of the RBOPF model . . . . .	83
6.5. Comparison of the 5 contingency solutions 1 . . . . .	86
6.6. Comparison of the 5 contingency solutions 2 . . . . .	86
A.1. New England network bus data . . . . .	92
A.2. New England network generator data . . . . .	93
A.3. New England network generator dynamic data . . . . .	93
A.4. New England network turbine governor data . . . . .	94
A.5. New England network automatic voltage regulator data . . . . .	95
A.6. New England network load data . . . . .	96
A.7. New England network branch data . . . . .	98

# 1. Introduction

Today's society is increasingly dependent on energy. Our lifestyle and behaviour are built on the mentality of an inexhaustible supply of energy. It is only when there is a blackout that we realise how much we are dependent on it.

Although renewable energies are advancing the world is still greatly dependent on fossil energy resources. In Germany, the decision to phase-out nuclear power (22.4% of the total energy produced in 2010) by 2022, means that other energy sources now need to compensate for this energy deficit. The share of the remaining fossil energy sources, hard coal, lignite and liquefied gas, rose to 57.2% of overall production in 2011, an increase on previous years (Source: Bundesnetzagentur). Figure 1.1 depicts the development of the producer price index in Germany for hard coal, lignite and liquefied gas from 2000 to 2011.

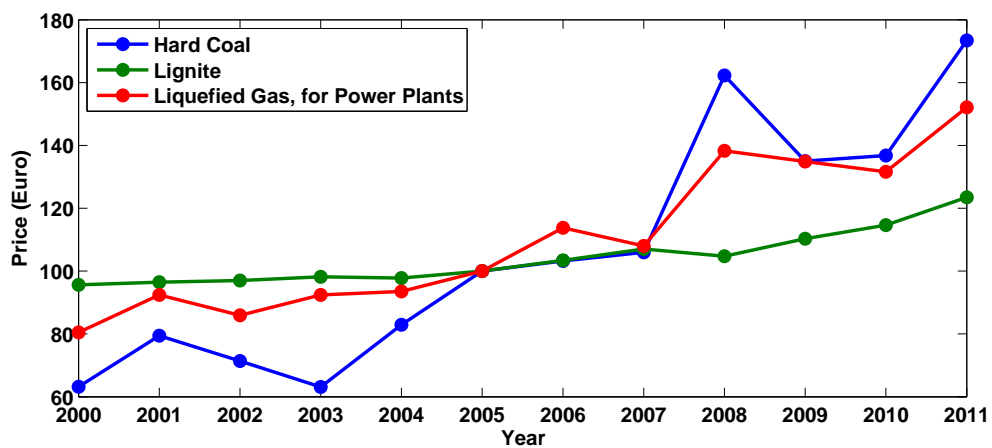


Figure 1.1.: Development of prices for hard coal, lignite and liquefied gas. As prices rise, the use of existing resources must be optimized. (Source: Bundesnetzagentur)

However, this is not a national problem. As natural resources become increasingly scarce the exploitation of fossil energy sources becomes more complex, technically as well as financially. New investments in the power system infrastructure are necessary worldwide to meet increasing demand as well as the integration of renewable

energies. As a result, the cost of producing energy can be assumed to be growing continuously. This growth is amplified by an ongoing boost in energy consumption due to increasing electrification in almost every aspect of our life. As prices rise it becomes more important to optimize the use of existing resources. This need for maximum efficiency has intensified as the traditionally regulated power industry has undergone a liberalization process and the energy market has become competitive. Energy companies are reliant to maximize their profit in order to remain profitable. Unfortunately the climb of electricity prices is not accompanied by increased security of supply. Several large-scale blackouts of power networks have occurred in recent years. In 2003 blackouts happened in Sweden [11] and Italy [1] as well as the US/Canada [7], where an estimated 55 million people were left without power, some for more than 12 hours. In November 2006 the European UCTE grid split into three islands [2] after the reaction of automatic protection devices caused a cascade of tripped lines. However, the largest power outage in history is the most recent. In July 2012 large parts of the Indian power network collapsed leaving more than 300 million people without power [14]. Overall about 670 million were affected, which is about 9% of the world population.

The reasons for blackouts are manifold. However, the deregulation of electricity markets, introduced with the aim of improving the efficiency of production, has driven system operators to run their networks closer to the security limits. When one component fails subsequent failures become more probable increasing the risk of a cascading blackout. The danger of instability is worsened by the advancing integration of renewable energy sources, especially wind power. Despite all of their benefits, they do bring a great deal of uncertainty into power systems. An inaccurate prediction of their generation can increase stress in a system.

These reasons can be seen as common driving factors for the danger of blackouts. Providing a stable and secure energy supply can be considered as a key issue in the future. The problems that engineers face are not only to meet the increasing demand but also to ensure system stability when network failures occur. In the future there is likely to be a great need for the planning of new extensions of grid networks. This provides a unique opportunity to improve networks such that the risk of cascading blackouts is kept to a minimum.

If the consequences of a contingency event could be estimated more accurately many blackouts could be prevented. This work deals with a new approach of operating

systems based on an optimal power flow (OPF) formulation, the risk-based OPF. The risk-based OPF attempts to, first, estimate the risk of a system and then, consequently, minimize that risk. Hence, the applications in planning as well as operating power systems are vast.

## 2. Power Systems

An electrical power system in its entirety, consisting of generation, transmission, distribution and consumption of electric power, can be seen as a very large dynamic system. In engineering such dynamic systems can be represented and analysed by mathematical models, which try to accurately capture the physical behaviour of the involved components. According to Machowski et al. [13], electrical power systems feature the unique attribute that demand must be exactly met by supply at all times, as there is still no possibility of storing electric energy in sufficiently large capacities. This can be seen as the key issue of power systems and has a great influence in the structure of a power system as well as dictating the characteristic of operation.

This chapter gives a brief introduction to the most important components of power systems as well as the derivation of the power flow equations, which compute the behaviour of the interaction of these components.

### 2.1. Power System Components

#### Generating Units

Generating units, embedded in plants, consist of the turbine or engine and the generator. The turbine or engine, the so-called prime mover, is connected by a shaft to the generator and transforms fuel into a rotational mechanical moment, which generates electrical power. The most common types of plants are hydro plants, which are driven by water, and thermal plants, which are fuelled by nuclear or fossil resources such as coal, oil or natural gas. Most plants are equipped with three-phase synchronous generators along with various protection and control devices, such as turbine governors, excitation regulators and circuit breakers, to guarantee safe operation.

The concept of a generating unit is visualised in Figure 2.1. The prime mover drives the synchronous generator applying its mechanical torque by a shaft. The nominal speed of the shaft depends on the type of plant and usually ranges from 500 rpm

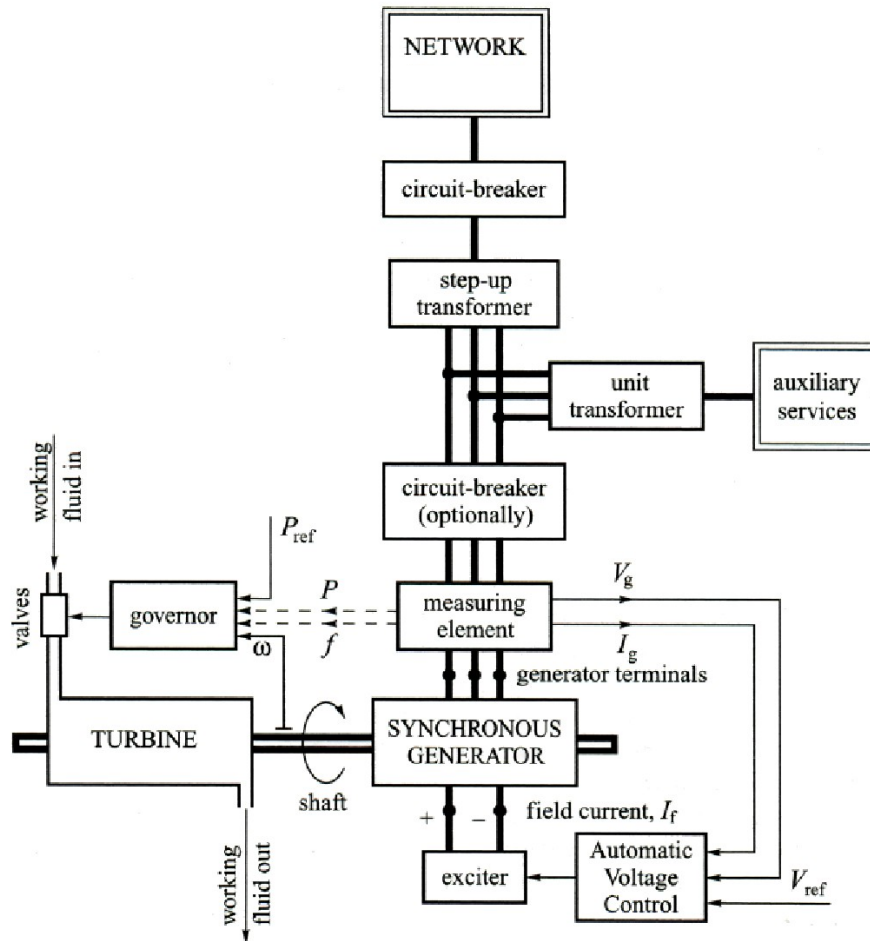


Figure 2.1.: Conceptual design of a generating unit taken from Machowski et al. [13]. The governor regulates the frequency by controlling the turbine inlet valve. The automatic voltage control fixes the output voltage.

(hydro) to 3000 rpm (thermal). The generator transforms this mechanical torque into electrical power. Therefore, it consists of two magnetic segments, one rotating, driven by the prime mover (rotor), and one static, mounted to the chassis (stator). The relative movement of those two magnetic fields induces an electrical current, which is fed into the transmission system.

As all plants of a power system are interconnected, it is essential that they operate at synchronous speed and nominal voltage in order to maintain the correct direction of power flow from the generating units to the loads. If the generators lose synchronism they start working against each other, putting great stress on the system. Two of the regulating devices that ensure this can be seen in Figure 2.1. The Turbine Governor (TG) regulates the fuel inlet valve of the turbine such that changes in real power and hence torque fluctuations can be balanced. The Automatic Voltage Regulator (AVR) monitors the terminal voltage of the generator and balances changes in reactive

power by adjusting the field voltage.

### **Transmission Lines**

The transmission lines in a power system allow to transmit electrical energy from generation sites to centres of load. Ideally they form a grid network that interconnects the various power stations with the consumers, often separated by large distances. Most lines are implemented as overhead lines operating at high voltages in the transmission system (220 kV – 756 kV), at medium voltages in subtransmission systems (110 kV) and at low voltages in distribution networks (10 kV – 30 kV) [20]. In residential and urban areas there is the possibility of using underground cables because overhead lines are too dangerous due to lack of space. However, they suffer from technical problems and cannot be used for long distances. For details see Heuck et al. [9].

Due to the series admittance and the shunt capacitance of the lines, the real and reactive power flowing in at either end of the line do not normally add up to zero.

### **Transformers**

Losses in transmission lines increase to the square of the line current, according to  $P_{Loss} = RI^2$ . In order to transmit the same amount of power at less current, the transmission voltage is increased resulting in reduced losses. Due to isolation and design problems, generators have a voltage limit usually of about several 10 kV (see Crastan [5]). In order to connect the power plants to the high voltage transmission network, operating at several 100 kV, transformers need to be integrated, transforming the low generator voltage to the high line voltage.

### **Buses**

Throughout the network there are common nodes that resemble important branch points within the grid network. These nodes are called buses and operate at a defined voltage level and phase angle, forming the complex bus voltage. Generally, there are three types of busses in a power network, namely the load bus, the generator bus and the slack bus.

### **Loads**

Loads consume electrical power by either a resistive, inductive or capacitive behaviour or a combination of these. Due to their immense number they are merged locally so that each one load in the system can resemble one big industrial complex as well as a few thousand private homes. The loads are distributed over the whole network and in total represent the so-called total demand of the system. Depending

on whether they represent an industrial, commercial or residential customer, they can vary greatly in quantity as well as electrical characteristics. Various load models have been introduced, taking into account voltage and frequency dependencies as well as day, month and year cycles.

Two load types that are used in this work are the PQ and the ZIP load. The PQ load characteristic is the simplest one. It sees the load as a constant demand of real and reactive power that does not change with any external influences. The ZIP load uses a combination of impedance ( $Z$ ), depending quadratically on the voltage, current ( $I$ ), depending linearly on the voltage, and constant power demand ( $P$ ). For more information see Section 3.3.

## 2.2. Power Flow

Power flow, also called load flow, is a very important calculation in power system studies. Its aim is to find a steady state operating point of the system under normal, balanced conditions, providing a snapshot of all the important variables of the system. Power flow studies are widely utilised in practice, where they are applied in the planning of power systems, network state estimation, e.g. if components have to be disconnected for maintenance purposes, security and economic analysis. Power flow is also the basis for time-domain simulation as can be seen in Chapter 3.

Therefore, a set of network equations needs to be solved obtaining all values for voltage magnitude and phase and injected real and reactive power. The derivation of these equations is given in the following sections. In order to obtain the general network equations it is helpful to understand the power balance equations for a single transmission line first.

### 2.2.1. Derivation of Single Line Equations

The impedance of an inductance  $L$  and the admittance of a capacity  $C$  are given by

$$\begin{aligned} Z_L &= j\omega L \\ Y_C &= j\omega C \end{aligned} \tag{2.1}$$

Depending on the values for  $L$  and  $C$  the inductive and capacitive properties of a conductor can be neglected if the frequency is low enough. A change of the input

signal can be considered to be instantaneously available along the conductor. As frequency rises the signal propagates as a wave of voltage and current through the conductor. If the line is long enough or if the frequency is high enough, changes in the signal cannot happen simultaneously at every point anymore. As power is usually transmitted by alternating currents with a nominal frequency, its wave properties have to be taken into consideration.

Two widely used models of transmission lines have evolved, the T-model, depicted in Figure 2.2 (a) and the  $\pi$ -model, depicted in Figure 2.2 (b). The difference between these two models is the way they approximate the line shunt capacitance, which is normally equally distributed along the line. The T-model assumes that the total line capacitance  $\underline{Y}_C$  is located at the centre of the line with two equal line impedances  $\underline{Y}_L/2$  at either side. The  $\pi$ -model on the other hand splits the total capacitance into two equal parts  $\underline{Y}_C/2$ , which are located near the ends of the line with the series impedance  $\underline{Y}_L$  in between.

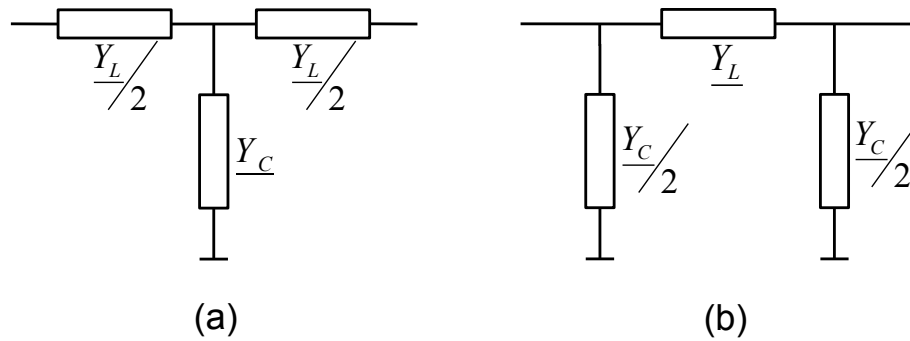


Figure 2.2.: (a) T-model and (b)  $\pi$ -model of a transmission line. The two models use different approaches to approximate the shunt capacitance  $\underline{Y}_C$ .

Higher order models are obtained by cascading these basic cells. However, the high order models are only required if the length of the line is greater than the wavelength of the voltage and current wave that propagates through the line. Considering most transmission systems work at a frequency of 50 Hz or 60 Hz, the corresponding wavelength can be computed to

$$\lambda = \frac{c}{f} = \frac{3 \cdot 10^8 \frac{m}{s}}{60 Hz} = 5 \cdot 10^6 m = 5 \cdot 10^3 km \quad (2.2)$$

Since even the longest transmission lines do not exceed 5000 km, the use of the first order model consisting of only one  $\pi$ - or T-element is justified.

To be able to understand the origin of the constraints that are used in the optimization models (see Chapter 4), the power flow equations are derived in the following. As the  $\pi$ -model is incorporated in PSAT, this model will be used; for the T-model the basic approach remains the same, as do the resulting equations. Only the parameters representing the equivalent impedance and shunt admittance are different. Figure 2.3 depicts the nominal single phase  $\pi$ -model of a transmission line with the sending end to the left and the receiving end to the right. The series admittance is denoted  $\underline{Y}_L$  and the shunt admittance  $\underline{Y}_C/2$ , which is purely capacitive. Complex variables are marked with an underline in the following equations.

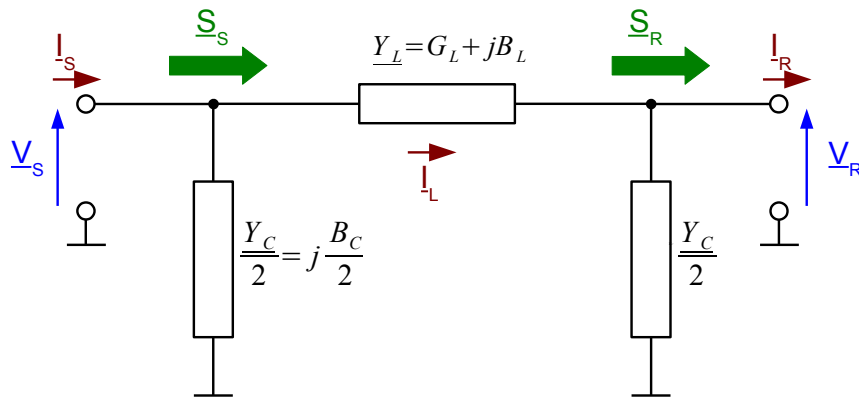


Figure 2.3.: Transmission line  $\pi$ -model incorporating the directions of the electric quantities [9]. Power is transmitted from the left (sending) end to the right (receiving) end.

Applying the Kirchhoff laws in Figure 2.3, the sending and receiving currents can be calculated as

$$\begin{aligned} \underline{I}_S &= -\underline{Y}_C \underline{V}_S + \underline{I}_L \\ &= -\underline{Y}_C \underline{V}_S + \underline{Y}_L (\underline{V}_R - \underline{V}_S) \end{aligned} \quad (2.3)$$

$$\begin{aligned} \underline{I}_R &= \underline{Y}_C \underline{V}_R + \underline{I}_L \\ &= \underline{Y}_C \underline{V}_R + \underline{Y}_L (\underline{V}_R - \underline{V}_S) \end{aligned} \quad (2.4)$$

For a clearer notation they can be expressed in matrix form

$$\begin{aligned} \begin{pmatrix} \underline{I}_S \\ \underline{I}_R \end{pmatrix} &= \begin{pmatrix} -\underline{Y}_C - \underline{Y}_L & \underline{Y}_L \\ -\underline{Y}_L & \underline{Y}_C + \underline{Y}_L \end{pmatrix} \begin{pmatrix} \underline{V}_S \\ \underline{V}_R \end{pmatrix} \\ \begin{pmatrix} \underline{I}_S \\ \underline{I}_R \end{pmatrix} &= \begin{pmatrix} \underline{Y}_{11} & \underline{Y}_{12} \\ \underline{Y}_{21} & \underline{Y}_{22} \end{pmatrix} \begin{pmatrix} \underline{V}_S \\ \underline{V}_R \end{pmatrix} \end{aligned} \quad (2.5)$$

Using polar form for complex voltages and admittances

$$\begin{aligned} \underline{V}_x &= |V_x| e^{j\delta_x} \\ \underline{Y}_x &= |Y_x| e^{j\theta_x} \end{aligned} \quad (2.6)$$

it is possible to derive equations for the apparent power at the sending and receiving end

$$\begin{aligned} \underline{S}_R &= \underline{V}_R \underline{I}_R^* = \underline{V}_R (\underline{Y}_{21} \underline{V}_S + \underline{Y}_{22} \underline{V}_R)^* \\ &= \underline{V}_R (\underline{Y}_{21}^* \underline{V}_S^* + \underline{Y}_{22}^* \underline{V}_R^*) \\ &= |V_R| e^{j\delta_R} (\underline{Y}_{21}^* |V_S| e^{-j\delta_S} + \underline{Y}_{22}^* |V_R| e^{-j\delta_R}) \\ &= \underline{Y}_{22}^* |V_R|^2 e^{j(\delta_R - \delta_R)} + \underline{Y}_{21}^* |V_S| |V_R| e^{j(\delta_R - \delta_S)} \\ &= \underline{Y}_{22}^* |V_R|^2 + \underline{Y}_{21}^* |V_S| |V_R| e^{j(\delta_R - \delta_S)} \end{aligned} \quad (2.7)$$

$$\begin{aligned} \underline{S}_S &= \underline{V}_S \underline{I}_S^* = \underline{V}_S (\underline{Y}_{11} \underline{V}_S + \underline{Y}_{12} \underline{V}_R)^* \\ &= \dots \\ &= \underline{Y}_{11}^* |V_S|^2 + \underline{Y}_{12}^* |V_S| |V_R| e^{j(\delta_S - \delta_R)} \end{aligned} \quad (2.8)$$

The apparent power can be split into its real and imaginary part corresponding to real and reactive power at the sending and receiving end of the line.

$$\begin{aligned} \underline{S} &= \text{Re}\{S\} + j\text{Im}\{S\} = P + jQ \\ P &= \text{Re}\{S\} \quad Q = \text{Im}\{S\} \end{aligned} \quad (2.9)$$

Making use of Equation (2.6) the real power at the sending end can be calculated to

$$\begin{aligned}
 P_S &= \text{Re}\{S_S\} \\
 &= |V_S|^2 \text{Re}\{\underline{Y}_{11}^*\} + |V_S| |V_R| \text{Re}\{\underline{Y}_{12}^* e^{j(\delta_S - \delta_R)}\} \\
 &= |V_S|^2 \text{Re}\{|Y_{11}| e^{-j\theta_{11}}\} + |V_S| |V_R| \text{Re}\{|Y_{12}| e^{j(\delta_S - \delta_R - \theta_{12})}\} \\
 &= |V_S|^2 |Y_{11}| \cos(\theta_{11}) + |V_S| |V_R| |Y_{12}| \cos(\delta_S - \delta_R - \theta_{12})
 \end{aligned} \tag{2.10}$$

Using the cosine identity

$$\cos(\alpha - \beta) = \cos(\alpha) \cos(\beta) + \sin(\alpha) \sin(\beta) \tag{2.11}$$

Equation (2.10) can be rewritten as

$$\begin{aligned}
 P_S &= |V_S|^2 |Y_{11}| \cos(\theta_{11}) + \\
 &\quad + |V_S| |V_R| |Y_{12}| (\cos(\delta_S - \delta_R) \cos(\theta_{12}) + \sin(\delta_S - \delta_R) \sin(\theta_{12})) \\
 &= |V_S|^2 \underbrace{|Y_{11}| \cos(\theta_{11})}_{g_{11}} + \\
 &\quad + |V_S| |V_R| (\underbrace{|Y_{12}| \cos(\theta_{12})}_{g_{12}} \cdot \cos(\delta_S - \delta_R) + \underbrace{|Y_{12}| \sin(\theta_{12})}_{b_{12}} \cdot \sin(\delta_S - \delta_R)) \\
 &= |V_S|^2 g_{11} + |V_S| |V_R| (g_{12} \cos(\delta_S - \delta_R) + b_{12} \sin(\delta_S - \delta_R))
 \end{aligned} \tag{2.12}$$

Bearing in mind that the real part of admittance is conductance and the imaginary part is susceptance,  $\underline{Y}$  can be split into two parts denoted  $g$  and  $b$ . For example  $\underline{Y}_{11}$

$$\begin{aligned}
 \underline{Y}_{11} &= |Y_{11}| e^{j\theta_{11}} \\
 &= |Y_{11}| \cos(\theta_{11}) + j |Y_{11}| \sin(\theta_{11}) \\
 &= g_{11} + j b_{11}
 \end{aligned} \tag{2.13}$$

This denotation is done for all four elements of the matrix in (2.5)

$$g_{11} = |Y_{11}| \cos(\theta_{11}) \quad , \quad b_{11} = |Y_{11}| \sin(\theta_{11}) \tag{2.14}$$

$$g_{12} = |Y_{12}| \cos(\theta_{12}) \quad , \quad b_{12} = |Y_{12}| \sin(\theta_{12}) \tag{2.15}$$

$$g_{21} = |Y_{21}| \cos(\theta_{21}) \quad , \quad b_{21} = |Y_{21}| \sin(\theta_{21}) \tag{2.16}$$

$$g_{22} = |Y_{22}| \cos(\theta_{22}) \quad , \quad b_{22} = |Y_{22}| \sin(\theta_{22}) \tag{2.17}$$

Using the sine and cosine identities, the real and reactive parts of the power at the sending and the receiving end calculate to

$$P_S = |V_S|^2 g_{11} + |V_S| |V_R| (g_{12} \cos(\delta_S - \delta_R) + b_{12} \sin(\delta_S - \delta_R)) \quad (2.18)$$

$$Q_S = -|V_S|^2 b_{11} + |V_S| |V_R| (g_{12} \sin(\delta_S - \delta_R) - b_{12} \cos(\delta_S - \delta_R)) \quad (2.19)$$

$$P_R = |V_R|^2 g_{22} + |V_S| |V_R| (g_{21} \cos(\delta_R - \delta_S) + b_{21} \sin(\delta_R - \delta_S)) \quad (2.20)$$

$$Q_R = -|V_R|^2 b_{22} + |V_S| |V_R| (g_{21} \sin(\delta_R - \delta_S) - b_{21} \cos(\delta_R - \delta_S)) \quad (2.21)$$

These are the power flow equations for a single transmission line. Equations (2.14)–(2.17) can be further generalised for the case of a tap changing transformer and/or a phase shifter applied at the sending end of the line. A tap-changing transformer with tap ratio  $\tau$  at the sending end changes the voltage to

$$|\tilde{V}_S| = \frac{1}{\tau} |V_S| \quad (2.22)$$

Similarly, a phase-shifting transformer changes the phase angle of the transmission line admittance by adding a phase offset  $\theta^{shift}$ . Using sine and cosine identities, the original line admittance  $\underline{Y}_L$  becomes  $\tilde{\underline{Y}}_L$ .

$$\begin{aligned} \tilde{\underline{Y}}_L &= \underline{Y}_L e^{j\theta^{shift}} = |Y_L| e^{j\theta_L + \theta^{shift}} \\ &= |Y_L| \cos(\theta_L + \theta^{shift}) + j |Y_L| \sin(\theta_L + \theta^{shift}) \\ &= |Y_L| \left( (\cos(\theta_L) \cos(\theta^{shift}) - \sin(\theta_L) \sin(\theta^{shift})) \right. \\ &\quad \left. + j(\sin(\theta_L) \cos(\theta^{shift}) + \sin(\theta^{shift}) \cos(\theta_L)) \right) \\ &= |Y_L| \cos(\theta_L) \left( \cos(\theta^{shift}) + j \sin(\theta^{shift}) \right) - \\ &\quad |Y_L| \sin(\theta_L) \left( \sin(\theta^{shift}) - j \cos(\theta^{shift}) \right) \end{aligned} \quad (2.23)$$

In Figure 2.3,  $\underline{Y}_L$  and  $\underline{Y}_C$  are defined as

$$\begin{aligned} \underline{Y}_L &= G_L + jB_L = |Y_L| \cos(\theta_L) + j |Y_L| \sin(\theta_L) \\ \frac{\underline{Y}_C}{2} &= j \frac{B_C}{2} \end{aligned} \quad (2.24)$$

Hence Equation (2.23) can be rewritten as

$$\begin{aligned}\tilde{\underline{Y}}_L &= G_L(\cos(\theta^{shift}) + j \sin(\theta^{shift})) - B_L(\sin(\theta^{shift}) - j \cos(\theta^{shift})) \\ &= (G_L \cos(\theta^{shift}) - B_L \sin(\theta^{shift})) + j(G_L \sin(\theta^{shift}) + B_L \cos(\theta^{shift}))\end{aligned}\tag{2.25}$$

Replacing  $|V_S|$  and  $\underline{Y}_L$  by  $|\tilde{V}_S|$  and  $\tilde{\underline{Y}}_L$ , respectively, as well as using Equations (2.5) and (2.24), Equations (2.14) - (2.17) can be formulated as

$$g_{11} = \frac{1}{\tau^2} G_L \tag{2.26}$$

$$g_{12} = -\frac{1}{\tau} (G_L \cos(\theta^{shift}) - B_L \sin(\theta^{shift})) \tag{2.27}$$

$$g_{21} = -\frac{1}{\tau} (G_L \cos(\theta^{shift}) + B_L \sin(\theta^{shift})) \tag{2.28}$$

$$g_{22} = G_L \tag{2.29}$$

$$b_{11} = \frac{1}{\tau^2} (B_L + \frac{B_C}{2}) \tag{2.30}$$

$$b_{12} = -\frac{1}{\tau} (B_L \cos(\theta^{shift}) + G_L \sin(\theta^{shift})) \tag{2.31}$$

$$b_{21} = -\frac{1}{\tau} (B_L \cos(\theta^{shift}) - G_L \sin(\theta^{shift})) \tag{2.32}$$

$$b_{22} = B_L + \frac{B_C}{2} \tag{2.33}$$

Thus, Equations (2.18) - (2.21) provide an explicit relationship between the real and reactive powers and the voltages at either side of the line whilst only requiring the line parameters.

### 2.2.2. Network Equations and Power Flow Problem Formulation

In order to solve the power flow problem for an entire system the full network equations need to be obtained.

At each bus there are two complex variables that define the state of the system, namely the injected apparent power  $\underline{S}$  and the bus voltage  $\underline{V}$  (see Figure 2.4). The apparent power can be split into its real and reactive part and bus voltage can be

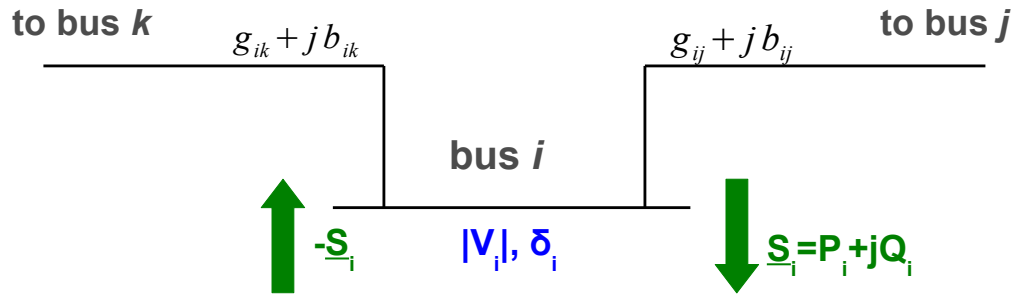


Figure 2.4.: Two of the four bus variables –  $P$ ,  $Q$ ,  $V$  and  $\delta$  – are unknown prior to the power flow computations. The line from bus  $i$  to bus  $j$  is described by its conductance  $g_{ij}$  and its susceptance  $b_{ij}$ .

represented by its magnitude and phase angle.

$$\begin{aligned} \underline{S} &= P + jQ \\ \underline{V} &= |V| e^{j\delta} \end{aligned} \quad (2.34)$$

Just as in the previous section it is desired to find the relationship between  $P$ ,  $Q$ ,  $|V|$  and  $\delta$ . Whereas so far there was only a sending and receiving end that influenced the equations, now an equation for each individual bus is needed that takes into account every other bus of the system. If more than one line is considered the direction of a line is specified by its ‘*from*’ (sending end) and ‘*to*’ (receiving end) bus locations. In order to derive the power flow equations for a system of arbitrary size Equations (2.18) – (2.21) need to be generalized. First, a two-bus system (see Figure 2.5 (a)) is considered, equivalent to the situation in Figure 2.3, where two buses are connected by a single line.

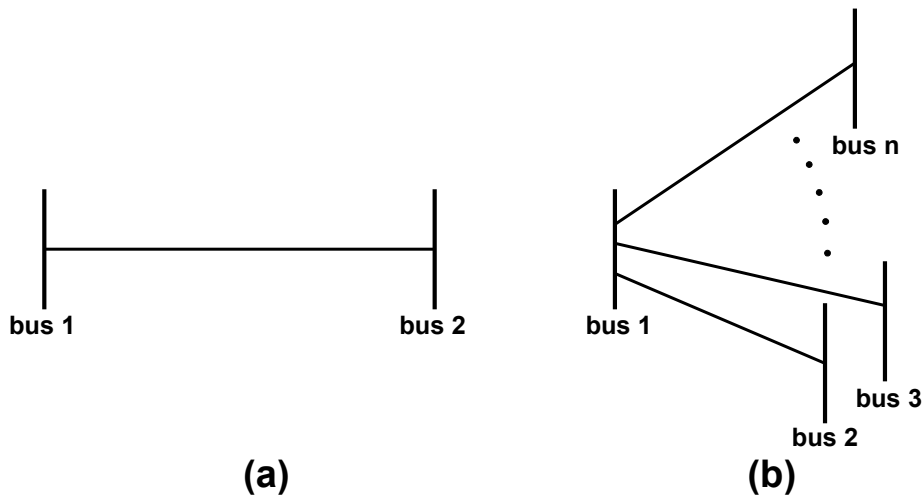


Figure 2.5.: For the derivation of the load flow equations, first a 2-bus system (a) is considered. Then, the results are generalised for an  $n$ -bus system (b).

Equation (2.18) for the injected real power still holds for this case, but instead of labelling the two ends of the line as sending and receiving, they are now indexed 1 and 2, corresponding to bus 1 and bus 2. Further, the equation can be transformed such that it is represented by a sum.

$$\begin{aligned}
 P_{12} &= |V_1|^2 g_{11} + |V_1| |V_2| (g_{12} \cos(\delta_1 - \delta_2) + b_{12} \sin(\delta_1 - \delta_2)) \\
 &= |V_1| \left( |V_1| \underbrace{(g_{11} \cos(\delta_1 - \delta_1))}_{=1} + \underbrace{b_{11} \sin(\delta_1 - \delta_1)}_{=0} \right) + \\
 &\quad |V_2| (g_{12} \cos(\delta_1 - \delta_2) + b_{12} \sin(\delta_1 - \delta_2)) \\
 &= |V_1| \sum_{k=1}^2 |V_k| (g_{1k} \cos(\delta_1 - \delta_k) + b_{1k} \sin(\delta_1 - \delta_k)) \tag{2.35}
 \end{aligned}$$

Now, if more buses are connected by additional transmission lines (Figure 2.5 (b)), the same relationship must also be true for those lines and the sum of Equation (2.35) can simply be extended to the number of connected lines. Hence, if  $n$  busses are connected to bus 1,  $P_1$  can be written as

$$P_1 = |V_1| \sum_{k=1}^n |V_k| (g_{1k} \cos(\delta_1 - \delta_k) + b_{1k} \sin(\delta_1 - \delta_k)) \tag{2.36}$$

Consequently, as this holds for every bus in the network, Equation (2.36) can be changed to the general case of bus  $i$ . Analogue to the injected real power, a general equation can be derived for the reactive power injection of bus  $i$ . Equations (2.37) and (2.38) show the polar form of the network equations,

$$P_i = |V_i| \sum_{k=1}^n |V_k| (g_{ik} \cos(\delta_i - \delta_k) + b_{ik} \sin(\delta_i - \delta_k)) \tag{2.37}$$

$$Q_i = - |V_i| \sum_{k=1}^n |V_k| (g_{ik} \sin(\delta_i - \delta_k) - b_{ik} \cos(\delta_i - \delta_k)) \tag{2.38}$$

where the parameters  $g_{ik}$  and  $b_{ik}$  are a generalisation of Equations (2.26)–(2.33).

The two cases  $i = k$  and  $i \neq k$  have to be distinguished.

$$g_{ik} = \sum_{k=1}^n \frac{1}{\tau_{ik}^2} G_{ik} \quad i = k \quad (2.39)$$

$$g_{ik} = -\frac{1}{\tau_{ik}} (G_{ik} \cos(\theta_{ik}^{shift}) - B_{ik} \sin(\theta_{ik}^{shift})) \quad i \neq k \quad (2.40)$$

$$b_{ik} = \sum_{k=1}^n \frac{1}{\tau_{ik}^2} (B_{ik} + \frac{B_{C,ik}}{2}) \quad i = k \quad (2.41)$$

$$b_{ik} = -\frac{1}{\tau_{ik}} (B_{ik} \cos(\theta_{ik}^{shift}) + G_{ik} \sin(\theta_{ik}^{shift})) \quad i \neq k \quad (2.42)$$

Here  $G_{ik}$  and  $B_{ik}$  are the conductance and susceptance of the line's series admittance and  $B_{C,ik}$  is the susceptance of the line's shunt admittance from bus  $i$  to bus  $k$ . If there is no tap ratio and no phase shift applied to the line,  $g_{ik}$  and  $b_{ik}$  are simply equal to the line conductance  $G_{ik}$  and susceptance  $B_{ik}$ , respectively.

The equations for the sending edge of the transmission line, Equations (2.18) and (2.19), were used as a base for the above derivation. Thus, all powers calculated by the formulas in Equations (2.37) and (2.38) represent power flowing *out* of the bus. By using Equations (2.20) and (2.21) for the receiving end, similar equations can be derived characterising power flowing *into* the bus.

The matrix formed by the elements  $y_{ik} = g_{ik} + jb_{ik}$  is called the admittance matrix  $\underline{Y}$  of the network. An element  $y_{ii}$  is called self-admittance and equals the sum of all admittances connected to bus  $i$ . If a bus  $l$  is not connected to another bus  $m$  the corresponding entry of the admittance matrix is  $y_{lm} = 0$ .

$$\underline{Y} = \begin{pmatrix} y_{11} & y_{12} & \cdots & y_{1n} \\ y_{21} & \ddots & & \vdots \\ \vdots & & \ddots & \vdots \\ y_{n1} & \cdots & \cdots & y_{nn} \end{pmatrix} \quad (2.43)$$

Taking into account loads at a bus  $i$  with a constant power demand  $S_i^D = P_i^D + jQ_i^D$  and generators, which supply the power  $S_i^G = P_i^G + jQ_i^G$  the load flow equations can

be written as

$$P_i^{fr} = P_i^G - P_i^D = |V_i| \sum_{k=1}^n |V_k| (g_{ik} \cos(\delta_i - \delta_k) + b_{ik} \sin(\delta_i - \delta_k)) \quad (2.44)$$

$$Q_i^{fr} = Q_i^G - Q_i^D = -|V_i| \sum_{k=1}^n |V_k| (g_{ik} \sin(\delta_i - \delta_k) - b_{ik} \cos(\delta_i - \delta_k)) \quad (2.45)$$

$$P_i^{to} = P_i^G - P_i^D = |V_i| \sum_{k=1}^n |V_k| (g_{ik} \cos(\delta_i - \delta_k) - b_{ik} \sin(\delta_i - \delta_k)) \quad (2.46)$$

$$Q_i^{to} = Q_i^G - Q_i^D = |V_i| \sum_{k=1}^n |V_k| (g_{ik} \sin(\delta_i - \delta_k) + b_{ik} \cos(\delta_i - \delta_k)) \quad (2.47)$$

For a network with  $n$  buses (2.44) – (2.45) provide  $2n$  equations. However, there are  $4n$  variables in the system, two for voltage and two for power at every bus. This implies that at least  $2n$  of the variables, 2 at each bus, must be specified in advance to be able to solve this problem.

As mentioned earlier, the demand of the individual loads as well as the generation level of the connected power plants are usually known. When the power is transmitted through the transmission system line losses will occur, which are not previously known but have to be supplied by the generators. Therefore, at least one generator cannot have a fixed generation so that these losses can be balanced.

Generally, buses are classified as shown in Table 2.1. The slack bus, also called swing or reference bus, is the only type of bus that has a specified voltage phase angle. The phase angles of all the other buses are measured relative to the reference bus. As the slack bus also has to balance the losses in the network it is the only one that can adjust its real power. PQ buses have loads with a defined real and reactive power demand connected, where the voltage magnitude and angle is unspecified. PV buses are linked to generators, which can control their real power output and voltage level.

<i>bus type</i>	<i>specified quantity</i>	<i>unknown quantity</i>
slack bus	$ V , \delta$	$P, Q$
generator bus (PV bus)	$P,  V $	$Q, \delta$
load bus (PQ bus)	$P, Q$	$ V , \delta$

Table 2.1.: The different bus types in the load flow problem. Loads consume power at a PQ-bus, generators feed power into the system at a PV-bus. The slack bus is needed to compensate for the unknown system losses.

To solve the load flow problem, the information about the various bus types has to

be put into Equations (2.44) and (2.45), which need to be solved numerically. As a result the four quantities  $P$ ,  $Q$ ,  $|V|$  and  $\delta$  can be obtained.

### 2.2.3. Solution Techniques

Finding a solution of the power flow equations requires solving a non-linear function. There are various iterative solution techniques that find the roots of non-linear functions and that can be adapted for the nodal power equations. All of these approaches have in common that an initial guess for the unknown voltage magnitudes and angles is required. The following methods are mentioned by Milano [18] and Saadat [19].

- Gauß-Seidel
- Newton-Raphson
- Fast Decoupled Load Flow
- Runge-Kutta

Since PSAT, the program used in this study, uses primarily the Newton-Raphson (NR) algorithm, only this solution technique is explained. The NR algorithm is based on Taylor's Theorem. The Taylor series expansion about a point  $x^0$  is given by the  $k$ -th order Taylor polynomial.

$$f(x) = f(x^0) + f'(x^0)(x - x^0) + \frac{f''(x^0)}{2!}(x - x^0)^2 + \dots + \frac{f^{(k)}(x^0)}{k!}(x - x^0)^k \quad (2.48)$$

Here the left hand side  $f(x)$  is the true value at point  $x$  and the right hand side an approximation based on  $x^0$ . The NR algorithm uses the linear term as an approximation to  $f(x)$ .

$$f(x) \approx f(x^0) + f'(x^0)(x - x^0) \quad (2.49)$$

Instead of solving  $f(x) = 0$ , the approximation can be set to zero and rearranged.

$$\begin{aligned} f(x^0) + f'(x^0)(x - x^0) &= 0 \\ x^1 &= x^0 - \frac{f(x^0)}{f'(x^0)} \end{aligned} \quad (2.50)$$

Depending on the initial value  $x^0$ , Equation (2.50) provides a solution that is reasonably close to the real root  $x$ . If a better approximation is needed this step has to be repeated iteratively bringing the approximation closer towards the real value  $x$ . The general iterative step is described by

$$x^{r+1} = x^r - \frac{f(x^r)}{f'(x^r)} \quad (2.51)$$

and is repeated until  $\|x^{r+1} - x^r\| \leq \epsilon$ .

For the multi-dimensional case  $\mathbf{x}$  and  $\mathbf{f}$  are vectors so that the derivative becomes a Jacobian matrix  $\mathbf{J}$

$$\mathbf{J} = \frac{\partial \mathbf{f}}{\partial \mathbf{x}} = \begin{bmatrix} \frac{\partial f_1}{\partial x_1} & \frac{\partial f_1}{\partial x_2} & \dots & \frac{\partial f_1}{\partial x_n} \\ \frac{\partial f_2}{\partial x_1} & \frac{\partial f_2}{\partial x_2} & \dots & \frac{\partial f_2}{\partial x_n} \\ \vdots & \vdots & \ddots & \vdots \\ \frac{\partial f_n}{\partial x_1} & \frac{\partial f_n}{\partial x_2} & \dots & \frac{\partial f_n}{\partial x_n} \end{bmatrix} \quad (2.52)$$

and the iteration step of Equation (2.51) becomes

$$\mathbf{x}^{r+1} = \mathbf{x}^r - \mathbf{J}^{-1} \cdot \mathbf{f}(\mathbf{x}^r) \quad (2.53)$$

In power systems vectors  $\mathbf{x}$  and  $\mathbf{f}$  are given by

$$\mathbf{x} = \begin{bmatrix} \delta_1 \\ \delta_2 \\ \vdots \\ \delta_n \\ V_1 \\ V_2 \\ \vdots \\ V_n \end{bmatrix} \quad \mathbf{f} = \begin{bmatrix} f_1^P(V, \delta) \\ f_2^P(V, \delta) \\ \vdots \\ f_n^P(V, \delta) \\ f_1^Q(V, \delta) \\ f_2^Q(V, \delta) \\ \vdots \\ f_n^Q(V, \delta) \end{bmatrix} = \begin{bmatrix} P_1(V, \delta) + P_1^D - P_1^G \\ P_2(V, \delta) + P_2^D - P_2^G \\ \vdots \\ P_n(V, \delta) + P_n^D - P_n^G \\ Q_1(V, \delta) + Q_1^D - Q_1^G \\ Q_2(V, \delta) + Q_2^D - Q_2^G \\ \vdots \\ Q_n(V, \delta) + Q_n^D - Q_n^G \end{bmatrix} \quad (2.54)$$

## 3. Power System Analysis Toolbox

The core computational tool of this work is the public domain software PSAT, which was first published in 2001 by Milano [17]. PSAT is an open-source MATLAB toolbox for the static and dynamic analysis of power systems that can be operated by a graphical user interface (GUI) or by a command-line version.

In addition of being free of charge, PSAT features several useful properties. It incorporates many routines such as power flow (PF), continuous power flow (CPF), small signal stability analysis (SSSA), optimal power flow (OPF) and time domain simulation (TD). Moreover it features a great number of component models, such as different load types (e.g. voltage dependent loads, frequency dependent loads), generators (synchronous and induction motor), various controllers (e.g. Turbine Governors (TG), Automatic Voltage Regulators (AVR), Power System Stabilizer (PSS)), FACTS components and wind turbine models. In particular the time domain simulation tool is vital to this project as it is one of the main supports for later analysis. However, the biggest advantages of PSAT are its availability, as an open-source application, and the fact that it allows changes to be made to the code. This is especially of great value as the program can be altered to meet the very specific requirements of the project. Also it enables the routines to be embedded within a MATLAB script and hence lets the simulation run repeatedly.

This chapter gives a detailed introduction to PSAT and its command line usage. First, the general usage of the program is explained and a description of the main routines is given. After an overview of the changes made to PSAT within this project, a case study is carried out, in order to demonstrate the functionality of some of the applied changes. Unless stated differently, variable names are written in bold, function names in italic letters.

### 3.1. Basic Operation and Available Cases

In this work it was desired to embed PSAT into MATLAB and call the program from a MATLAB script. Therefore PSAT has to be set to command line usage, which is done when PSAT is initialised using the function *initpsat*. It immediately calls the routine *psat* that completes the following tasks:

- Check for OCTAVE and MATLAB versions.
- Define all important global variables (*fm\_var*).
- Define and initialise the struct variables **clpsat** and **Settings**. These contain important settings for the control of the different routines as well as general parameters (the difference between those two is that the first is especially for command line usage).
- Define and initialise various structs representing routines (eg. **OPF**, **CPF**, **SSSA**), tools (eg. **History**, **Varout**, **Snapshot**) and interfaces (eg. **GAMS**, **UWPFLOW**).
- Define the struct variable for the Differential Algebraic Equations **DAE**.

After the initialisation of the framework of the program, PSAT needs to be fed with a data file containing the necessary information about the components and the topology of the network. This is done by the command *runpsat(data\_file, 'data')*, where the file 'data\_file' must be of a specific structure and must at least contain the variables **Bus**, **Lines**, **PV**.

Optionally, a so-called 'perturb' file can be loaded. This file is called at every step during the time-domain simulation (see Section 3.2.2) and allows the user to build in additional functions or routines that are executed during the simulation. This file, loaded by the command *runpsat(pert\_file, 'pert')*, is of great practical value as special requirements can easily be added without changing the whole structure of the program. Thus it offers the great advantage that certain aspects of a routine can be changed significantly by exchanging only one file (< 1kB) rather than the whole program directory (~ 10MB). Therefore it is desirable to put any additional code into this file, if changes are to be made. However, since some changes need to make major modifications to the program structure, this is not always possible (see Section 3.3).

When the data and perturb file are loaded, the main routines can be accessed, again by executing the function *runpsat*. A command indicates which routine is to be chosen, e.g. ‘pf’ for power flow, ‘n1cont’ for an N-1 contingency analysis, ‘opf’ for optimal power flow, ‘td’ for time-domain simulation; the full list can be seen in the header of the function *runpsat*.

As an example, the following series of commands will perform a power flow:

```
initpsat  
runpsat(data_file, ‘data’)  
runpsat(‘pf’)
```

This will result in the following command line output:

---

```
< P S A T >
```

```
Copyright (C) 2002-2010 Federico Milano
```

```
Version 2.1.6
```

```
May 13, 2010
```

```
PSAT comes with ABSOLUTELY NO WARRANTY; type ‘gnuwarranty’  
for details. This is free software, and you are welcome to  
redistribute it under certain conditions; type ‘gnulicense’  
for details.
```

```
Host: Matlab 7.12.0.635 (R2011a)
```

```
Session: 01-Jan-2099 00:00:00
```

```
Usage: Command Line
```

```
Usage: Command Line
```

```
Path:
```

```
Load data from file...
```

```
Newton-Raphson Method for Power Flow Computation
```

```
Data file "/home/v1awank/thesis/d_case39"
```

```
Writing file "fm_call" ...
```

```
PF solver: Newton-Raphson method
```

```
Single slack bus model
```

```
Iteration = 1 Maximum Convergency Error = 0.0006023
```

```
Iteration = 2 Maximum Convergency Error = 4.2002e-06
```

```
Power Flow completed in 0.019334 s
```

---

Figure 3.1.: PSAT command line output for a simple power flow computation.

The solution of the injected real and reactive powers for the generators and the loads can be accessed in the fields **Bus.Pg**, **Bus.Qg**, **Bus.Pl** and **Bus.Ql** of the **Bus**

structure. The solution of the bus voltages and phase angles can be accessed in the algebraic variables of the **DAE** structure (field ‘y’). The whole solution is captured in the **Snapshot** structure, if enabled. More detail will be given in Section 3.2.1.

For this project data files were available for more than 15 different networks of a great variety. They range from very basic 3-bus test networks with only three generators to a vast reconstruction of the polish network with over 2000 nodes. However, often the data is limited to the very core information of bus data and generator capacity and does not provide high order generator models or data for controlling tools such as turbine generators and automatic voltage controllers which are necessary for a realistic simulation. PSAT requires data files of a special format but is capable of converting from other common data file formats, such as MATPOWER, by an integrated function.

## 3.2. Structure and Main Routines

The two PSAT routines that were predominantly used in this work will be explained in detail. In order to get a better understanding of their functioning, special attention must be paid to the structure of the component models in PSAT as well as to the variable **DAE**.

Incorporating the differential algebraic equations, **DAE** is the most important variable in PSAT and essential to all computations. Every time there are load flow computations to be carried out, e.g. in every time step of the simulation, the variables of the **DAE** structure are computed and stored anew. The **DAE** structure contains every quantity included in the load flow problem. Some important fields of the structure are shown in Table 3.1.

x	the vector of state variables (e.g. $\omega, \delta$ )
y	the vector of algebraic variables (e.g. $V, \theta, p, q$ )
m	dimension of <b>DAE.y</b>
n	dimension of <b>DAE.x</b>
g	algebraic equations
f	differential equations
$A_c$	Jacobian matrix

Table 3.1.: The main entries of the DAE structure consisting of variables, dimensions, equations and Jacobian matrix.

As PSAT has an efficient but complex way to create the DAE entries (see Section

3.2.3), there is no unique form of the variables of the structure. This stems from the fact that only the component models for which data is provided in the data file are actually considered. Thus the dimensions of the variables in the DAE structure depend on the number of models that are included and the variables are arranged differently for each network.

Every physical component of the power system that is required in the computations needs a mathematical model. All models that can be defined in the data file consist at least of a ‘con’, ‘store’ and ‘n’ field. The initial values for the models must be written to the ‘con’ field while any changes made to the model parameters after the first power flow need to be addressed to the ‘store’ field. The ‘n’ field indicates the number of units of the component. This is also used to detect and consequently ignore ‘empty’ models in order to reduce the dimension of the Jacobian matrix and the state vectors.

For every component in PSAT there is an individual setup function defined in order to perform initial computations of the corresponding model and hence pre-set the fields of the structure. Most of the setup functions check initially if data for the model exists at all, using the ‘con’ field. While inactive models are not taken into account, each active model adds to the dimension of the **DAE** structure. This is the reason why there is no definite shape to the **DAE** variables. However, if a system consists of a number of  $n$  buses, the first  $2n$  entries of the **DAE.y** vector are always the phase angles followed by the voltage magnitude of the buses. The meaning of the rest of the vector depends on the included models.

### 3.2.1. Standard Power Flow Routine *fm\_spf*

The power flow computation is the most important calculation in PSAT as it is needed for almost every routine. Provided there is a valid data file, the function *fm\_spf* solves a standard power flow (called by the function *runpsat('pf')*). A flowchart of this routine can be seen in Figure 3.2.

The first four functions are only executed the first time the routine is called and are needed to set up the models and initialise the **DAE** structure. The function *fm\_ncomp* consists of a full list of setup functions for every component. Here, all the included models are set as well as the **DAE.y** variable. If it is desired to create a new, user-defined model in PSAT, a setup function has to be written and placed

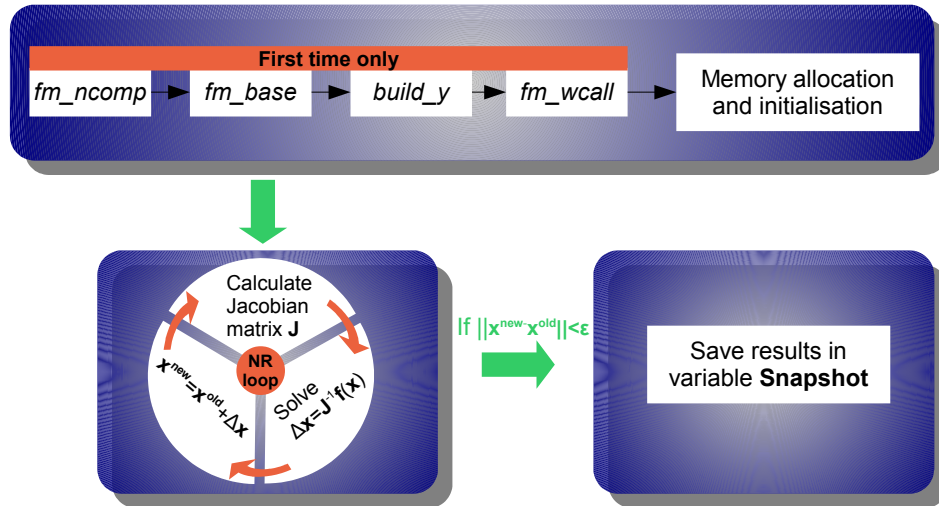


Figure 3.2.: The flowchart of the standard power flow routine (*fm\_spf*). The core element of this routine is the Newton-Raphson loop in the lower left box.

here. For a full list of files that have to be modified check Chapter 25 in the PSAT manual [17]. If a common power base is set in PSAT, the function *fm\_base* converts all corresponding parameters with respect to that conform base, followed by the computation of the admittance matrix of the network (stored in **Line.Y**).

After some memory allocation, e.g. for the Jacobian matrix, and initialisations of important variables, e.g. maximum iteration number and tolerance, the actual computation loop begins. It should be noted that in the flow chart only the Newton-Raphson loop is shown, while PSAT is capable of many different routines, such as Fast Decoupled Power Flow and Runge Kutta to name but two. According to Milano [17] the following linear problem is solved in a loop.

$$\begin{aligned}
 \begin{bmatrix} \Delta x^i \\ \Delta y^i \end{bmatrix} &= - \begin{bmatrix} F_x^i & -F_y^i \\ G_x^i & G_y^i \end{bmatrix}^{-1} \begin{bmatrix} f^i \\ g^i \end{bmatrix} \\
 \begin{bmatrix} x^{i+1} \\ y^{i+1} \end{bmatrix} &= \begin{bmatrix} x^i \\ y^i \end{bmatrix} + \begin{bmatrix} \Delta x^i \\ \Delta y^i \end{bmatrix}
 \end{aligned} \tag{3.1}$$

where  $F_x = \nabla_x f$ ,  $F_y = \nabla_y f$ ,  $G_x = \nabla_x g$  and  $G_y = \nabla_y g$  are the Jacobians of  $f$  and  $g$  with respect to  $x$  and  $y$ , respectively. If every single entry of the vector of increments is less than a pre-defined tolerance the calculations are stopped and the results are saved in the **Snapshot** variable. If the number of iterations exceeds a maximum, no feasible load flow solution can be found due to a singularity and the simulation is aborted.

Another efficient solution of PSAT is given by the function *fm\_wcall*. This function creates another file called *fm\_call*, which is not stored in the PSAT directory but in the current directory and is central to many computations. *fm\_wcall* checks which models are active and then writes the calls of those components only in the *fm\_call* function. A list of the active models is deposited in the **Comp** structure. The reason for this solution must be to improve the time consumption of the calculations as this function is called in every load flow computation and hence, in PSAT, in every step of the time-domain simulation.

### 3.2.2. Time-Domain Simulation Routine *fm\_int*

The time-domain simulation in PSAT includes dynamic behaviour and therefore adds differential equations to the Jacobian matrix. This extended problem is solved continuously for a great number of time steps, until a pre-defined stopping time is reached. The function that is executing the time-domain simulation is *fm\_int* and is called by `runpsat('td')`. Figure 3.3 shows a flow chart of the routine.

After some initial settings the output structure **Varout** is defined. At the end of the simulation **Varout** will contain the complete set of algebraic and state variables for every time step as well as the real and reactive power line flows. In general, this structure contains all the information about the time-domain simulation, which makes it the main output variable, similar to **Snapshot** in the power flow computations. If applied, the intervention times of the circuit breaker or fault events are set. If the correct flag is set, the load data, which is given as constant real ( $P$ ) and reactive ( $Q$ ) power consumptions, is converted into impedances. The impedance is computed as

$$Z = \frac{P}{V_{ref}^2} \quad V_{ref}: \text{reference voltage computed during the initial load flow} \quad (3.2)$$

This is done in the function *pqshunt*, which is hidden within the settings. The impedance calculation is done in each time step as part of the function *gcall* of the **PQ** class.

The time-domain simulation uses two different time variables. The “original time”  $t$  is the time of the last feasible load flow solution and is set to zero at the start of the simulation. The other variable, **actual\_time**, is the prospective time used in the computations of the NR loop. The relationship between the two times is

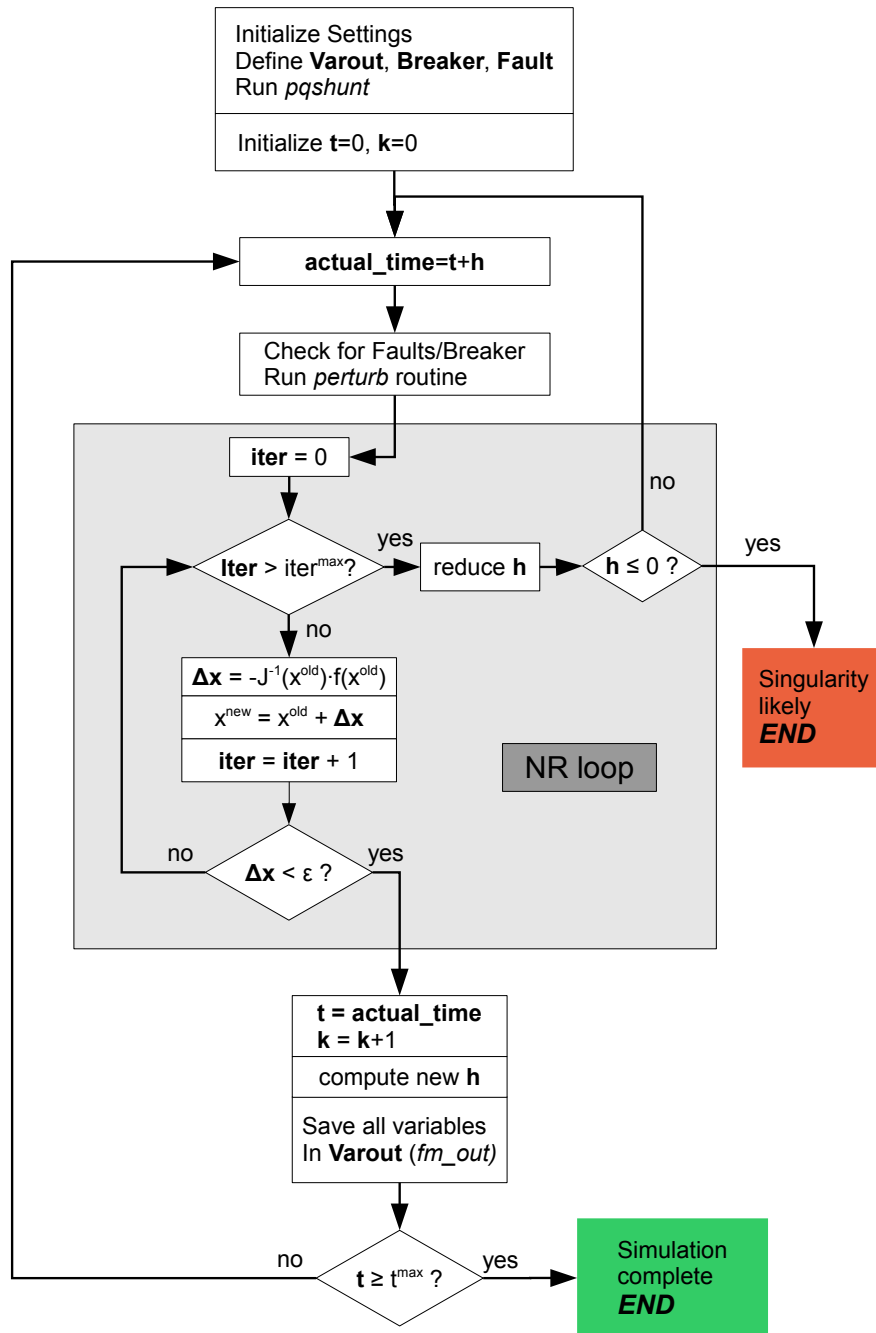


Figure 3.3.: The flowchart of the time-domain simulation routine (*fm\_int*). The perturbation file, which is executed in every step of the routine, allows the user additional interventions or observations.

**actual\_time** = **t** + **h**, where **h** is the time step. If the time step is chosen too big, it is possible that the NR loop does not converge. The time step has to be reduced and a new **actual\_time** has to be calculated. For this reason the original time **t** needs to be stored. After the **actual\_time** has been calculated the routine checks for breaker or fault interventions and, in case an intervention is detected, adjusts the time step. This is to calculate the state of the system an instant before

an intervention event – typically  $10^{-6}$  seconds – and an instant after. At this stage of the code, the perturbation file is loaded to allow any additional interventions or observations made by the user.

After, the Newton-Raphson loop is completed as described in the function *fm\_spf*. If the number of iterations exceeds a limit the calculations are stopped, the time step **h** is reduced by a time step algorithm and the NR algorithm is repeated. If the NR algorithm cannot find a solution until the time step reaches zero, the simulation is aborted and stopped. If it does converge the time **t** and the output variable **Varout** are updated. If **t** is greater than the pre-defined simulation time the simulation is completed and stops.

### 3.2.3. Implementation of the State Vectors

Finally, using the example of the 39-bus New England network it is shown how the **DAE.x** and **DAE.y** vectors are built. For the New England network there is data available for the component models **Bus**, **PV**, **SW**, **PQ**, **Syn**, **Tg** and **Exc** (see Table 3.2). The network consists of 39 buses, 10 machines and 21 loads. The layout of the vector of the algebraic variables and of the state variables is shown in Tables 3.3 and 3.4.

<i>Var</i>	<i>Description</i>
<b>Bus</b>	Bus model and load flow solution
<b>PV</b>	Static generator model
<b>SW</b>	Slack/Swing bus model
<b>PQ</b>	Load model
<b>Syn</b>	Dynamic generator model
<b>Tg</b>	Turbine governor model
<b>Exc</b>	Automatic voltage regulator model

Table 3.2.: Explanation of the meaning of the available 39-bus models. Models, for which there is no data provided are not taken into account in the computations.

<b>DAE.y</b>		
<i>Index</i>	<i>Description</i>	<i>model idx</i>
1-39	Bus phase angles $\theta$	<b>Bus.a</b>
40-78	Bus voltage magnitude $V$	<b>Bus.v</b>
79,84,...,115	Synchronous generators injected real power $p$	<b>Syn.p</b>
80,85,...,116	Synchronous generators injected reactive power $q$	<b>Syn.q</b>
81,86,...,117	Synchronous generators field voltage $v_f$	<b>Syn.vf</b>
82,87,...,118	Synchronous generators mechanical power $p_m$	<b>Syn.pm</b>
119-128	Turbine governors reference speed $\omega_{ref}$	<b>Tg.wref</b>
129-138	Automatic voltage regulators reference voltage $v_{ref}$	<b>Exc.vref</b>

Table 3.3.: Structure of the algebraic variables **DAE.y** for the 39-bus network including synchronous generators, TG's and AVR's.

<b>DAE.x</b>		
<i>Index</i>	<i>Description</i>	<i>model idx</i>
1,4,...,36 <sup>1</sup>	Synchronous machine angle $\delta$	<b>Syn.delta</b>
2,5,...,37	Synchronous machine speed $\omega$	<b>Syn.omega</b>
3,6,...,38	q-axis transient voltages $e1q$	<b>Syn.e1q</b>
7,11,...,39	d-axis transient voltages $e1d$	<b>Syn.e1d</b>
40,44,...,76	AVR regulator voltage $v_m$	<b>Exc.vm</b>
41,45,...,77	AVR reference voltage 1 $v_{r1}$	<b>Exc.vr1</b>
42,46,...,78	AVR reference voltage 2 $v_{r2}$	<b>Exc.vr2</b>
43,47,...,79	AVR field voltage $v_f$	<b>Exc.vf</b>
80,83,...,107	TG state variable $t_{g1}$	<b>Tg.tg1</b>
81,84,...,108	TG state variable $t_{g1}$	<b>Tg.tg2</b>
82,85,...,109	TG state variable $t_{g1}$	<b>Tg.tg3</b>

Table 3.4.: Structure of the state variables **DAE.x** for the 39-bus network including synchronous generators, TG's and AVR's.

### 3.3. Extensions to PSAT

One of the big advantages in using PSAT is the fact that changes can easily be made to meet the specific needs and requirements of the project. This was used several times in this work to make both, small and major adjustments to the existing program code in order to fix bugs in the program as well as adding new features to it. The most important changes are listed below.

<sup>1</sup>Note that the number of indices of the synchronous machines depends on the model type. In the 39-bus network, 9 generators are of model type 4 (4 state variables) and one is of model type 3 (3 state variables). This is the reason why there are only 39 indices for 10 synchronous machines.

**Start from previously computed operating point**

As explained earlier in this chapter, PSAT needs to be provided with a valid data file consisting of the network's structure, the parameters of its components as well as an initial guess of the bus voltage magnitudes, phase angles and the real power injection of the slack bus. The parameters of the (static) components include real and reactive power consumption of the loads, real power and voltage magnitude at the buses as well as voltage magnitude and phase angle for the bus. During this work it proved necessary to set the system to the optimal operating point computed by AMPL (see Section 4.1) and start the simulation from there. In order to avoid having to create an extra data file for each of those cases, the function *ModifyPSATdata* has been added to apply an AMPL solution to PSAT. This function did already exist prior to this project and is not considered a real extension to the program as it does not directly modify the code but takes place in the script from which PSAT is executed.

In the original version of PSAT it is not possible to save the state of the time-domain simulation in order to re-start the simulation from that point. This is of particular importance for the creation of “consequence tree” structures of contingencies (see Section 6.3.1). For that purpose it is necessary to simulate consecutive contingency sequences. Depending on the setting, a great number of these sequences have equal lines to start with before branching off. It is essential to avoid running the simulation from the base case for every sequence as the exploration of a full tree structure is very time consuming. For this purpose the time-domain simulation routine *fm\_int* has been changed so that it is possible to start the simulation from a previously saved operating point.

To save a simulation, all the local variables used in the routine have to be saved since those are lost after the function is executed. The various global components of the network, found in the field **Comp.names**, also have to be saved as during the simulation essential properties of the network can be changed, such as the topology (through line tripping) or the component states (e.g. through protective load shedding, generator outages, etc.). To load a previous point of the simulation, it is important to bypass the initialisations of the local variables.

**Breaking routine**

PSAT requires a pre-defined simulation time, which stops the simulation at a certain time instance. Often this cannot be known prior to the simulation. A workaround to this problem is setting the simulation time to a high value, in order to make sure of capturing all the important action. However, in the process of creating a

“consequence tree” (see Section 6.3.1), the simulation is likely to run over 100 times, so that a high simulation time would slow down the process immensely. In highly meshed networks a single line trip has but a small effect on the rest of the system and the system regains a stable point after 30 seconds or less. On the other hand if there is a greater outage in generation or the network breaks into one or multiple islands, vast oscillations can occur, which may also trigger further actions such as protective load shedding. In such a case calculations will take much longer time.

To resolve this problem the function `xCalculate_dx` has been embedded into the `perturb` file. In every time step this function calculates the difference between the last recorded and the current vector of algebraic ( $\mathbf{dy}$ ) and state variables ( $\mathbf{dx}$ ). The norm of the combined vector  $[\mathbf{dx} \ \mathbf{dy}]^T$  gives a measure of the stimulation of the system. If this norm is below a defined limit  $\sigma^{break}$  for a specific period of time  $t^{break}$ , the simulation is considered at a stable operating point and is broken. Typical values that were utilized were  $\sigma^{break} = 6 \cdot 10^{-5}$  and  $t^{break} = 75$  computational steps, which is about 9 seconds in the simulation (see Figure 3.4).

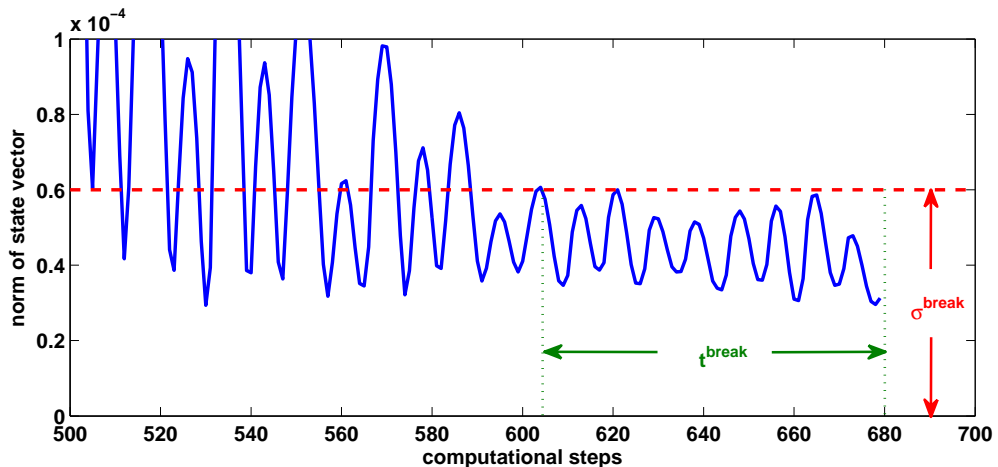


Figure 3.4.: Visualisation of the breaking routine stopping criterion. If the norm of the state vector is below a limit  $\sigma^{break}$  for a time slot of  $t^{break}$ , the simulation is stopped.

This procedure does not differentiate between the origin of the quantities incorporated in the state vector, many of which stem from very diverse physical backgrounds. In some situations this led to prolonged simulation times due to noise in the trajectories of the power injection of the generators. To take this into account, the function has been extended so that for each associated group of quantities an extra threshold can be defined.

This method has the disadvantage of not being completed at rest at the end of the

simulation. When it is used as a starting point for a consecutive simulation, the system will be slightly in motion. However, the simulation will have been started in order to undertake some action such as tripping a line. This primary motion can be considered negligible as the dimension of the upcoming interruption will be several orders greater than the initial movement. (see Figure 3.5)

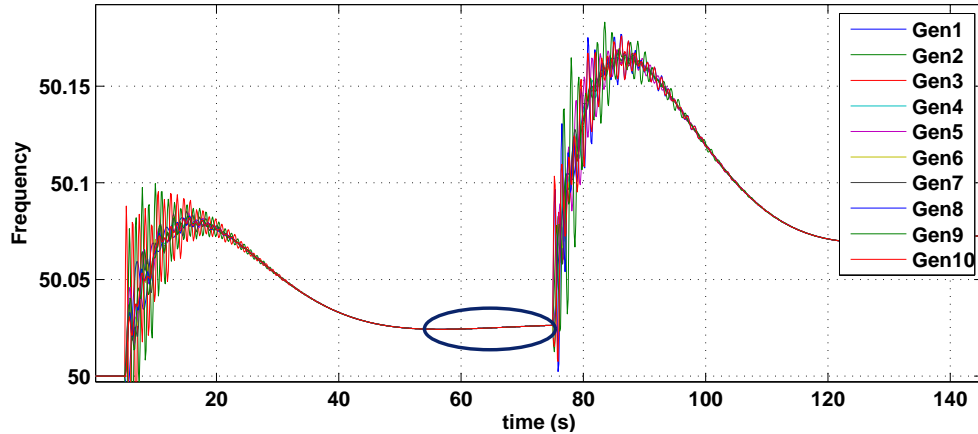


Figure 3.5.: Generator frequency of two consecutive line breaks. The frequency is not completely at rest when the simulation is stopped and the second line break is initialised. Yet, this motion (blue circle) is stable and small compared to the upcoming intervention.

### Protective load shedding routines

The aim of these extensions to PSAT is to make the time-domain simulation more realistic. Protective load shedding is a radical but effective method of preventing system collapse. The proportion of demand and supply is often altered in contingencies. Especially in islanding situations the balance between the generation and the consumption of power is significantly disturbed. Even if there is enough generating capacity in the system, the balance might not be restored fast enough or it might be a local phenomenon. In most contingencies the system would collapse under the stress caused by this imbalance. With automatic under-voltage and under-frequency load shedding, many of these situations can be saved by locally or globally reducing the load. The amount of load shed becomes an essential measure later in this work where it is used to judge the severity of a contingency (Chapter 6).

### Outages of generating units

The only contingencies that PSAT can simulate are three-phase faults to ground and line trips. Generator outages can be considerably more severe than line contingencies, especially in systems with a small number of large generating units. Therefore

the possibility of generator contingencies has been added to PSAT. The function *xGOintervention* works in a similar way to the **Breaker** handling. An outage time as well as an index of the failing generating unit need to be written to the variable **xGlob.GO**. If the outage time is within the time slot of the simulation, PSAT will simulate the failure of these units, setting all the corresponding parameters to zero, e.g. the frequency, real and reactive power, field voltage, etc. Therefore various changes must be made to the **DAE** structure as well as to the structures **Syn**, **Exc** and **Tg**. Since the nature of these changes is very complex and requires detailed study of various PSAT routines, the changes are not explained here.

### ZIP loads

Loads can be modelled in two ways in PSAT: Either as a unit that consumes constant active and reactive power, called PQ load, or as a constant impedance, which changes its power demand according to the square of the bus voltage. As many individual loads are often represented as a single large load the real characteristic might be better approximated as a mixture of different load behaviours. Although data did not exist for any of the network cases, the possibility of a more common load behaviour was provided by implementing the ZIP load model. The ZIP model is a mixture of impedance (Z), current (I) and constant power (P) demand. The real power consumption of a ZIP load  $d$  computes as

$$p_d^{D,ZIP} = P_d^D \cdot \left( \alpha + \beta \frac{v_b}{V_{ref}} + \gamma \frac{v_b^2}{V_{ref}^2} \right) \quad \forall d \in \mathcal{D}_b \quad (3.3)$$

where  $P_d^D$  is the original power demand from the data file. The reference voltage  $V_{ref}$  is computed in the function *pqshunt* before the time-domain simulation and based on the voltage of the power flow computations. The load parameters must add up to one.

$$\alpha + \beta + \gamma = 1 \quad (3.4)$$

### Islands

One big drawback of PSAT is that the time-domain simulation cannot properly handle situations when the network is split into one or multiple islands. Although designed to avoid convergence problems for single isolated buses, it fails to deal correctly with larger islands consisting of more than one bus.

Before load flow calculations as well as after every breaker intervention, PSAT checks

the connectivity state of the network topology. There is a function called *fm\_flows* with the main use of computing the power flow in the transmission lines using the bus bar voltage magnitudes and phase angles as well as the line admittance. However, by setting a flag, the routine completes other tasks, such as checking the connectivity. If an islanded bus is identified, it is written to the field ‘island’ of the **Bus** class. When the state matrix is created during the *fm\_call* routine, every bus registered in the **Bus.island** field gets all its entries removed from the matrix but the diagonal entry, which is set to one. This is to ensure that the variables of such a bus (voltage magnitude, phase angle, real and reactive power injections) are set to zero and do not influence the rest of the network. Thus an isolated bus is treated as a “dead” bus that is restricted from interacting with as well as having an influence on any other component within the network.

To be able to understand where the problem of PSAT lies, the function *fm\_flows* has to be analysed in more detail. As this is too long to describe at this point, it is stated without proof that, with the method incorporated in PSAT only single isolated buses can be identified while islands consisting of two or more buses remain undetected. Although fine in many cases there are situations when this can lead to convergence problems within the time-domain simulation if no additional action is undertaken. PSAT checks the connectivity state of the network before every load flow calculation as well as after breaker interventions using the function *fm\_flows*. As this is the only time when islanding can appear any additional code has to be placed at this point of the program. There are four cases to consider when a new islanded region evolves in the network (see Figure 3.6).

- a) The island consists of one or multiple buses having at least one generator and at least one load.
- b) The island consists of one or multiple buses hosting no generator but at least one load.
- c) The island consists of one or multiple buses hosting at least one generator but no load.
- d) The island consists of one or multiple buses hosting no generator and no load.

In the first case, no immediate action has to be taken. Of course, there is a good chance that the system does not cope with its new state but there is no influence on the convergence of the algorithm. In the second case, load flow can never converge to a solution as the islanded load cannot be supplied and thus would cause a singularity

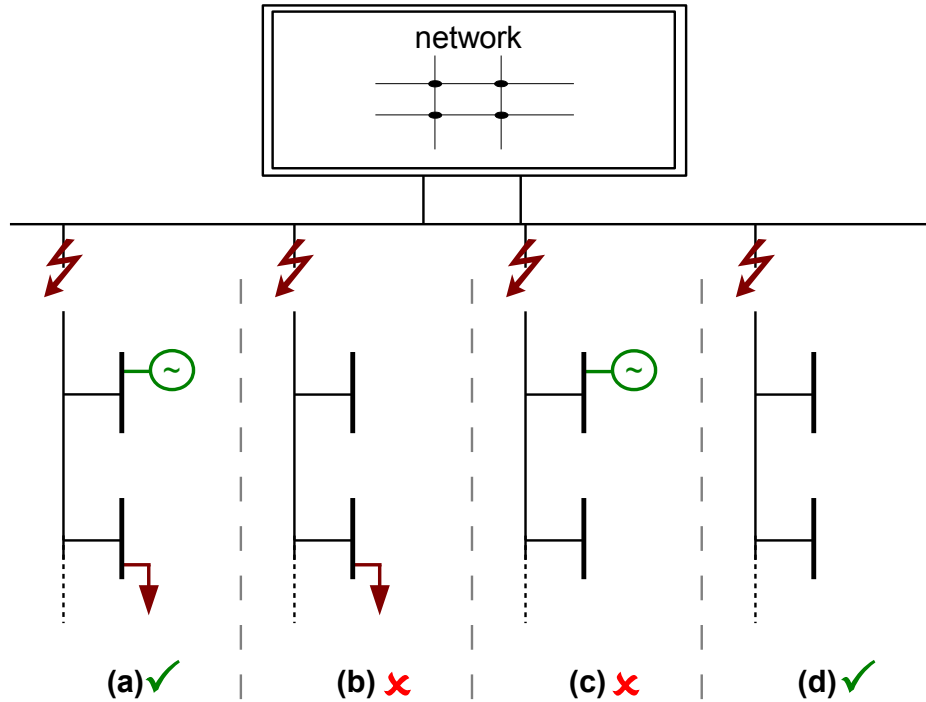


Figure 3.6.: Four different islanding types. Types (a) and (d) do not require any immediate action. Types (b) and (c) need to be shut down manually in order to prevent singularity problems.

in the computation. Therefore the worst-case measure has to be undertaken and the full load in the isolated part of the network has to be disconnected. This is done by setting the corresponding load to zero in the **PQ** class and registering each bus number in the **Bus.island** field. Similarly, in the third case every generator within the island has to be shut down using the generator shutdown routine and again all buses have to be registered in the **Bus.island** field. The latter also is the only action that has to be applied in the fourth case where it has to be made sure that the voltage magnitude and angle of the respective buses are set to zero and do not interfere with the rest of the network.

## 4. Optimization in Power Systems

In today's deregulated electricity market, system operators aim to run the network at maximum profit. To achieve this, a power network needs to be operated at its optimal economic point, i.e. at minimum cost. This can be formulated as an optimization problem. Demand is not a fixed parameter but dependent on a great number of customers, each acting with individual, arbitrary behaviour. To balance supply and demand at every instant of time, efficient optimization procedures are needed to be able to adjust generation continuously.

The load flow problem as introduced in Chapter 2 usually has one unique solution. This is a result of the fact that two of the four variables at each bus are previously known and two can be determined by the real and reactive power balance equations. At a PQ bus, the two known variables – P and Q – are defined by the mean demand averaged over thousands of customers and therefore, in general, are not within the area of influence of the system operator. At a PV bus however, where P and V are the known variables, the system operator can indeed vary these, at least to a certain extent. Taking this into account, two additional degrees of freedom arise as the number of unknowns exceeds the number of equations and the system is under-determined. Since the voltage is generally limited to a value relatively close to 1 p.u., the main variable to differ is the real power generation  $p^G$ . With a growing number of generating units more possibilities appear to schedule generation.

It lays in the nature of the diversity of energy sources that generating units differ considerably in their operating costs. This is a result of different fuel types and conceptual designs as well as geographical position. If load flow and losses are considered geographical position especially has an influence as power plants are not located all at the same point or share an equal distance from the centre of loads. Also, they might be connected to the system by different types of transmission networks.

A widely applied method to approximate the generation cost of thermal plants is by using a quadratic fuel cost function. According to Saadat [19] the fuel cost curve of

a generating unit  $g$  is usually described by

$$GenCost_g(p_g^G) = c_g^{(0)} + c_g^{(1)}p_g^G + c_g^{(2)}p_g^{G^2} \quad (4.1)$$

where  $p_g^G$  is the real power output and the cost coefficients  $c_g^{(i)}$  are constant for any one plant and are measured in  $\$/h$ ,  $\$/MWh$  and  $\$/MW^2h$ , respectively. The offset  $c_g^{(0)}$  can be seen as a fixed cost, which only has to be applied once e.g. to start up the plant. The coefficients  $c_g^{(1)}$  and  $c_g^{(2)}$  are the costs for operation and maintenance. Even for considerably small systems this can lead to a great diversity in cost. This will be illustrated in Section 4.5 by an example of a system with four generators.

Running a power network at its most economic operating point is the main goal that is shared by all the models introduced in this chapter. The models range from basic and simple to very extensive formulations. As feasible load flow solution and consequently security aspects for both cases, DC and AC, are taken into account, the problem formulations gain more and more complexity.

## 4.1. Optimization Problems

Optimization problems deal with the task of finding an optimal solution to a problem formulation.

$$\begin{aligned} \min \quad & \mathbf{f}(\mathbf{x}) \\ \text{subject to} \quad & g_i(\mathbf{x}) = 0 \quad i = 1, \dots, k \\ & h_j(\mathbf{x}) \leq 0 \quad j = 1, \dots, m \end{aligned} \quad (4.2)$$

where  $g_i(\mathbf{x})$  are the equality constraints and  $h_j(\mathbf{x})$  the inequality constraints.  $\mathbf{f}$  is called the objective function or objective.

If the objection function is of linear form

$$\mathbf{f}(\mathbf{x}) = \mathbf{c}^T \mathbf{x} \quad (4.3)$$

the problem is referred to as linear programming ( $LP$ ) problem.

For an objective of the form

$$\mathbf{f}(\mathbf{x}) = \mathbf{c}^T \mathbf{x} + \frac{1}{2} \mathbf{x}^T \mathbf{H} \mathbf{x} \quad (4.4)$$

it is called a quadratic programming (QP) problem. In case the objective is a nonlinear function it is called a non-linear programming (NLP) problem.

There are two types, constrained and unconstrained optimization. In unconstrained problems, there are no equality or inequality constraints and the solution conditions are simply given by

$$\frac{\partial \mathbf{f}}{\partial \mathbf{x}} = 0 \quad (4.5)$$

According to Saadat [19], the solution conditions in an constrained problem are obtained from the LaGrange multiplier method. The problem is converted to (4.6) and solution conditions are given by (4.7) – (4.9)

$$L = \mathbf{f} + \sum_{i=1}^k \lambda_i g_i + \sum_{j=1}^m \mu_j h_j \quad (4.6)$$

$$\frac{\partial L}{\partial \mathbf{x}} = 0 \quad (4.7)$$

$$\frac{\partial L}{\partial \lambda_i} = 0 \quad (4.8)$$

$$\frac{\partial L}{\partial \mu_j} \leq 0 \quad (4.9)$$

where  $\lambda_i$  and  $\mu_j$  are LaGrange multipliers.

In this study the program AMPL was used in combination with an interior point solver (ipopt) to solve the optimization problems.

## 4.2. Economic Dispatch Calculation (EDC)

The aim of the Economic Dispatch Calculation is to find a schedule of power generation such that the operating cost of the total system is minimized. As mentioned at the beginning of this chapter, this also is the main objective in all of the following models. The EDC model is the most basic. It is subject to only one

constraint, which represents a power balance equation. Thus, the EDC minimizes the instantaneous operation cost such that the current real power demand is matched by the generation.

For a set  $\mathcal{G}$  of generators and a set  $\mathcal{D}$  of loads this model can be described mathematically as

$$\begin{aligned} \min \quad & \sum_{g \in \mathcal{G}} c_g^{(0)} + c_g^{(1)} p_g^G + c_g^{(2)} p_g^{G^2} \\ \text{subject to} \quad & \sum_{g \in \mathcal{G}} p_g^G = \sum_{d \in \mathcal{D}} p_d^D \end{aligned} \quad (4.10)$$

The objective is the sum of all cost functions of the generators. The cost for each generator is given by Equation 4.1 with the cost parameters  $c_g^{(i)}$ . The real output of generating unit  $g$  is denoted as  $p_g^G$  and the real power demand of load  $d$  as  $p_d^D$ .

This model can be represented by the theoretical network topology of Figure 4.1. Assuming that all generators as well as the system total load are connected to a single busbar shows the simplicity of the model.

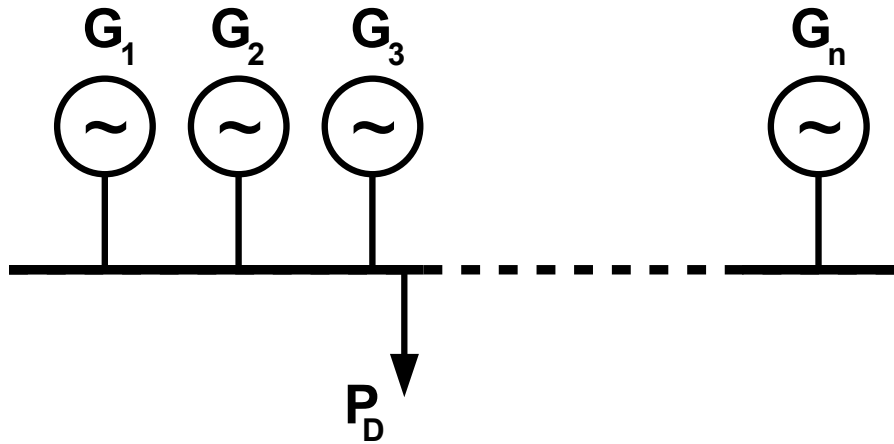


Figure 4.1.: EDC theoretical network topology. The assumption that all generating units as well as the total demand are connected to one bus is strongly simplified. It does not take into account power flow or line losses.

Since the power output of one generating unit is usually limited in both its maximum and minimum output, this model can be extended by an appropriate constraint. As the generating units are not located directly at the consuming loads but connected via a transmission system, an approximation of the line losses can also be included

for greater accuracy.

Taking these considerations into account the extended problem becomes

$$\begin{aligned}
 \min \quad & \sum_{g \in \mathcal{G}} c_g^{(0)} + c_g^{(1)} p_g^G + c_g^{(2)} p_g^{G^2} \\
 \text{subject to} \quad & \sum_{g \in \mathcal{G}} p_g^G = \sum_{d \in \mathcal{D}} p_d^D + p^{Loss} \\
 & P_{g-}^G \leq p_g^G \leq P_{g+}^G \quad \forall g \in \mathcal{G}
 \end{aligned} \tag{4.11}$$

where the losses  $p^{Loss}$  can be evaluated by various approximations, e.g. Kron's loss formula [19], which will not be discussed any further.  $P_{g-}^G$  and  $P_{g+}^G$  represent the minimum and maximum limit of real power generation of unit  $g$ , respectively.

### 4.3. Optimal Power Flow (OPF)

As mentioned in the previous section the EDC considers all the generating units and the load connected to the same one bus, which is far from the circumstances found in real power systems. Also, it does not take into account either line flows and their limits or bus phase voltages and angles. For a more practical approach it is required to incorporate a feasible load flow solution to ensure the computed solution is applicable to the network.

In order to achieve this the Optimal power flow incorporates additional constraints featuring the nodal network equations. The set  $\mathcal{G}_b$  is a compound set of  $\mathcal{G}$  and the set of buses  $\mathcal{B}$ . Similarly, the set  $\mathcal{D}_b$  is a combination of the sets  $\mathcal{D}$  and  $\mathcal{B}$  and  $\mathcal{L}$  is the set of Lines. Hence, Kirchhoff's current law (KCL) for real and reactive powers can be formulated for every bus by the following constraints.

$$\left. \begin{aligned}
 \sum_{g \in \mathcal{G}_b} p_g^G &= \sum_{d \in \mathcal{D}_b} p_d^D + \sum_{l \in \mathcal{L}: b=b^{fr}} p_l^{L,fr} + \sum_{l \in \mathcal{L}: b=b^{to}} p_l^{L,to} + g_b v_b^2, \quad \forall b \in \mathcal{B} \\
 \sum_{g \in \mathcal{G}_b} q_g^G &= \sum_{d \in \mathcal{D}_b} q_d^D + \sum_{l \in \mathcal{L}: b=b^{fr}} q_l^{L,fr} + \sum_{l \in \mathcal{L}: b=b^{to}} q_l^{L,to} - b_b v_b^2, \quad \forall b \in \mathcal{B}
 \end{aligned} \right\} KCL \tag{4.12}$$

where  $p_g^G$  ( $q_g^G$ ) represents the generated real (reactive) power of unit  $g$ ,  $p_d^D$  ( $q_d^D$ ) the real (reactive) demand of load  $d$  and  $p_l^{L,fr}$  ( $p_l^{L,to}$ ) the flow of real power from (to) line  $l$ , with reactive flows respectively. The bus voltage magnitude is indicated by  $v_b$ , the shunt conductance and susceptance of bus  $b$  by  $g_b$  and  $b_b$ .

Similarly, Kirchhoff's voltage law (KVL) can be expressed. Equations (4.13) give the KVL for a line  $l$ , based on Equations (2.18) – (2.21). Every line is defined by its sending and receiving bus location, denoted by the superscripts  $fr$  and  $to$ .  $v_l^{fr}$  ( $v_l^{to}$ ) is the voltage magnitude of the sending (receiving) bus of line  $l$ ,  $\delta_l^{fr}$  ( $\delta_l^{to}$ ) the corresponding phase angle. The parameters  $g_{l11}, \dots, g_{l22}, b_{l11}, \dots, b_{l22}$  refer to the parameters (2.26) and (2.33) and describe the conductance and susceptance of line  $l$ .

$$\left. \begin{aligned} p_l^{L,fr} &= v_l^{fr^2} g_{l11} + v_l^{fr} v_l^{to} (g_{l12} \cos(\delta_l^{fr} - \delta_l^{to}) + b_{l12} \sin(\delta_l^{fr} - \delta_l^{to})) \\ q_l^{L,fr} &= -v_l^{fr^2} b_{l11} + v_l^{fr} v_l^{to} (g_{l12} \sin(\delta_l^{fr} - \delta_l^{to}) - b_{l12} \cos(\delta_l^{fr} - \delta_l^{to})) \\ p_l^{L,to} &= v_l^{to^2} g_{l22} + v_l^{fr} v_l^{to} (g_{l21} \cos(\delta_l^{to} - \delta_l^{fr}) + b_{l21} \sin(\delta_l^{to} - \delta_l^{fr})) \\ q_l^{L,to} &= -v_l^{to^2} b_{l22} + v_l^{fr} v_l^{to} (g_{l21} \sin(\delta_l^{to} - \delta_l^{fr}) - b_{l21} \cos(\delta_l^{to} - \delta_l^{fr})) \end{aligned} \right\} KVL \quad (4.13)$$

In order to make the formulations clearer, the KCL equations (4.12) and the KVL equations (4.13) will be denoted as a single vector equality.

$$\mathbf{g}^{KCL}(\mathbf{x}) = \mathbf{0} \quad (\text{KCL equations according to (4.12)})$$

$$\mathbf{g}^{KVL}(\mathbf{x}) = \mathbf{0} \quad (\text{KVL equations according to (4.13)})$$

where  $\mathbf{x}$  is a vector containing all the real and reactive powers, phase angles and voltage magnitudes.

In the EDC model transmission line flows are not modelled. Here variables for real and reactive power flows are included, which need to be limited for safe operation. The same holds for the voltage levels and reactive power generation. Therefore some extra inequality constraints must be formulated and added to the model.

$$p_l^{L^2} + q_l^{L^2} \leq S_l^{L^2} \quad (4.14)$$

$$Q_{g-}^G \leq q_g^G \leq Q_{g+}^G \quad (4.15)$$

$$V_{b-} \leq v_b \leq V_{b+} \quad (4.16)$$

Here,  $S_l^L$  is the apparent power limit for line  $l$ ,  $Q_{g-}^G$  ( $Q_{g+}^G$ ) are the lower (upper) limit for the reactive power generation of unit  $g$  and  $V_{b-}$  ( $V_{b+}$ ) is the lower (upper) bound

for the bus voltage magnitude at bus  $b$ . The line flows are computed as

$$\begin{aligned} p_l^L &= \max(p_l^{L,fr}, p_l^{L,to}) \\ q_l^L &= \max(q_l^{L,fr}, q_l^{L,to}) \end{aligned} \quad (4.17)$$

There are two versions of the standard OPF. The *full AC formulation*, shown in Section 4.3.1, provides a solution for generated real and reactive powers, the line flows as well as the phase angle and magnitude of the bus voltages. The line flow equations described by (4.13) incorporate sine and cosine functions and hence form a non-linear programming (NLP) problem. If the full description is not required or if fast computation is necessary, the model can be simplified to the *DC linearisation*. This is an easier linear programming (LP) problem providing an approximate solution for the real powers and the bus angles but neglecting line losses and reactive powers. The adjusted power equations for the linearisation are shown in Section 4.3.2.

### 4.3.1. Full AC OPF

Adding the constraints described above to the problem (4.11) gives the full AC formulation

$$\min \sum_{g \in \mathcal{G}_b} c_g^{(0)} + c_g^{(1)} p_g^G + c_g^{(2)} p_g^{G^2}$$

$$\text{subject to } \mathbf{g}^{KCL}(\mathbf{x}) = \mathbf{0} \quad \forall b \in \mathcal{B} \quad (4.18)$$

$$\mathbf{g}^{KVL}(\mathbf{x}) = \mathbf{0} \quad \forall l \in \mathcal{L} \quad (4.19)$$

$$\delta_0 = 0 \quad (4.20)$$

$$P_{g-}^G \leq p_g^G \leq P_{g+}^G \quad \forall g \in \mathcal{G} \quad (4.21)$$

$$Q_{g-}^G \leq q_g^G \leq Q_{g+}^G \quad \forall g \in \mathcal{G} \quad (4.22)$$

$$V_{b-} \leq v_b \leq V_{b+} \quad \forall b \in \mathcal{B} \quad (4.23)$$

$$p_l^{L^2} + q_l^{L^2} \leq S_l^{L^2} \quad \forall l \in \mathcal{L} \quad (4.24)$$

The power flow equations, consisting of KCL (4.18) and KVL (4.19), together with the reference phase angle constraint (4.20) form the equality constraints. Generator output limits (4.21) and (4.22), thermal limits (4.24) and voltage level limits (4.23)

give the the inequality constraints.  $p_i^L$  and  $q_i^L$  are calculated as introduced in Equation (4.17).

### 4.3.2. Linearized DC OPF

In order to simplify and linearise the power flow equations various assumptions are made:

- Reactive power flows are neglected
- Voltages are constant and normalised,  $v_b = 1.0$
- Phase angle differences of neighbouring buses are small

$$\begin{aligned}\cos(\delta_i^{fr} - \delta_i^{to}) &\approx 1 \\ \sin(\delta_i^{fr} - \delta_i^{to}) &\approx \delta_i^{fr} - \delta_i^{to}\end{aligned}$$

- Line resistance is small compared to reactance,  $g_{l_{ik}} \ll b_{l_{ik}}$

Taking these simplifications into account the real powers in (4.13) simplify to

$$\begin{aligned}p_i^{L,fr} &= v_i^{fr^2} \underbrace{g_{l_{11}}}_{\approx 0} + \underbrace{v_i^{fr} v_i^{to}}_{\approx 1} (\underbrace{g_{l_{12}}}_{\approx 0} \underbrace{\cos(\delta_i^{fr} - \delta_i^{to})}_{\approx 1} + b_{l_{12}} \underbrace{\sin(\delta_i^{fr} - \delta_i^{to})}_{\approx \delta_i^{fr} - \delta_i^{to}}) \\ &\approx b_{l_{12}} (\delta_i^{fr} - \delta_i^{to}) \\ p_i^{L,to} &\approx b_{l_{21}} (\delta_i^{to} - \delta_i^{fr}) = -b_{l_{12}} (\delta_i^{fr} - \delta_i^{to})\end{aligned}$$

This implies that opposite flows in the same line have opposite signs but equal magnitude and can be treated as one single variable  $p_i^L$ . Hence, neglecting the equations for the reactive powers, (4.12) and (4.13) simplify to

$$\begin{aligned}\sum_{g \in \mathcal{G}_b} p_g^G &= \sum_{d \in \mathcal{D}_b} p_d^D + \sum_{l \in \mathcal{L}_b} p_l^L & \forall b \in \mathcal{B} \\ p_l^L &= b_{l_{12}} (\delta_l^{fr} - \delta_l^{to}) & \forall l \in \mathcal{L}\end{aligned}$$

The linearised OPF formulation becomes a convex LP problem, which is considerably easy to solve as there exist efficient solvers.

$$\begin{aligned}
 \min \quad & \sum_{g \in G} c_g^{(0)} + c_g^{(1)} p_g^G + c_g^{(2)} p_g^{G^2} \\
 \text{subject to} \quad & \sum_{g \in \mathcal{G}_b} p_g^G = \sum_{d \in \mathcal{D}_b} p_d^D + \sum_{l \in \mathcal{L}_b} p_l^L \quad \forall b \in \mathcal{B} \\
 & p_l^L = b_{l_{12}} (\delta_l^{fr} - \delta_l^{to}) \quad \forall l \in \mathcal{L} \\
 & \delta_0 = 0 \\
 & P_{g-}^G \leq p_g^G \leq P_{g+}^G \quad \forall g \in \mathcal{G} \\
 & p_l^L \leq P_{l,max}^L \quad \forall l \in \mathcal{L}
 \end{aligned}$$

## 4.4. Security Constrained OPF (SCOPF)

In the previous sections it was assumed that an electricity network is in its *optimal* state if it operates at minimal cost. For an abstract model this solution might be satisfactory. In real power systems however, the components of a network are exposed to environmental impacts, construction faults and human errors. Thus, a *contingency* such as a line or generator outage has to be taken into account as a possibly event. When a contingency occurs, the flows in the network rearrange immediately according to Kirchhoff's laws and try to reach a new steady state. For line contingencies this usually results in an increase of line flows in parts of the network. As a consequence, further lines could be tripped by automatic protection devices that detect the overflow. In the worst case, this can lead to a cascading blackout. To account for such a scenario it is desirable to find a system state that is not only low in operating cost but also aware of security aspects such as the possibility of line outages. These requirements are met by the Security Constrained OPF (SCOPF), an extension to the standard OPF that features additional constraints to ensure feasible post-contingency load flow solutions. These extra constraints restrict the space of feasible solutions so that the cost of the SCOPF is always higher or equal to the corresponding OPF. The difference in cost between the OPF and the SCOPF can be seen as the “cost of security”.

Mathematically the SCOPF features the same constraints as the standard OPF, denoted as the base case constraints. Additionally needs to incorporate a whole new

set of constraints for one each considered contingency  $c$ .

$$\begin{aligned} \sum_{g \in G_b} p_{g,c}^G &= \sum_{d \in D_b} p_{d,c}^D + \sum_{l \in L} p_{l,c}^{L,fr} + \sum_{l \in L} p_{l,c}^{L,to} + g_b v_{b,c}^2, \quad \forall b \in \mathcal{B} \\ \sum_{g \in G_b} q_{g,c}^G &= \sum_{d \in D_b} q_{d,c}^D + \sum_{l \in L} q_{l,c}^{L,fr} + \sum_{l \in L} q_{l,c}^{L,to} - b_b v_{b,c}^2, \quad \forall b \in \mathcal{B} \end{aligned} \quad (4.25)$$

$$\begin{aligned} p_{l,c}^{L,fr} &= v_{l,c}^{fr^2} g_{l11} + v_{l,c}^{fr} v_{l,c}^{to} (g_{l12} \cos(\delta_{l,c}^{fr} - \delta_{l,c}^{to}) + b_{l12} \sin(\delta_{l,c}^{fr} - \delta_{l,c}^{to})) \\ q_{l,c}^{L,fr} &= -v_{l,c}^{fr^2} b_{l11} + v_{l,c}^{fr} v_{l,c}^{to} (g_{l12} \sin(\delta_{l,c}^{fr} - \delta_{l,c}^{to}) - b_{l12} \cos(\delta_{l,c}^{fr} - \delta_{l,c}^{to})) \\ p_{l,c}^{L,to} &= v_{l,c}^{to^2} g_{l22} + v_{l,c}^{fr} v_{l,c}^{to} (g_{l21} \cos(\delta_{l,c}^{to} - \delta_{l,c}^{fr}) + b_{l21} \sin(\delta_{l,c}^{to} - \delta_{l,c}^{fr})) \\ q_{l,c}^{L,to} &= -v_{l,c}^{to^2} b_{l22} + v_{l,c}^{fr} v_{l,c}^{to} (g_{l21} \sin(\delta_{l,c}^{to} - \delta_{l,c}^{fr}) - b_{l21} \cos(\delta_{l,c}^{to} - \delta_{l,c}^{fr})) \end{aligned} \quad (4.26)$$

$$\delta_{0,c} = 0 \quad (4.27)$$

$$P_{g-}^G \leq p_{g,c}^G \leq P_{g+}^G \quad \forall g \in \mathcal{G} \quad (4.28)$$

$$Q_{g-}^G \leq q_{g,c}^G \leq Q_{g+}^G \quad \forall g \in \mathcal{G} \quad (4.29)$$

$$V_{b-} \leq v_{b,c} \leq V_{b+} \quad \forall b \in \mathcal{B} \quad (4.30)$$

$$p_l^{L^2} + q_l^{L^2} \leq S_l^{L^2} \quad \forall l \in \mathcal{L} \quad (4.31)$$

These constraints are basically the same as in the base case. For line contingencies the flows in the broken lines are set to zero in the KVL. Similarly, the generated powers  $p_g^G$  and  $q_g^G$  are set to zero in case of generator contingencies. The contingency variables, denoted by a subscripted  $c$ , provide the result of the power flow in the case of a contingency. However, so far the variables of the base case and the variables of the contingency case are independent of each other. The formulation only checks for the existence of a feasible load flow solution in the contingency case. To allow for this to effectively influence the objective another constraint needs to be added linking the contingency case with the base case.

According to Capitanescu [3] there are two main types of SCOPFs, the preventive SCOPF (P-SCOPF) and the corrective SCOPF (C-SCOPF). The preventive SCOPF is designed to strongly improve security in the network and does not allow any change of the control variables in post-contingency states, such as active and reactive generator powers, tap ratios, shunt reactances, load apparent powers, etc. The corrective SCOPF on the other hand is designed more towards economy, as it allows rescheduling the control variables up to a certain extend.

In this work the only control variable considered for the linking are the generator

outputs  $p_g^G$  and  $p_{g,c}^G$ . Hence, the preventive and corrective SCOPF can be defined as follows

<b>preventive SCOPF</b>	<b>corrective SCOPF</b>
$\min \quad GenCost$	$\min \quad GenCost$
$\text{subject to } \mathbf{g}^{base}(\mathbf{x}) = \mathbf{0}$	$\text{subject to } \mathbf{g}^{base}(\mathbf{x}) = \mathbf{0}$
$\mathbf{h}^{base}(\mathbf{x}) \leq \mathbf{0}$	$\mathbf{h}^{base}(\mathbf{x}) \leq \mathbf{0}$
$\mathbf{g}^{con}(\mathbf{x}_c) = \mathbf{0}$	$\mathbf{g}^{con}(\mathbf{x}_c) = \mathbf{0}$
$\mathbf{h}^{con}(\mathbf{x}_c) \leq \mathbf{0}$	$\mathbf{h}^{con}(\mathbf{x}_c) \leq \mathbf{0}$
$p_{g,c} = p_g$	$-\rho p_g \leq p_{g,c} \leq \rho p_g$

where  $\mathbf{g}^{base}$  ( $\mathbf{h}^{base}$ ) form the equality (inequality) constraints of the base case.  $\mathbf{g}^{con}$  ( $\mathbf{h}^{con}$ ) on the other side refer to the contingency equality (inequality) constraints.  $\mathbf{x}$  are the algebraic variables of the base case,  $\mathbf{x}_c$  of the contingency case  $c$ . It can be seen that for the preventive SCOPF the output  $p_{g,c}^G$  must be the same in all contingency cases as  $p_g^G$  in the base case. For the corrective SCOPF however, it is allowed to change by a constant factor  $\rho$ . The limits on the line flows, voltage, etc. still apply in the contingency case but it is possible to loosen the bounds in order to improve feasibility of the model.

## 4.5. Visualisation

### 4.5.1. 3-Bus Model

A lossless, DC, N-1 insecure model from Dent [6] was chosen as a basis which was then extended to a full AC model by applying suitable extensions. The network topology is depicted in Figure 4.2, the network data are given in tables 4.1 – 4.3. The system consists of three buses, which are each interconnected by three single lines. Bus 1 holds two of the four generators, buses 2 and 3 each hold one. There are three loads to be supplied, one at each bus.

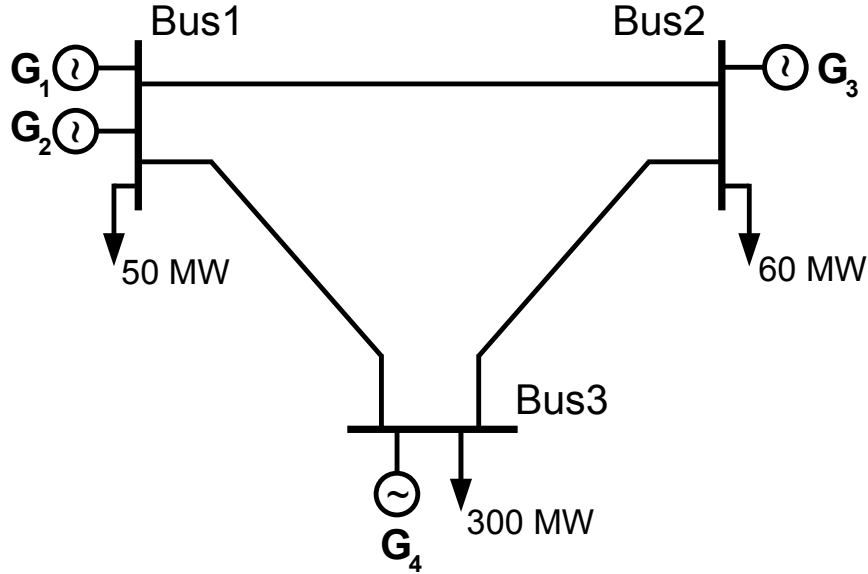


Figure 4.2.: 3-Bus test network

Load data			
#	Bus	$P^D$ [MW]	$Q^D$ [MVar]
1	1	50	8.66
2	2	60	1.24
3	3	300	50

Table 4.1.: Load data of the 3-bus test system

Generator data								
#	Bus	$P_{max}$ [MW]	$P_{min}$ [MW]	$Q_{max}$ [MVar]	$Q_{min}$ [MVar]	$c^{(0)}$ [\$/h]	$c^{(1)}$ [\$/MWh]	$c^{(2)}$ [\$/MW <sup>2</sup> h]
1	1	140	0	70	0	0	7.5	0
2	1	285	0	100	0	0	6.0	0
3	2	85	0	50	0	0	14.0	0
4	3	90	0	60	0	0	10.0	0

Table 4.2.: Generator data of the 3-bus test system

Branch data							
#	fr bus	to bus	$r$ [pu]	$x$ [pu]	$b$ [pu]	$S_{max}^L$ [MVA]	$S_{max}^{L,emgy}$ [MVA]
1	1	2	0.02	0.2	0.001	126	200
2	1	3	0.02	0.2	0.001	250	400
3	2	3	0.02	0.1	0.001	130	230

Table 4.3.: Branch data of the 3-bus test system

In the branch data, the parameters  $S_{max}^L$  and  $S_{max}^{L,emgy}$  correspond to thermal limits of the line flow.  $S_{max}^L$  is a long-term limit and  $S_{max}^{L,emgy}$  a 15min emergency limit, which is raised by 60%. In the DC case the same values are adapted for the real power limits  $P_{max}^L$  and  $P_{max}^{L,emgy}$ .

In order to keep the example simple, the cost function is approximated by a linear function without fixed costs. Generator 2 is the cheapest to run followed by generators 1, 4 and finally 3. The minimum values for real and reactive power generation are neglected and set to zero. It should be noted that the lower limit for the real power generation  $P_{g-}^G$  is usually greater than zero whereas the lower limit for the reactive power can range to negative values as well. The reason for the non-zero bound is that plants would suffer from stability problems if their real power output is decreased to an arbitrary low level. Rective power on the other hand can be consumed or provided dependent on the power factor.

#### 4.5.2. EDC

This EDC problem can be solved using the network data of the 3-Bus system. The solution can be seen in Table 4.4, including generator limits but neglecting any losses in the system. To meet the total demand of 410 MW the cheapest generator, Generator 2 is used up to its maximum capacity while the remaining power is provided by Generator 1, the second cheapest. Thus, the total generation cost per hour computes to 2647.5 \$/h.

Total demand	410 MW
Total generation	410 MW
Generator 1	125 MW
Generator 2	285 MW
Generator 3	0 MW
Generator 4	0 MW
Total cost per hour	2647.5 \$/h

Table 4.4.: Solution of the EDC optimization problem

#### 4.5.3. DC and AC OPF

The results of the DC OPF model are visualised based on the 3-Bus network. In Figure 4.3 the system is solved without line limits applied and in Figure 4.4 with line

limits applied. The solution without the line limits applied is the same as the EDC model. For this solution the flow on Line 1 is too high since the thermal limit for this line is given by 126 MW (Table 4.3). When the thermal constraints are applied, the power sent over the lines is limited and a more expensive generator has to be switched on (Figure 4.3). Consequently, the operation cost increases.

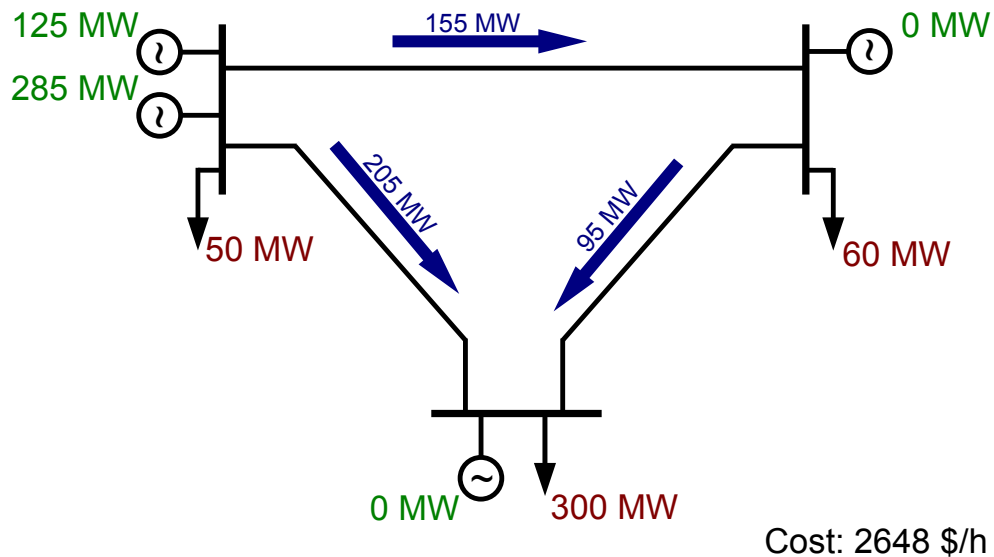


Figure 4.3.: Solution of the DC OPF without line limit constraints. The flow in line 1 exceeds its limit of 126 MW.

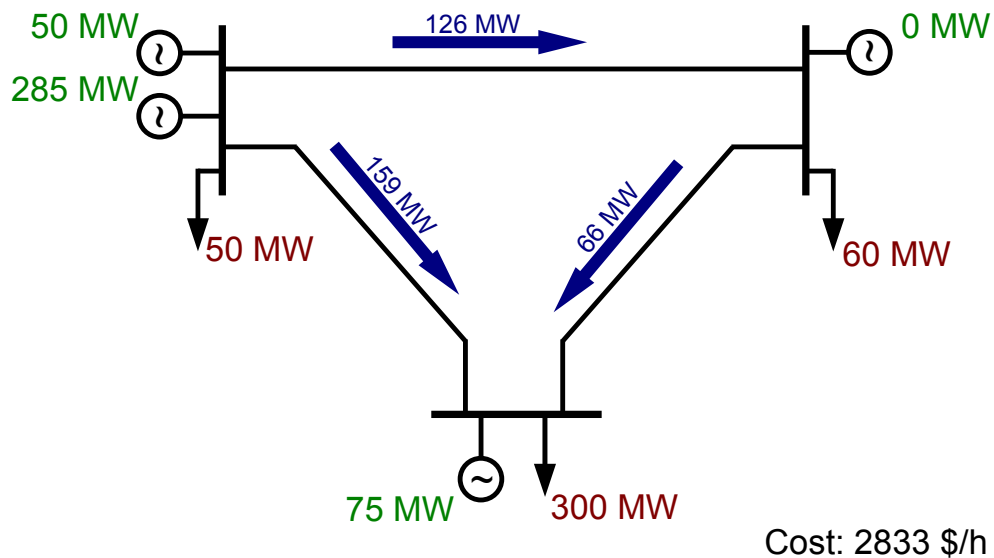


Figure 4.4.: Solution of the DC OPF with line limit constraints. The More expensive generator at bus 3 needs to be switched on.

In the AC model reactive powers need to be considered for the loads, the generators and the line flows. Also, the voltage magnitudes are not normalised.

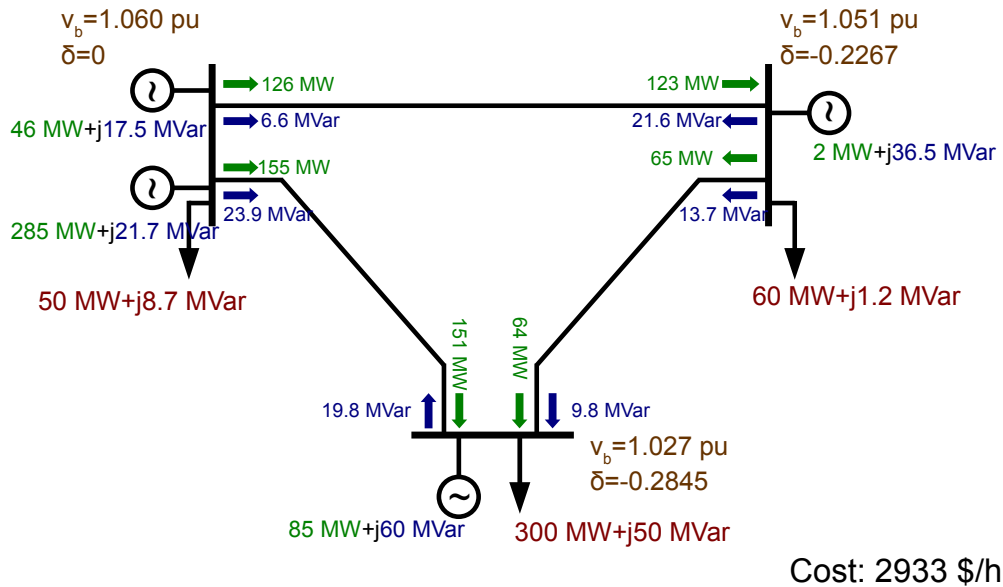


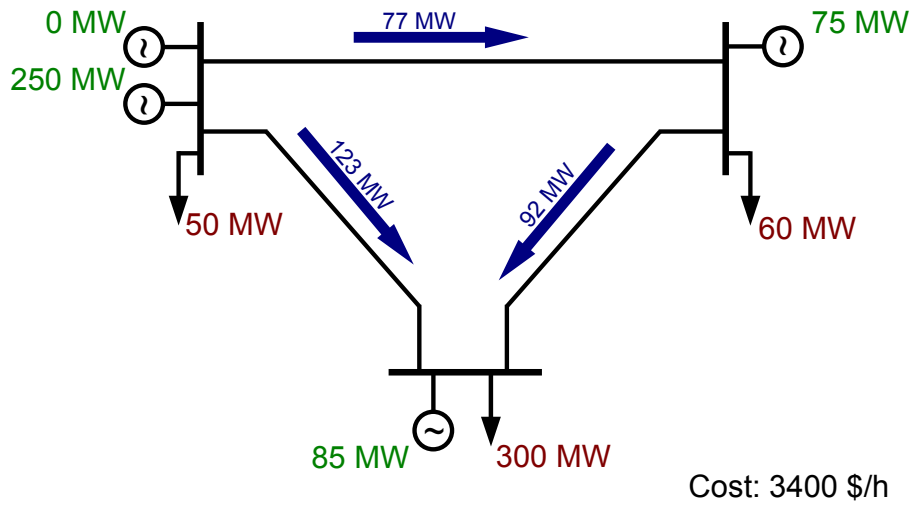
Figure 4.5.: Solution of the AC OPF. Reactive powers and voltage magnitudes are considered as well as line losses. The loads are modelled as constant PQ.

The lines consume real and reactive power resulting in losses in the system. Yet, these losses have to be supplied and paid for, increasing the operating cost in comparison to the lossless DC solution.

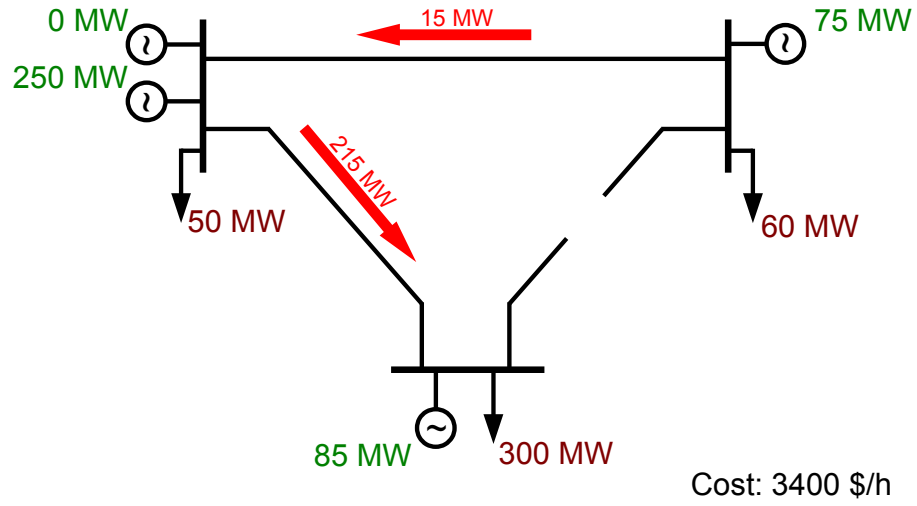
#### 4.5.4. DC SCOPF

The SCOPF solution is depicted in Figures 4.6 and 4.7 for the preventive and the corrective case, respectively. The solutions are only given for the DC case.

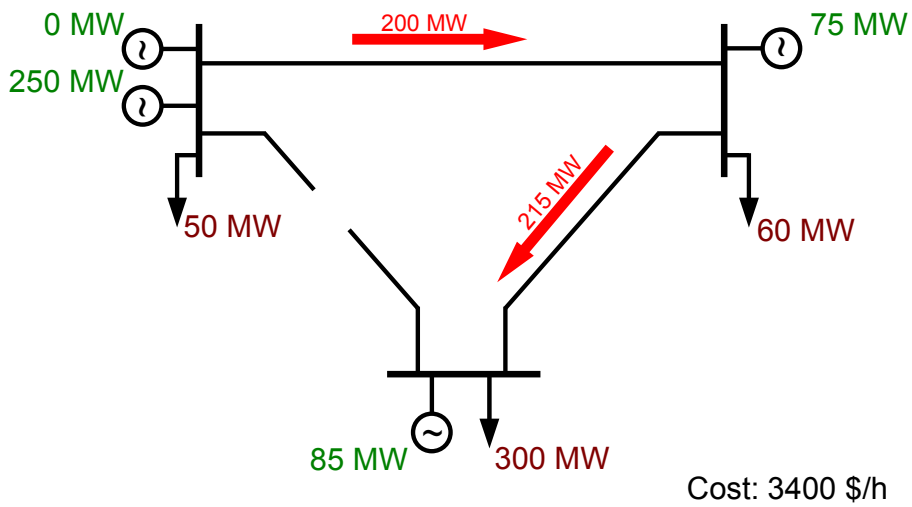
preventive SCOPF



(a)



(b)



(c)

Figure 4.6.: Solution of the DC P-SCOPF (a) base case (b) Line 3 contingency (c) Line 2 contingency

corrective SCOPF

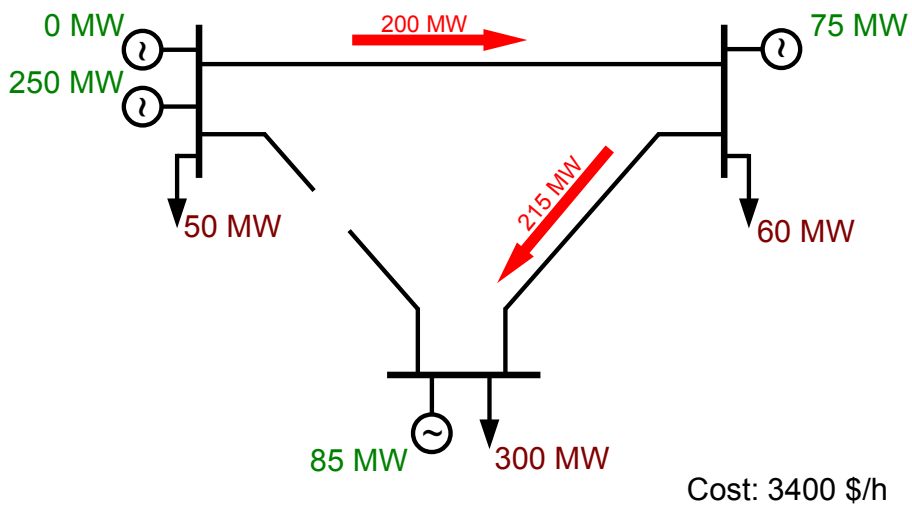
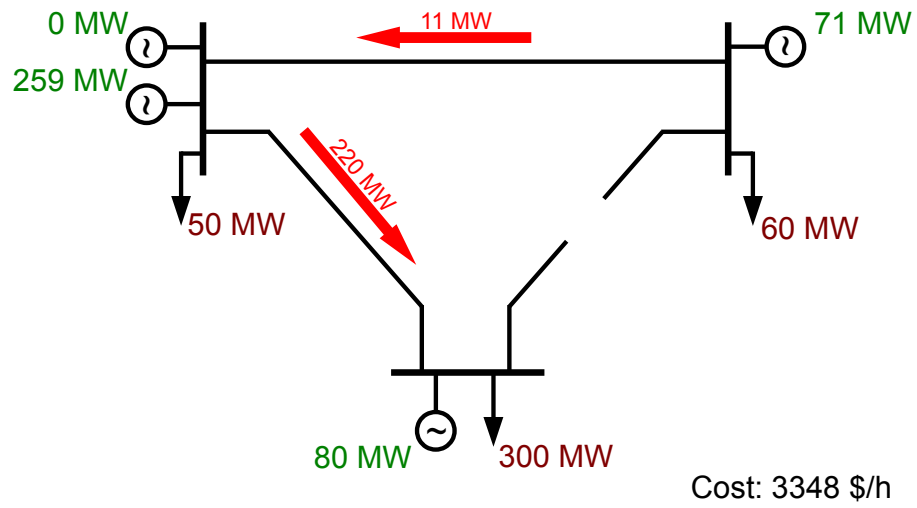
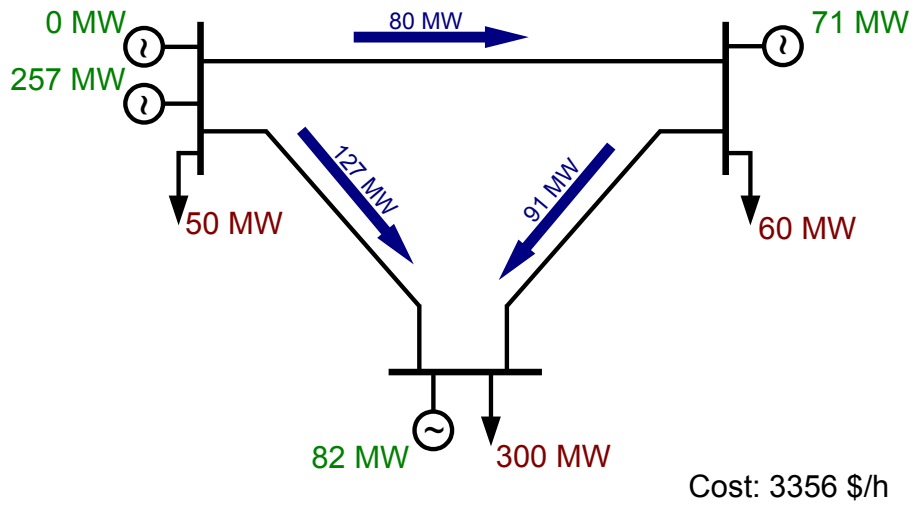


Figure 4.7.: Solution of the DC C-SCOPF (a) base case (b) Line 3 contingency (c) Line 2 contingency

## 4.6. Summary

In this chapter various optimization models for power systems were introduced. The most basic is the EDC, which only looks at the generation and demand. The OPF extends this model by applying load flow constraints to the problem. The SCOPF does not look for the cheapest solutions at all cost but also considers security aspects.

Table 4.5 gives an overview of the constraints used in the various models. Table 4.6 gives an overview of distribution of generation of the various models.

<i>Constraints</i>	EDC	OPF		SCOPF	
		DC	AC	DC	AC
Generation cost	✓	✓	✓	✓	✓
power balance	✓				
KVL & KCL		✓	✓	✓	✓
reference angle		✓	✓	✓	✓
real power generation limits		✓	✓	✓	✓
real power line limits		✓		✓	
reactive power generation limits			✓		✓
voltage limits			✓		✓
apparent power line limits			✓		✓
contingency KVL & KCL				✓	✓
contingency limits				✓	✓

Table 4.5.: Constraints of the various models.

	EDC	OPF		C-SCOPF		P-SCOPF	
		DC	AC	DC	AC	DC	AC
Total generation	410	410	418.02	410	415.66	410	416.15
Total demand	410	410	410	410	410	410	410
Total losses	-	-	8.02	-	5.66	-	6.15
Generator 1	125	50	45.97	0	0	0	0
Generator 2	285	285	285	257	252.91	250	246.95
Generator 3	0	0	2.05	71	81.8	75	85.04
Generator 4	0	75	85	82	80.95	85	84.16
Total cost per hour \$/h	2647.5	2832.5	2933.4	3355.2	3472.2	3400.2	3513.8

Table 4.6.: Dispatch of generation of the various models. The AC solutions are less expensive as they can effectively reduce the load by setting a low bus voltage at the load buses.

## 5. Risk Based Optimal Power Flow (RBOPF)

This chapter introduces the concepts of risk and security as they are used in this work. The general idea of the risk-based approach to optimal power flow is described and the differences to the SCOPF are highlighted. The formulation of the proposed model is followed by a detailed discussion. Finally, some problems with risk-based OPFs are pointed out.

### 5.1. Concept of Risk and Security

“Risk” plays a vital part in this thesis and especially in this chapter. As this term is rather vague and somewhat intangible, some brief comments about risk are given in the following section.

Since it is used and applied in many fields, such as finance, economics or IT security, risk has many definitions, each one being slightly different but ultimately leading to the same principle. The *Stanford Encyclopedia of Philosophy* defines risk rather fundamental as “an unwanted event that may or may not occur”, whereas the *IEEE Standard Dictionary Of Electrical And Electronics Terms* takes a more mathematical approach and specifies risk simply as the “product of probability and consequence”. If an event is unwanted, it is safe to assume that the consequence of the event is as well, and hence implying some sort of loss. In other words risk can be considered as a collective of uncertain and unwanted events, which, in their consequence, result in a loss.

In power systems an unwanted event is the malfunction of a component with the possible consequence of a disruption of normal operation of parts of the network or of the entire network. Under normal conditions demand and generation are in balance observing line flow, voltage and other limits. A disruption means that one of those limits is violated and/or the balance is disturbed. For a network operator

mostly those consequences that directly affect a consumer are important. Most customers won't notice a situation where the voltage or the frequency deviates from their nominal levels, as long as within reasonable limits. But they will be highly affected if the situation results in their disconnection from the power network. This suggests that the relevant 'loss' in power systems is represented by the disconnection of customers and hence by the loss of load. There is also a financial risk for operators to consider, but this study concentrates on the risk of the disconnection of customers. Taking all of these considerations into account, risk in power systems can be seen as an expectation of the cost of the consequential load loss, covering both impact and likelihood of that loss.

Both the SCOPF and the RBOPF claim to offer solutions for operating points that make a power system "secure". However, as both are mathematical optimization models, the term "security" needs to be used with caution. Actual security of a power system implies that the system is in a state of continuous safe operation. Unsafe situations are prevented altogether or at least the severity of their consequences is reduced. The models can only provide an approximation of this actual security. They are based on an assumption on how to interpret security. The SCOPF makes the assumption that a system can be considered secure if all line flows are below 100% of their capacity, under normal operating conditions as well as in contingencies. The RBOPF approach will change this assumption and state a different interpretation of security as will be seen in the course of this chapter.

It needs to be clarified that whenever "secure" is being mentioned, it always must be put in the context of the underlying model and hence of its corresponding assumption of security. The real, physical implementation of the provided solutions may not be secure at all, even though it satisfies all of the criteria of the model's understanding of security.

## 5.2. Description of RBOPF

McCalley [12] transferred the idea of risk to optimization problems in power systems by introducing the risk-based OPF (RBOPF). It should be pointed out that whenever the RBOPF method is mentioned in this chapter, it directly refers to the original version introduced by McCalley. For the analysis in the next chapter however, the original version will be varied and RBOPF will in general refer to the modification

unless stated differently. According to McCalley, “dynamic security limits based on the most severe contingency and scenario often result in operating restrictions corresponding to low or no risk but very high costs.” [16]. Moreover, there are several other drawbacks to the SCOPF approach as introduced in the previous chapter, such as:

- The N-1 secure SCOPF does not take into account any contingencies that involve more than one component failing, even though it might be more important to take into consideration.
- For a greater number of contingencies, the operating cost will increase and the problem can even become infeasible.
- The contingency constraints are hard constraints.
- A state where all lines operate at full load (100% line flow) is considered “secure”, which is certainly not true for most cases.
- The most severe events are usually the least probable.

These problems can be avoided by introducing the concept of risk. In the following, it is explained how this is achieved giving a greater understanding of the differences of the RBOPF to the SCOPF.

As introduced in Chapter 4 there are two types of SCOPF. If a very secure solution is desired, the preventive SCOPF can be used. However, this security comes with high operating costs. To run the system at lower operating costs the corrective SCOPF can be used, which naturally provides a less secure solution. The proposed RBOPF tries to combine the advantages of both the preventive and the corrective SCOPF and provides a low cost operating point at a relatively high level of security. According to Li et al. [12] this is enabled by shifting towards the corrective solution for contingencies with a relatively small risk and getting closer to the preventive solution if the risk is relatively large. The risk is thereby defined as product of probability and severity (Equation 5.1, taken from Xiao et al. [22]), which means that the RBOPF approach requires contingency probabilities as well as a measure of the severity of the impact of future events.

$$Risk = Probability \times Severity \tag{5.1}$$

Unlike the SCOPF where the resulting operating state provides the least costs that ensure maintaining all contingency constraints, the RBOPF attempts not just to find any solution but the least risky one. In fact, it seeks for a trade-off between the lowest generation cost and the lowest risk. To get a better understanding of this difference, it is necessary to conceive how the optimal solutions of the individual approaches are obtained.

First of all it should be clarified that “solution” here means the computed operating state of the system for the base case satisfying all underlying constraints. The computed operating state includes values for the voltage levels, phase angles and dispatch of generation. As introduced in Chapter 4, base case (base state) refers to the state of the system when all components are working normally and no contingency is active. If one or more contingencies occur, and a component, such as a line, fails it is referred to as a contingency case. It is essential to understand that a different system state in the base state results in a whole different behaviour in case of a contingency. This concept is demonstrated in the following example.

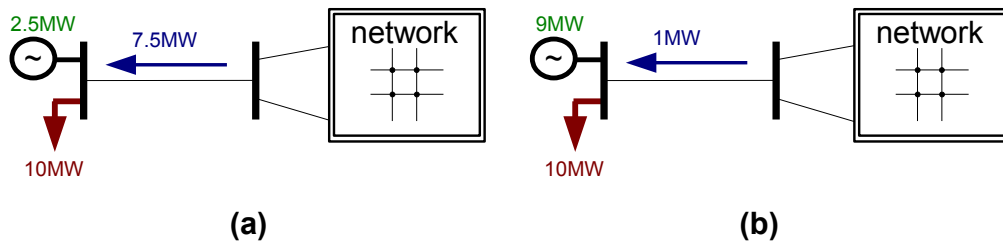


Figure 5.1.: This example demonstrates how the generation dispatch influences the security of the system. A line contingency in case (a) is more severe than in case (b).

A bus that has a 10 MW load and a generator connected to it is linked to the rest of the network by one line only. The generator is considered to be very costly but capable of supplying the load on its own. In case 1 (Figure 5.1 (a)) the generator only runs at 2.5 MW while in case 2 (Figure 5.1 (b)) it is 9 MW. It is obvious that in case 1 the impact of a possible line contingency is much greater than in case 2. In case 1 the generator would have to increase its output by 400% putting the system into a state of severe stress, if not even causing a collapse, whereas in case 2 this increase would be much smaller and could be captured more easily. Generally speaking, the line flow levels are changed by shifting the dispatch of generation. Although this situation cannot be considered to be very realistic, it demonstrates well how the base case solution can have an influence on the system’s security. The different ways

how the SCOPF and the RBOPF obtain their optimal solutions is explained in the following.

The SCOPF produces an operating state that ensures a feasible load flow for every contingency considered satisfying all hard limits for bus voltages, line flows, etc. in the base case as well as in all the contingency cases. However, there is no measure as to how good these contingency operating states are and there is no influence to change them. The SCOPF approach does not at all differentiate between the contingencies that have a severe impact on the system and those that do not. The only objective of the SCOPF is to minimize the cost subject to ensuring feasible solutions for all contingency events. In other words, the SCOPF only guarantees that there exists a feasible solution for the contingency cases but does not take into account possible differences in the quality of that solution in respect of the system's security.

Actually, the SCOPF is a “worst-case” approach. Since it does not have a measure of probability it expects that at least one contingency will happen for definite. Usually the most severe events are the least likely. The SCOPF must account for these events at all cost, even if economically the security benefit is completely disproportionate to that cost. There is another aspect to the “worst-case” character of the SCOPF. Since only the cost is included in the objective function, there will always be one constraint at its limit. Otherwise the corresponding variable could be relaxed more in order to reduce the cost further. This aspect can be seen in Figure 5.2, which

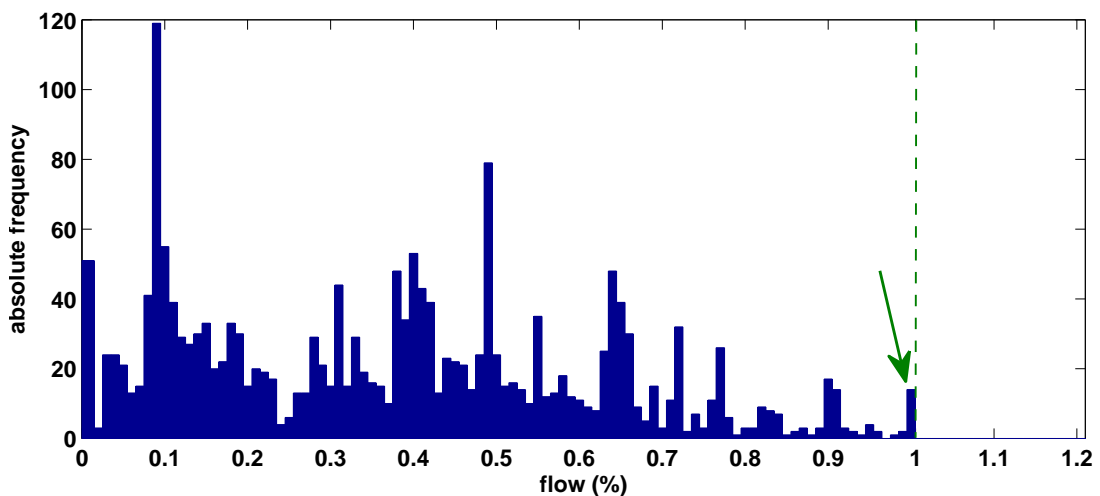


Figure 5.2.: The contingency histogram for the SCOPF solution. The dashed line indicates the 100% mark. The green arrow highlights 14 contingency flows at 100%.

shows a histogram of the contingency line flows. In the figure there is a peak of 14 at 100% flow. This proves that there are 14 flows within the 46 contingencies that feature a line flow of 100%.

The RBOPF on the other hand tries to optimize precisely this quality by manipulating the solutions of the contingency cases in order to make them, and hence the overall system, more secure and less exposed to failure. It takes into account the severity of the contingencies as well as their probability. Thus the objective is not only to minimize the cost but also the system's exposure to failure, the risk. In order to achieve that, it removes some of the hard contingency constraints but introduces penalty terms instead. These penalty terms represent a severity index and added up give a measure of the risk. Every contingency case as well as the base case is assigned such a severity index, which is meant to give a measure of the stress the system is exposed to in this state. McCalley assumes that the severity index is directly related to the number of overloaded lines as well as the extent of that overload. The task of the optimization problem is to minimize the operating cost while, at the same time, find solutions to the contingency cases that feature a low risk. Severity indices are a measure of violations and can be based on voltage or overload violations, frequency deviations, system stability margin, etc. While McCalley considered overload and voltage violations for the severity index in the RBOPF approach, in this work only the overload is taken into account. More detail is given in the next section.

### 5.3. RBOPF Models

As mentioned in the previous section, the main characteristic of RBOPF is that the hard constraints are replaced by soft constraints featuring a penalty term. Thus, contingencies with unlimited line flows are allowed. However, every contingency has a special severity function assigned to it that defines the shape and rate of the penalty. Therefore it maps the line flow to a severity index. Figure 5.3 shows a severity function taken from McCalley [15].

In this severity function, every flow exceeding 90% of its maximum rating receives a severity index as a penalty. This is done for all line flows of the system for a given contingency  $c$ .

$$Sev_c^{con} = \sum_{l \in L} Sev_{l,c}^{line} \quad (5.2)$$

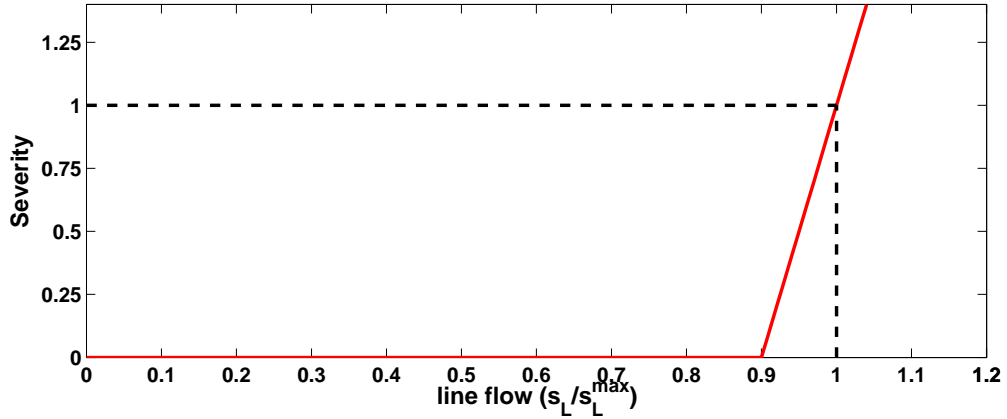


Figure 5.3.: The overload severity function as suggested by McCalley [15]. The area of non-zero severity, here starting at 90% line flow, is the so-called penalty area.

To evaluate the overall risk of the contingencies, the severities of the individual contingencies are accumulated, each one weighted by its corresponding probability  $Pr_c$ , which is a constant parameter of the model and can be derived from statistical data.

$$Risk = \sum_{c \in C} Pr_c \cdot Sev_c^{con} \quad (5.3)$$

Hence the risk represents a measure of the “mean consequence” of the operating point of a system. Yet, the most important impact on the system’s security has not been taken into consideration. The distribution of the flows in the base case greatly influences the subsequent contingency flows. For this major effect the base case needs to be part of the overall risk index, even though it is limited by hard constraints.

$$Risk = \sum_{c \in C} Pr_c \cdot Sev_c^{con} + \sum_{l \in L} Sev_l^{base} \quad (5.4)$$

It can be seen that the base case severity is not weighted while the contingency severities are weighted by their corresponding probability, which is usually very small. This emphasizes the importance of the base case flows. Any flow exceeding 90% contributes a term to the objective that will tend to reduce that flow. In order to influence the solution of the optimization problem, the risk term is included in the objective function.

Three different formulations that incorporate risk into OPF models are shown in Table 5.1.

	<i>Single Objective 1</i>	<i>Single Objective 2</i>	<i>Composite Objective</i>
<i>objective</i>	$\min GenCost$	$\min Risk$	$\min GenCost + \omega_R Risk$
<i>subject to</i>	$\mathbf{g}^{base}(\mathbf{x}) = \mathbf{0}$ $\mathbf{h}^{base}(\mathbf{x}) \leq \mathbf{0}$ $\mathbf{g}_c^{con}(\mathbf{x}_c) = \mathbf{0}$ $\mathbf{h}_c^{con}(\mathbf{x}_c) \leq \mathbf{0}$ $\mathbf{r}_c(\mathbf{x}_c) = \mathbf{0}$ $0 \leq Risk \leq R_{max}$	$\mathbf{g}^{base}(\mathbf{x}) = \mathbf{0}$ $\mathbf{h}^{base}(\mathbf{x}) \leq \mathbf{0}$ $\mathbf{g}_c^{con}(\mathbf{x}_c) = \mathbf{0}$ $\mathbf{h}_c^{con}(\mathbf{x}_c) \leq \mathbf{0}$ $\mathbf{r}_c(\mathbf{x}_c) = \mathbf{0}$ $0 \leq GenCost \leq GC_{max}$	$\mathbf{g}^{base}(\mathbf{x}) = \mathbf{0}$ $\mathbf{h}^{base}(\mathbf{x}) \leq \mathbf{0}$ $\mathbf{g}_c^{con}(\mathbf{x}_c) = \mathbf{0}$ $\mathbf{h}_c^{con}(\mathbf{x}_c) \leq \mathbf{0}$ $\mathbf{r}_c(\mathbf{x}_c) = \mathbf{0}$

Table 5.1.: Three ways to formulate the RBOPF. The first and the third approach are taken from Fu [8]. The second method is a modification of the first, swapping the function of *GenCost* and *Risk*. For this work the composite model was chosen.

As introduced in Chapter 4, *GenCost* represents the cost of generation.  $\mathbf{g}^{base}(\mathbf{x})$  and  $\mathbf{g}_c^{con}(\mathbf{x})$  are the equality equations for the base case and for the case of contingency  $c$ , respectively and  $\mathbf{h}^{base}(\mathbf{x})$  and  $\mathbf{h}_c^{con}(\mathbf{x})$  represent the limits on voltage levels, line flows and generation limits.  $\mathbf{r}_c(\mathbf{x}_c)$  denoted the risk constraints as in Equations (5.27) – (5.31).

The first approach (Single Objective 1) is the only method that does not put the risk into the objective function but adds an additional hard constraint that limits the level of total risk. Instead of the total risk, it is also possible to introduce multiple risk constraints for every individual contingency. This method is similar to the SCOPF and does not necessarily find the smallest risk. Yet, it ensures that the total risk does not exceed the defined limits. A guess of the value of the hard limit  $R_{max}$  has to be specified by the user.

The second approach (Single Objective 2) is very similar to the first. The risk measure is put in the objective function while the generation cost is subject to a hard limit in the constraints,  $GC_{max}$ . Again, it is also possible to introduce multiple generation cost constraints for every individual contingency. The smallest operation cost is not necessarily found but kept below the defined limits.

The third, composite objective approach puts the risk into the objective of the minimization problem weight by a factor  $\omega_R$ . Hence it effectively minimizes the risk trying to find the optimal balance of risk and generation cost. By changing the weighing constant  $\omega_R$  it can be specified which of the two objectives is granted

priority. Thus the focus can be laid more on security or more on economy. A model based on this method is used in this study. The full proposed formulation can be seen below.

$$\begin{aligned} \min \quad & GenCost + \omega_R \cdot Risk + \\ & \eta \cdot ShedCost + \xi \cdot GenCon \end{aligned} \quad (5.5)$$

subject to

— Base case constraints —

$$GenCost = \sum_{g \in G} c_g^{(0)} + c_g^{(1)} p_g^G + c_g^{(2)} p_g^{G^2} \quad (5.6)$$

$$\mathbf{g}^{KCL,base}(\mathbf{x}) = \mathbf{0} \quad \forall b \in B \quad (5.7)$$

$$\mathbf{g}^{KVL,base}(\mathbf{x}) = \mathbf{0} \quad \forall b \in B \quad (5.8)$$

$$p_d^D = P_d^D \cdot (\alpha + \beta v_b + \gamma v_b^2) \quad \forall d \in D \quad (5.9)$$

$$q_d^D = Q_d^D \cdot (\alpha + \beta v_b + \gamma v_b^2) \quad \forall d \in D \quad (5.10)$$

$$P_{g-}^G \leq p_g^G \leq P_{g+}^G \quad \forall g \in G \quad (5.11)$$

$$Q_{g-}^G \leq q_g^G \leq Q_{g+}^G \quad \forall g \in G \quad (5.12)$$

$$s_l^{L^2} = p_l^{L^2} + q_l^{L^2} \quad \forall l \in L \quad (5.13)$$

$$s_l^L \leq S_l^L \quad \forall l \in L \quad (5.14)$$

$$V_{b-} \leq v_b \leq V_{b+} \quad \forall b \in B \quad (5.15)$$

$$\delta_0 = 0 \quad (5.16)$$

— Contingency constraints —

$$\mathbf{g}^{KCL,con}_c(\mathbf{x}_c) = \mathbf{0} \quad \forall b \in B \quad (5.17)$$

$$\mathbf{g}^{KVL,con}_c(\mathbf{x}_c) = \mathbf{0} \quad \forall b \in B \quad (5.18)$$

$$p_{d,c}^D = (P_d^D - p_{d,c}^{LS}) \cdot (\alpha + \beta v_{b,c} + \gamma v_{b,c}^2) \quad \forall d \in D \quad (5.19)$$

$$q_{d,c}^D = (Q_d^D - q_{d,c}^{LS}) \cdot (\alpha + \beta v_{b,c} + \gamma v_{b,c}^2) \quad \forall d \in D \quad (5.20)$$

$$P_{g-}^G - p_{g,c}^{gencon} \leq p_{g,c}^G \leq P_{g+}^G \quad \forall g \in G \quad (5.21)$$

$$Q_{g-}^G - q_{g,c}^{gencon} \leq q_{g,c}^G \leq Q_{g+}^G \quad \forall g \in G \quad (5.22)$$

$$GenCon = \sum_{g \in G} \sum_{c \in C} p_{g,c}^{gencon} + q_{g,c}^{gencon} \quad (5.23)$$

$$V_{b,c-} \leq v_{b,c} \leq V_{b,c+} \quad \forall b \in B \quad (5.24)$$

$$\delta_{0,c} = 0 \quad (5.25)$$

$$-\rho p_g^G \leq p_{g,c}^G - p_g^G \leq \rho p_g^G \quad \forall g \in G \quad (5.26)$$

— Risk constraints —

$$Risk = \sum_{c \in C} Pr_c \cdot Sev_c^{con} + \sum_{l \in L} Sev_l^{base} \quad (5.27)$$

$$Sev_c^{con} = \sum_{l \in L} Sev_{l,c}^{line} \quad \forall c \in C \quad (5.28)$$

$$s_{l,c}^{L^2} = p_{l,c}^{L^2} + q_{l,c}^{L^2} \quad \forall l \in L \quad (5.29)$$

$$Sev_{l,c}^{line} = Z_{c,l}^1 \cdot \frac{s_{l,c}^L}{S_l^{L,max}} - Z_{c,l}^0 \quad \begin{cases} \forall c \in C \\ \forall l \in L \end{cases} \quad (5.30)$$

$$Sev_l^{base} = Z_l^{1,base} \frac{s_l^L}{S_l^{L,max}} - Z_l^{0,base} \quad \forall l \in L \quad (5.31)$$

— Load shedding constraints —

$$ShedCost = \sum_{c \in C} Pr_c \cdot ShedCost_c^{con} \quad (5.32)$$

$$ShedCost_c^{con} = \sum_{d \in D} LSC_d \cdot p_{d,c}^{LS} \quad \forall c \in C \quad (5.33)$$

$$P_d^D \cdot q_{d,c}^{LS} = Q_d^D \cdot p_{d,c}^{LS} \quad \begin{cases} \forall c \in C \\ d \in D \end{cases} \quad (5.34)$$

This formulation features a composite objective function (5.5) incorporating the generation cost, the risk, the load shedding and an auxiliary term 'GenCon', which will be explained below.

The base case constraints consist of the generation cost definition (5.6) as introduced in chapter 4 as well as the real and reactive power demand (5.9)–(5.10), generator, line and voltage limits (5.11)–(5.15) and reference bus angle definition (5.16). The demand is implemented as a ZIP model to provide the possibility of modelling a voltage dependent load. The parameters  $\alpha$ ,  $\beta$  and  $\gamma$  must add up to 1 but otherwise can be chosen as desired. In order to make the model clearer, the power flow Equations (5.7) and (5.8) are not displayed in the model but can be seen in their full form in (4.12) and (4.13) in section 4.3.

Equations (5.17)–(5.26) show the contingency constraints. Equation (5.26) gives the link between the generated real power of the base and the contingency cases. (5.19) and (5.20) are the real and reactive power demand in contingencies allowing

the possibility to shed some of the load by  $p^{LS}$  or  $q^{LS}$ , respectively. (5.21) and (5.22) model the generation limits. In generator contingencies or when a line contingency isolates a generator this generator has to be shut down and consequently has zero generation. In order to prevent feasibility problems in these situations the two variables  $p^{gencon}$  and  $q^{gencon}$  have been implemented, which allow zero generation. However, the sum of these variables (Equation (5.23)) is part of the objective. Hence, by setting the weight  $\xi$  to a very high value it can be assured that the limit will only be violated in the above situation. As in the base case, Equations (5.17) and (5.18) represent the power flow Equations as introduced in (4.25)–(4.26).

Finally, the risk constraints, as described in section 5.2, are given by Equations (5.27)–(5.31) and the load shedding constraints by Equations (5.32)–(5.34). Every load has a cost factor  $LSC_d$ , which gives the possibility to value the individual loads. The disconnection of a hospital is certainly more expensive than a company with a special contract. Due to lack of data  $LSC_d$  was uniformly set to 500 for all loads. Multiplied by the amount of shed real power  $p_{d,c}^{LS}$ , this gives the cost of the actually disconnected load in one contingency. The sum over all loads of an individual contingency results in the cost of disconnected load,  $ShedCost_c^{con}$  (Equation (5.33)). Finally, the cost of the total load shedding is obtained by summing up the costs of the individual contingencies, weighted by their corresponding probabilities, as shown in Equation (5.32). There are separate variables for the shedding of real and reactive load,  $p^{LS}$  and  $q^{LS}$ . Equation (5.34) ensures that the percentage of load shed is the same for the real and the reactive case. If the solution computes non-zero load shed for a contingency, the simulation is set to instantaneously shed the load after that contingency happened.

## 5.4. Discussion and Comparison to SCOPF

In order to evaluate the different approaches, an AMPL model has been implemented using an interior point solver (ipopt). The MATLAB routine *xSolveOpt* was written to coordinate this. It incorporates all different model types and so allows quickly computing and comparing solutions of different models. As input it requires a set of contingencies, e.g. line contingencies, and the model type ('EDC', 'OPF\_DC', 'OPF\_AC', 'SCOPF\_DC', 'SCOPF\_AC', 'RBOPF\_DC', 'RBOPF\_AC'). By using this and the MATPOWER data file of the network the script creates the *DAT*, *MOD* (corresponding to the model type) and *RUN* file and runs AMPL. The solution file

created by AMPL is read and the data is saved in an output structure along with the settings of the problem, such as runtime, limit values, etc.

For the following calculations the 39-bus New England network was used as a basis. The detail of this network can be taken from Figure 6.1 as well as Appendix A. The set of contingencies consisted of the 46 lines. Due to lack of data, the probabilities of the individual contingencies were assumed equal and arbitrarily chosen to 0.005. The severity function was taken from McCalley [15]. It is the same as shown in Figure 5.3. The cost parameters of Equation (5.6) were adapted from Tessema [21]. In both cases, load shedding was allowed.

Using the *xSolveOpt* routine, solutions to the AC models of the SCOPF and the RBOPF were computed. Figure 5.4 demonstrates illustrative the core difference of the SCOPF and the RBOPF as it was described earlier in this chapter. It shows a histogram of the contingency line flows of the SCOPF (a) and RBOPF (b), respectively. It can be seen that the SCOPF forces all its contingency line flows below 100%. The RBOPF on the other side does not have this hard limit and so allows one of the flows to go wide over the top at 150%. However, as much as it is possible it tries to push the flows out of the penalty area, i.e. the area with non-zero severity, which in this example starts at 90% (left of the red dashed line). If there are different probabilities for the contingencies, the flows of the least likely contingency are more easily allowed to have flows within the penalty area than a contingency with a high probability.

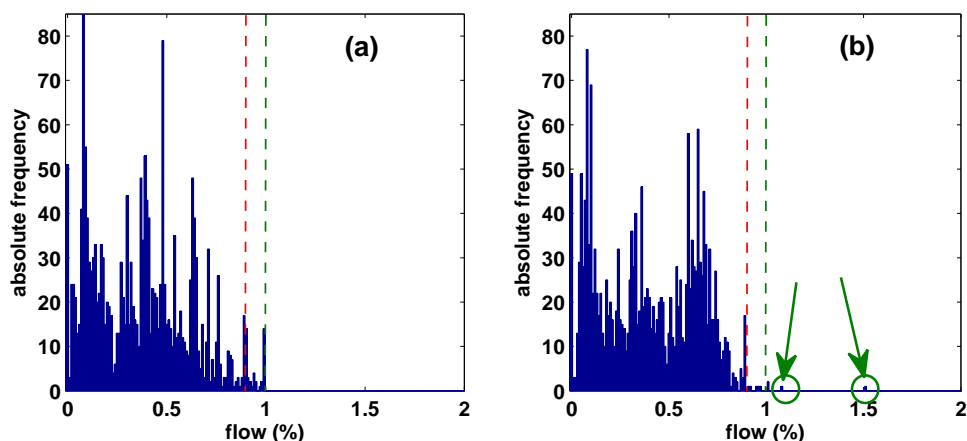


Figure 5.4.: On the left the contingency histogram for the SCOPF, on the right for the RBOPF. The SCOPF strictly does not allow any flows above 100% but has more contingency flows in the penalty area (90%–100%). The RBOPF has one flow at 134% but actively pushes flows below the penalty area.

Another feature of RBOPF is demonstrated in the following example. Figure 5.5 shows the histogram of the line flows for two different probability parameters. The given set of contingencies includes a 'troublesome' line contingency, which leads to a high overflow in one of the lines (namely in contingency #35 there is an overflow in line 38). In the Figure 5.5 (a) the probability of that contingency is set to the value of 0.0001, making this contingency very unlikely compared to the rest of the set (for the rest of the contingencies the probability is set to 0.005). Consequently, the solution of the corresponding problem allows a very high overflow of 170% for line 38 in contingency #35, marked with a green arrow in the left histogram. For the histogram in Figure 5.5 (b) the probability of the "troublesome" contingency #35 is set to the value of 0.01. This makes it very likely compared to the other contingencies and gives it a higher priority in the RBOPF. As a result the RBOPF finds a solution that lowers the flow of line 38 (again marked with a green arrow in the histogram) to about 140%. However, to balance this effect, other contingencies have to be granted higher flows corresponding to a shift to the right in the histogram. Examining Figure 5.5 (b), it can clearly be seen that a significant number of contingency flows are shifted right, towards and beyond the 90% mark (indicated by a dashed red line), while the green arrow is pushed towards the left. Thus, the example shows the functionality of the RBOPF to influence the contingency flows based on their probability.

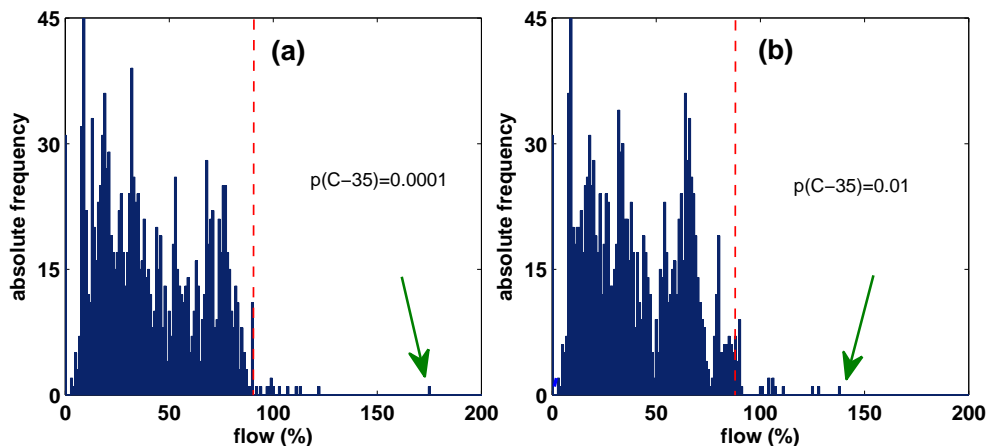


Figure 5.5.: The RBOPF accounts for different probabilities of the contingencies. On the left all contingencies are equally probable, with one contingency flow exceeding 170%. On the right the probability of that flow has been increased such that it is pushed below 140%.

To conclude this section, some final remarks on feasibility computation time and the use of load shedding should be noted.

*Remark 1:* Although not used in this work, the RBOPF method can be developed to the point where there are no limitations to the feasibility other than computational difficulty in considering a large set of contingencies. Especially the SCOPF suffers a lot from feasibility issues, which can only be solved by relaxing the model's hard constraints or allowing more load shed. The RBOPF on the other hand can introduce additional penalties similar to the line flow penalty. This is done by gradually replacing the hard limits, e.g. for voltage, and introducing severity functions instead. These severity functions capture the expected cost of further failures that may be caused by the constraint violations. Finally all the severities are included in the objective as an overall risk measure.

*Remark 2:* There is a big difference in the computation time of the two approaches. The computation of RBOPF solution needed 12 times as long to finish than the SCOPF solution. This is a considerable difference, especially when taking into account that the underlying system with 39 buses is rather small and the gap could widen for larger systems.

*Remark 3:* The RBOPF provides the best results only when implemented with load shedding. Unlike the SCOPF, the RBOPF considers the probabilities of individual contingencies and can apply more load shedding specifically in unlikely cases. This is a great advantage if there are any "troublesome", i.e. severe contingencies with small probabilities. As a result the system can be operated at much lower cost but at the same time offer a valid solution for these special cases. The SCOPF cannot favour any of the contingencies in this way and has to find a more costly solution.

## 5.5. Problems with RBOPF

According to Equation (5.1) risk is the product of probability and severity. While the severity is a function of the line flow, the probabilities of the various contingencies are constant and have to be chosen arbitrarily in case there is no data available. It can be assumed that the probability is a function of the line flow as well. Lines close to their capacity limits are certainly more likely to fail than lines that are barely loaded.

However, this point is only of secondary importance to the RBOPF method. Examining Equation 5.4 shows that the severity functions of the contingencies are weighted by their probabilities while the base case is unweighted. Since the probabilities

are in the range of 0.005, the base case takes a very high priority compared to the contingency cases. Therefore, the optimization problem will usually try to prevent any line flows in the penalty area for the base case. This leads to the conclusion that the probabilities would mostly depend on environmental influences, such as lightning strikes, and only marginally on the line flow.

Another drawback of the RBOPF method is that there is no proof of the validity of its measure of risk. Although there is a general and approved definition of risk (see section 5.1), there is no universal concept of how to get the severity index. The basic approach is comprehensible but there is no evidence yet that a solution that is computed to be less risky by the RBOPF, in fact is more secure than one with a higher computed risk. The RBOPF approach supposes that line flows in the penalty area imply a higher severity and consequently it tries to keep the line flows below a certain level. Due to the lack of hard constraints however, very high flows of more than 100% are possible. Even though this is only allowed for contingencies with a very small probability, there is a chance for it happening. By its own assumptions this circumstance makes the unlikely contingencies worse compared to a model solution with hard constraints. This leaves the question if a solution can actually be considered better if parts of it are made worse. After all the RBOPF method provides a trade-off between risk and cost.

Finally, the whole approach is based on the assumption that risk depends purely on the violation of contingency constraints.

## 6. Results

### 6.1. New England 39-bus Network

In the interest of analysing and verifying the different approaches, a suitable test system had to be chosen. As mentioned in Section 3.1, there was a great variety of different network cases available for this project. As the quality of the results depends very much on the accuracy of the model of the system, high order models for the generators as well as controlling devices were desired. These requirements fitted the 39-bus New England network, which features dynamic models of TG's and AVR's. For the sake of clearness and to reduce computation time, the 39-bus network was chosen as primary model.

The origin of the 39-bus network data is revealed in the header of the corresponding MATPOWER file, which can be seen in the appendix A.1. The full data can be found in Tables A.2–A.5 containing all the modifications and additions that have been made.

Figure 6.1, taken from Chakrabarti et al. [4], depicts the network topology of the New England System. It features 39 buses interconnected by 46 transmission lines. Tap changing transformers are installed at 11 of the lines. The total demand of the system is 6254 MW and is divided into 21 loads of various sizes throughout the network. The loads are supplied by 10 synchronous generators, 9 of which are of order 5 and one of order 4. The maximum capacitance of all generators is 8404 MW. Each generator is equipped with a turbine governor as well as an automatic voltage regulator. As the original data set included equal cost parameters for each generator, the parameters were taken from [21]. A complete description of the network data is given in the Appendix at A.

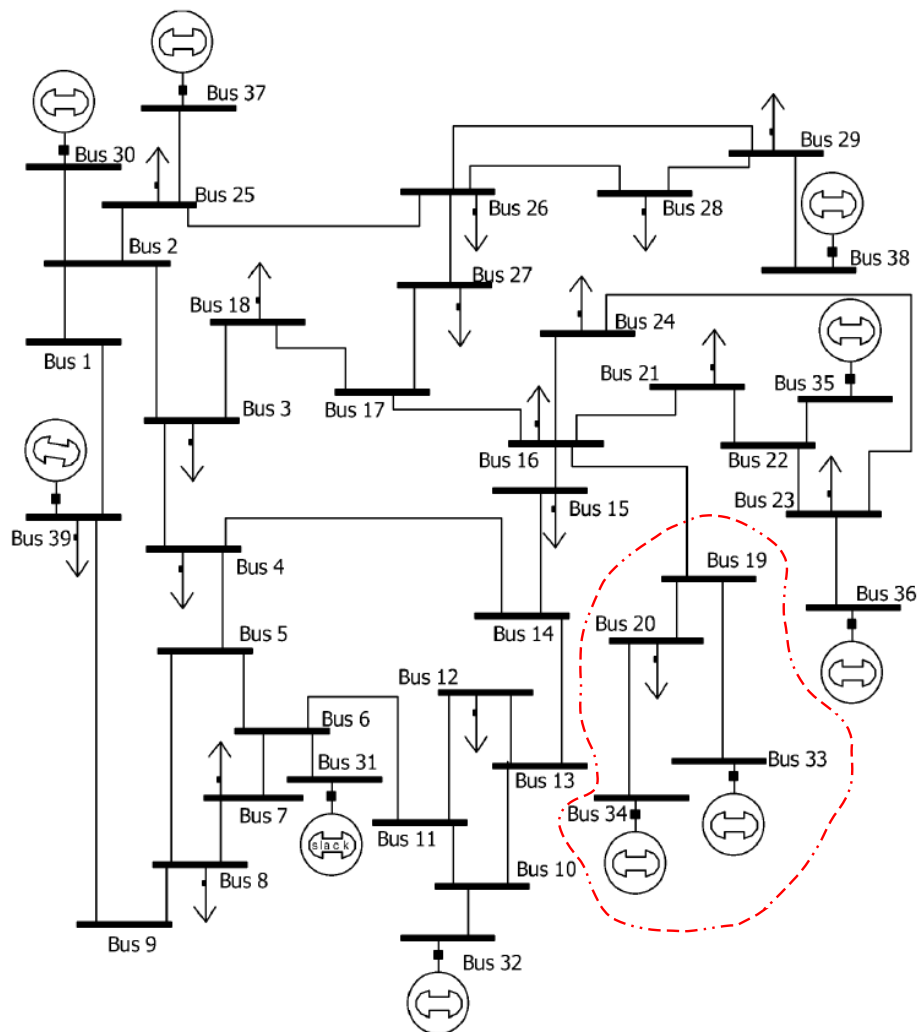


Figure 6.1.: The 39-bus network topology. The 21 loads are shown as arrows, the 10 generators as circles. Buses 19, 20, 33 and 34 form a semi-island (marked by a red line) being connected to the rest of the network by one line only.

The bus voltage limits are  $V_{b-} = 0.94$  p.u. and  $V_{b+} = 1.06$  p.u. for non-generator buses and  $V_{b-} = 0.98$  p.u. and  $V_{b+} = 1.04$  p.u. for generator buses in the base case. In a contingency case these limits are relaxed to  $V_{b-} = 0.90$  p.u. and  $V_{b+} = 1.10$  p.u. for non-generator buses and  $V_{b-} = 0.94$  p.u. and  $V_{b+} = 1.06$  p.u. for generator buses.

It should be noted that the four buses 19, 20, 33 and 34 have a prominent status within the system as they form a near-island being connected to the rest of the network only by the line 27. On this semi-island there is one large load accounting for about 11% of the total demand but also two generators that, depending on the operating state, make up for 18% of the total supply. Therefore, power is

usually exported to the rest of the system. If line 27 fails it has a severe impact on the system's stability as there is a large plus of power in the 4-bus island but a considerable lack of power in the rest of the system. Due to these circumstances, line 27 is likely to overload in many other contingencies and thus crucial to the network's security.

## 6.2. Solving the Optimization Problems

In order to solve the various optimization problems that were introduced in Chapter 4 and 5 the routine *xSolveOpt* was written. Based on a network model and a set of contingencies this script creates the necessary DAT-, MOD- and RUN-file for AMPL. Several database functions have been written, which store all the different variables (*xPdata*), constraints (*xModConstraint*) or objective functions (*xModCost*) that are needed for the various models. If a model – e.g. AC RBOPF – is specified, *xSolveOpt* calls those database functions and automatically chooses the right variables and constraints for this model. Parameter settings, such as the value of  $\omega_R$  can be defined in the function *xInitGset*.

The stated 39-bus network has been solved for all the different optimization models. The load model was set to 30% PQ and 70% impedance. Contingency load shedding was allowed and put in the objective with a weight  $\eta$  as in Section 5.3. The result is shown in Table 6.1. The set of contingencies had to be reduced because of feasibility

		OPF	SCOPF	RBOPF1	RBOPF2
Contingencies		–	Lines 1–26, 28–36, 40–46		
$\eta$		–	1	1	1
$\omega_R$		–	–	5000	1000
<i>Demand</i>	[MW]	6063	6088	6081	6077
<i>Generation</i>	[MW]	6121	6138	6132	6128
<i>Losses</i>	[MW]	58	49	50	51
Total load shed in contingencies	[MW]	–	7.27	2.92	2.77
<i>ShedCost</i>	[1/hr]	–	727.2	292.0	277.1
<i>Risk</i>	[1/hr]	–	–	0.0657	0.1167
<i>Generation Cost</i>	[\$/hr]	92991	94060	93206	93105

Table 6.1.: Comparison of different optimization solutions. Despite providing the most expensive solution the SCOPF uses the most load shed in contingencies.

issues of the SCOPF. *Demand*, *Generation* and *Losses* refer to the base case of the solution. Naturally the OPF provides the lowest cost. The RBOPF with the lower  $\omega_R$  has the second cheapest solution as the objective is biased more towards minimizing the generation cost than towards the risk. Although the SCOPF has the most expensive solution it uses the most load shed in the contingency cases.

Table 6.2 shows the actual risk (see Section 6.3) of the various approaches. The OPF solution is surprisingly safe. However, this can be considered a coincidence. The original RBOPF solution features the safest operating point, being significantly cheaper than the SCOPF solution.

	OPF	SCOPF	RBOPF1
$\Delta t$	1 hr	1 hr	1 hr
reaction time	15 min	15 min	15 min
GenCost	92991	94060	93206
tree risk	25.86	34.42	19.23

Table 6.2.: Comparison of the actual risk of the OPF, SCOPF and RBOPF. See Section 6.3 for information about the meaning of the risk measure.

As stated earlier, the RBOPF tries to find the optimal balance between the risk and the generation cost. The priority of these two quantities is controlled by the weighting factor  $\omega_R$ . In order to analyse the influence of this weighting factor, the routine *xSweepOmegaR* has been constructed. In a sweep over  $\omega_R$  the optimization problem is repeatedly solved and the generation cost as well as the risk is plotted in a diagram.

To determine the range of possible  $\omega_R$  values, the dimension of the two quantities, generation cost and risk, has to be considered. The generation cost is a result of the function *GenCost* (4.1). In the considered 39 bus network the capacity of the largest plant is of order  $10^3$  MW. Taking into account that the cost parameters are of order 10 for  $p^G$  and  $< 0.01$  for  $p^{G^2}$ , this means that in this constellation the maximum cost that one plant can contribute is of order  $10^4$ . Hence, all 10 plants added together give a total of order  $10^5$ . The risk on the other hand is a sum of products of probabilities and severities. As mentioned before the probabilities were arbitrarily set to 0.005. The majority of the lines can be considered to have a line flow below 90% and hence severity 0. A few lines might be in the 90-100% area (severity greater than 0 but less than 1) and even fewer above that (severity greater than 1). Overall the severity of a single contingency can be considered to be of order 1, so that the total risk will be no greater than of order  $10^{-1}$  ( 50 lines times 0.005 times 1). Hence, the maximum

values for  $GenCost$  and  $risk$  were derived to  $10^4$  and  $10^{-1}$ , respectively. This leads to the conclusion that  $\omega_R$  has to be chosen less than  $10^6$ , because the majority of the above values represents an upper limit. Based on this calculation the range was deliberately chosen large from  $10^1$  to  $10^6$ . The results can be seen in Figure 6.2.

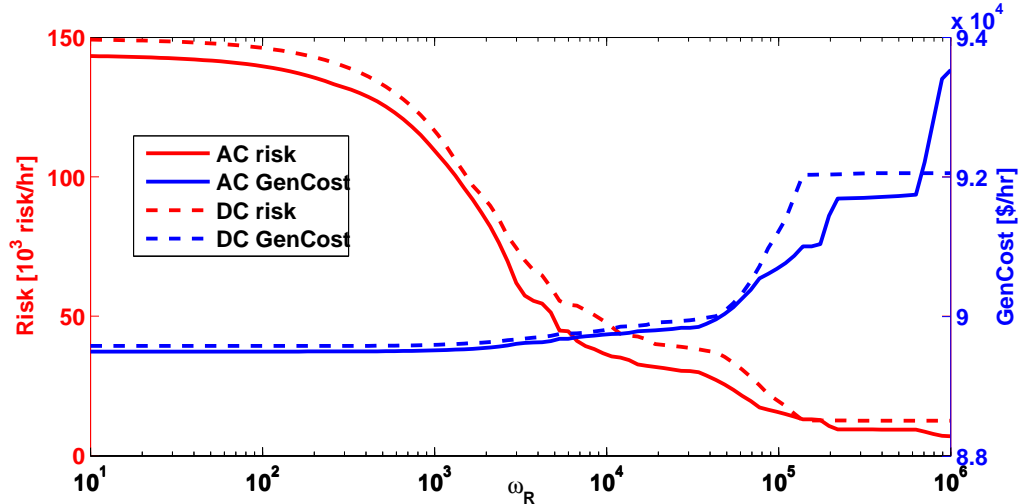


Figure 6.2.: Sweep over  $\omega_R$  with risk as red line and the generation cost as blue line (DC solution dashed, respectively).

The solid lines indicate the AC solutions, the dashed lines the corresponding DC solutions. The line of the DC generation cost (blue dashed) was shifted by an offset of 6000 in order to show the similarity of the AC and the DC graphs. Since there are no line losses in the DC case, the generation level is naturally smaller as the corresponding AC case. However, the loads in the AC case are dependent on the bus voltage  $v_b$ , such that there is less demand if the voltages are below 1 p.u.

As an interesting result it can be noted that for most parts the AC and DC graphs show an almost identical characteristic. Since the DC computations are a great deal faster compared to the AC computations (DC – 10mins, AC – 120mins) this is an important insight. It seems strange that the risk measure drops about 90% of its maximum value while the generation cost only rises about 5%. This can be explained by the fact that the risk measure based on the original severity functions is arbitrary and its absolute value has no meaning. Also, the generation cost is measured per hour and therefore a very costly quantity so that an increase of 5% can be considered high. Despite these inaccuracies, an initial guess for the optimal  $\omega_R$  can be assumed to be in between  $10^4$  and  $10^5$ . It should be noted that due to the arbitrariness of the risk measure the optimal point is not necessarily the intersection of the two graphs but can be estimated by their shape.

## 6.3. The Actual Measure of Risk

The severity functions are intended to capture the severity of the consequence of an individual contingency and should provide information about the expected impact on the system. The main problem of McCalley's measure of risk is that those severity functions are arbitrarily defined. The underlying concept however is true. A real measure of risk, as defined in Section 5.1, in fact does exist. McCalley's approach using the severity functions is one attempt of modelling this real risk. Yet, only the correct severity functions will result in a good approximation. Provided the data are correct the actual risk of a system can be derived and the true severity functions can be extracted. These functions are unique to the network and depend on the topology, the generation levels, the load settings, the protection scheme, etc.

The generation cost is usually defined as \$ per unit time, e.g. [\$/hr]. In order to achieve trade-off between risk and generation cost, the product  $\omega_R \cdot Risk$  has to match this unit. The weighing factor  $\omega_R$  specifies how important the risk is compared with the generating costs. Therefore,  $\omega_R$  must define the cost of one unit of risk and is given in [\$/risk]. Hence, *Risk* is measured in unit risk per unit time, e.g. [risk/hr].

This definition is backed up by the fact that in power systems contingency events are not triggered. For comparison, in the classic urn problem, the event 'drawing a ball' is a forced action. If the *risk of drawing a blue ball* is considered, no measure of time needs to be taken into account. In power systems however there is no such forced action, but the question of whether or not a contingency is going to happen over a certain interval of time, e.g. the *risk of a line failing within the next hour*, is considered.

### 6.3.1. Consequence Trees

Having clarified that the true measure of risk exists and what it looks like, the next question is how it can be obtained. There seems to be only one solution to this problem: realise the contingencies and observe the consequences. As this cannot be done on a real system, the consequences need to be simulated. The more exact the model of the considered system, the better is the produced approximation of the actual risk. The components of the network as well as the operation schemes have to be adapted as precisely as possible to get an exact system model. The extended

PSAT simulator is used for this task. A “consequence tree” is developed, which visualizes the progress of the system after contingencies. The risk deduced from the “consequence tree” is denoted as “tree-risk”. An example is shown in Figure 6.3.

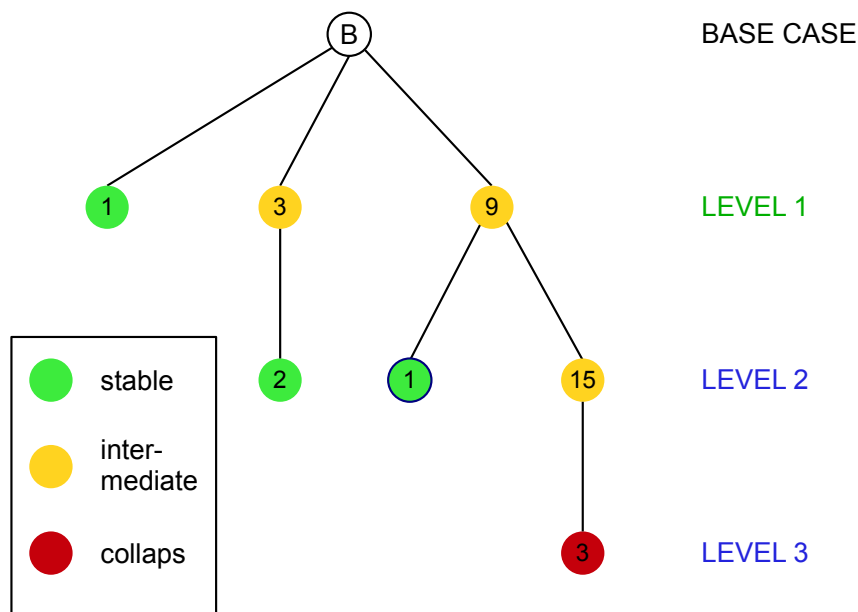


Figure 6.3.: Example of a consequence tree. The white top node represents the base case, the other nodes contingency cases. The system is in a stable state for a green node, in an intermediate state for an amber node and collapsed for a red node.

The consequence trees are created by the routine *xtree*. From the base case state, shown as white node at the top level, pre-defined contingencies are consequently simulated. After a contingency has happened the system reaches a new state, displayed by a node at level 1. The line connecting various nodes symbolizes the time-domain simulation that was carried out to go from one state to the next. Generally time moves on when going down the tree.

The consequence trees assume that after a contingency the system can generally be in three different states:

- **Stable** (green)

The system is in a stable state if the simulation of the contingency did not end in a singularity and all line flows are below a defined limit.

- **intermediate** (amber)

The system reaches an intermediate state if the simulation is completed but there are highly loaded or even overloaded lines that are likely to be tripped by the protection devices.

- **collapse** (red)

If the simulation did end in a singularity the system is supposed to have collapsed.

In Figure 6.3 each state is represented by a coloured disc containing a label. The white node at the top, labelled 'B', represents the base case of the system. The labels of the other nodes stand for the corresponding line contingency that led to this state. For example, line1 was tripped to reach the state of the node labelled '1' at level 1. If the system reaches an intermediate state, all lines that exceed a defined limit are stored in a new set. These lines are tripped, starting from the corresponding amber operating point. This procedure is repeated until the system reaches either a stable point or collapses. A blue ring means that the system is split at least into two separate islands in this state.

Figure 6.4 depicts the flowchart of the routine. The tree is developed vertically. It forms different levels, the top level, level 0, being the base case only. Level 1 consists of the forced line trips and from level 2 onwards the lines have been tripped automatically as a result of their high load.

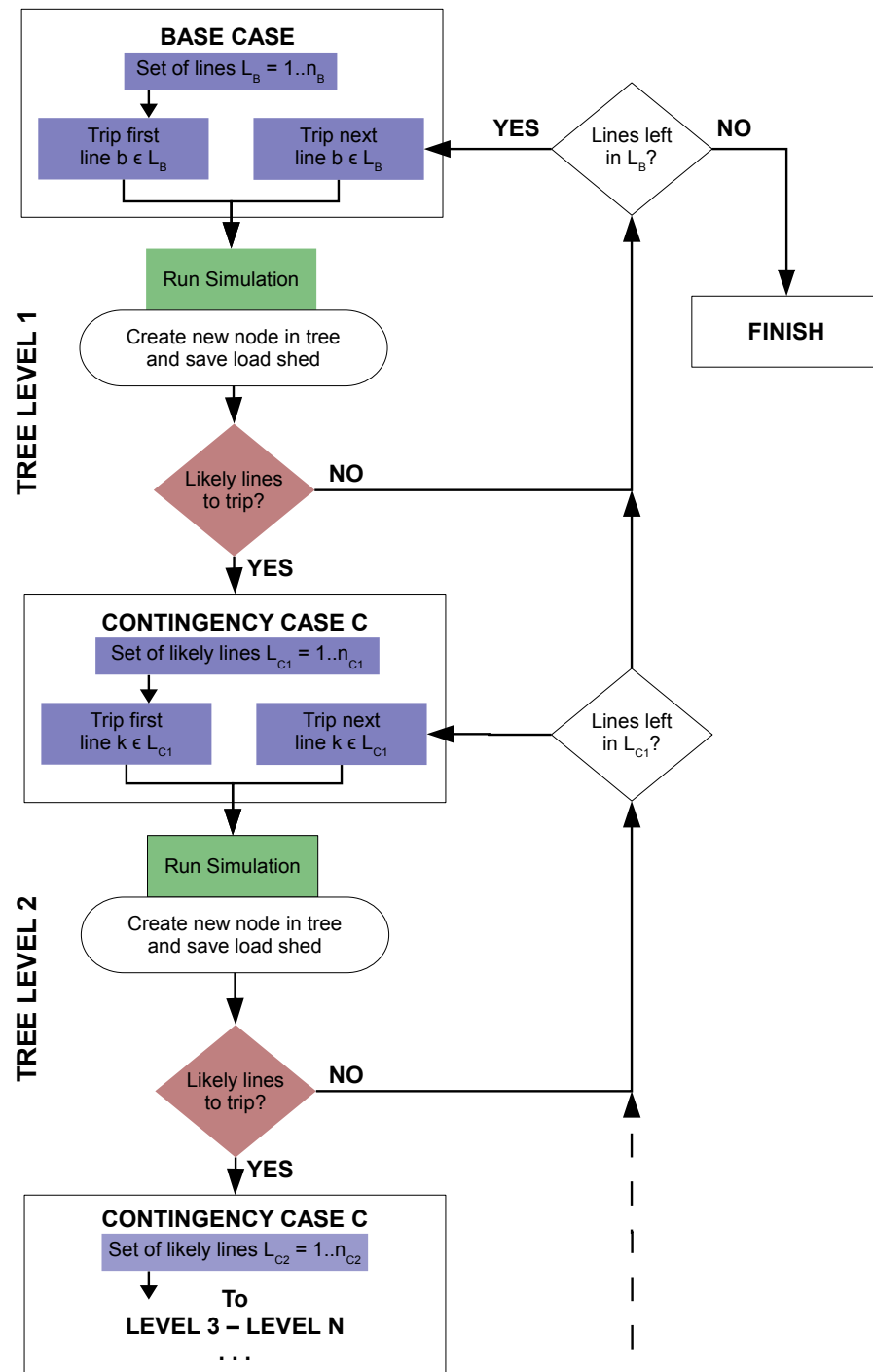


Figure 6.4.: Flow chart of the routine *xtree*, which creates the consequence trees.

### 6.3.2. Risk Computation

For each state a probability measure and a severity index is computed. Their derivation is explained in the following.

As stated in Section 5.1, it is not the voltage or frequency level, as long as within

reasonable limits, that is important to customers but the issue of whether or not they are disconnected from the network. Thus, the interesting quantity of regret in a power system is the loss of load. Therefore, a reasonable assumption is to define the severity index as the amount of lost load in a state. For the consequence trees the load loss is calculated as the accumulated amount of load that was shed during the simulations, given in percent. In Figure 6.8 the severity is shown below every node. In case of a collapse, the load shed and therefore the severity is 100%.

The probability index is more complex to derive. As explained at the beginning of this section, risk is measured per unit time. Since the severity is defined as a percentage the time dependency has to come from the probability measure. Calculating the probability of a component functioning during an interval of time is an issue of reliability theory. It is assumed that each line  $k$  has a failure rate  $\lambda_k$  assigned to it. Modelling the failure rate as an exponential distribution, the probability of line  $k$  failing in a time slot of  $\Delta t$  is given by

$$p(\lambda_k, \Delta t) = 1 - e^{-\lambda_k \Delta t} \quad (6.1)$$

The failure rate  $\lambda_k$  is itself a function of the line flow. There is no data available for this but it can be assumed that the failure rate is very small for flows well below 100%, increasing for high flows and eventually becoming asymptotic for overloads. Figure 6.5 shows an example of how this dependency could look. If an ideal protection device is installed that trips the line at a defined flow, e.g. 105%, the graph would

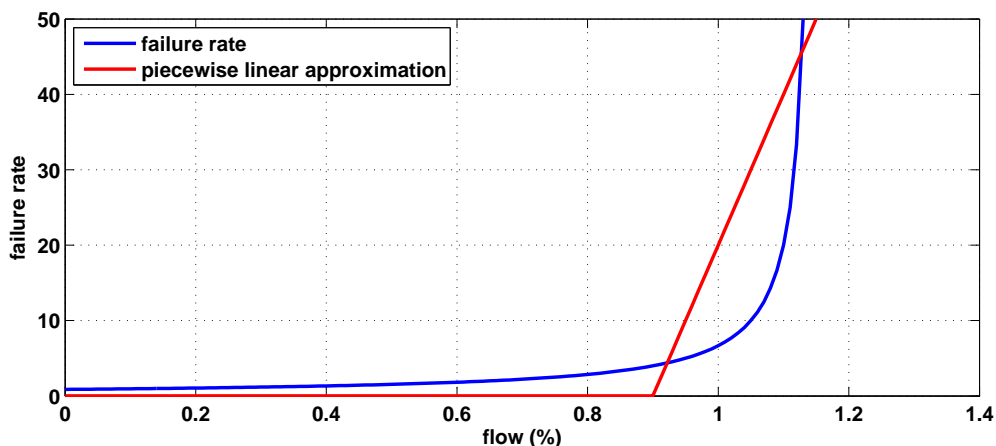


Figure 6.5.: Hypothetic flow to failure rate dependency. The rate is supposed to be very low for low line flows, rising around 100% flow and increasing asymptotically towards higher line flows.

step up to infinity at this line flow. However, every device is slightly different and none is perfect so that uncertainties such as errors in line current measurement will smooth the curve.

As the true shape of this graph is unknown, it can be approximated by a piecewise linear function (red line in Figure 6.5). If the approximation is substituted into Equation 6.1 a graph similar to the following shape is obtained.

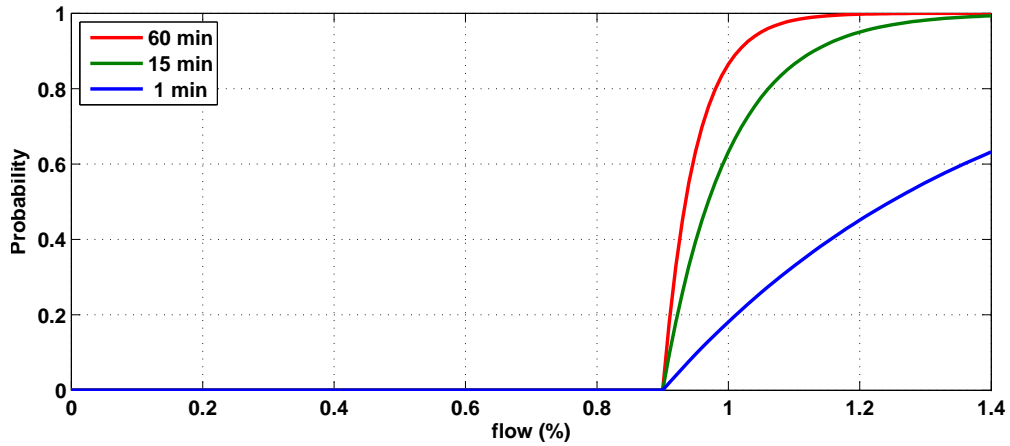


Figure 6.6.: Flow to probability dependency based on a linear approximation of the failure rate. This graph is for visualisation only and does not correspond to actual values.

Figure 6.6 shows the dependency of the probability measure from the line flow. The different graphs in the figure mark different examined time slots  $\Delta t$ . It can be seen how the probability of a line of equal flow gets smaller the smaller the considered time slot. The value of the failure rate of low line flows can be approximated using statistical data, such as the *mean time between failures* (MTBF) or *failure in time* (FIT) data. Additional information about these failure measures can be found in Krasich [10]. In Figure 6.8 the probability is shown on top of each node.

With these definitions for the severity and the probability of the states in the consequence tree the tree-risk can be calculated. The probabilities of level 1 of the tree depend on the considered time interval  $\Delta t$ . All the following events of the tree have a *fixed time interval*. The reason for this is that it is assumed that after a fixed time the system operator has chance to interact and improve the system state, e.g. by manually shedding more load, changing generation levels, or activating back-up generators. The fixed time in which the system is left on its own is set to 15 minutes for this work. This arrangement is visualised in Figure 6.7.

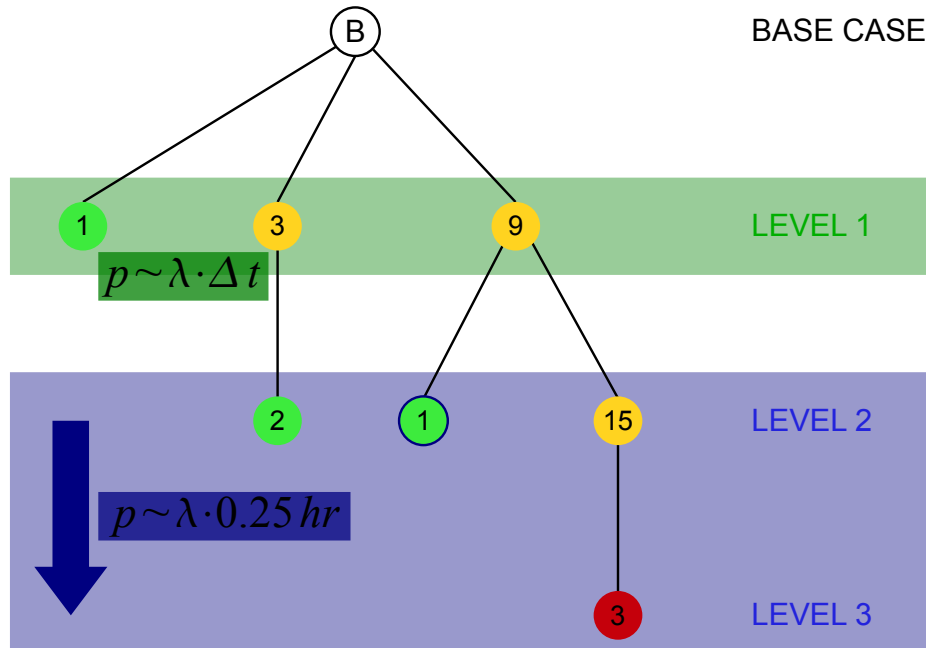


Figure 6.7.: Visualisation of the risk computation. The probabilities of the first level are based on the time slot  $\Delta t$ , the probabilities of the subsequent levels are based on a 15 minutes reaction time. The severity is computed as the accumulated amount of load shed.

For each end point of a “failure path” in the tree, its probability is multiplied by the severity, i.e. the accumulated amount of load shed. The probability of an end point is the product of the branch probabilities that led to that end point. The sum over all end points gives the tree-risk, which provides a good approximation of the true risk of the system.

If the risk of an individual contingency is required only those endpoints associated with this contingency are summed up. The result is a measure of the expected consequences of that one contingency. Figure 6.8 illustrates this computation.

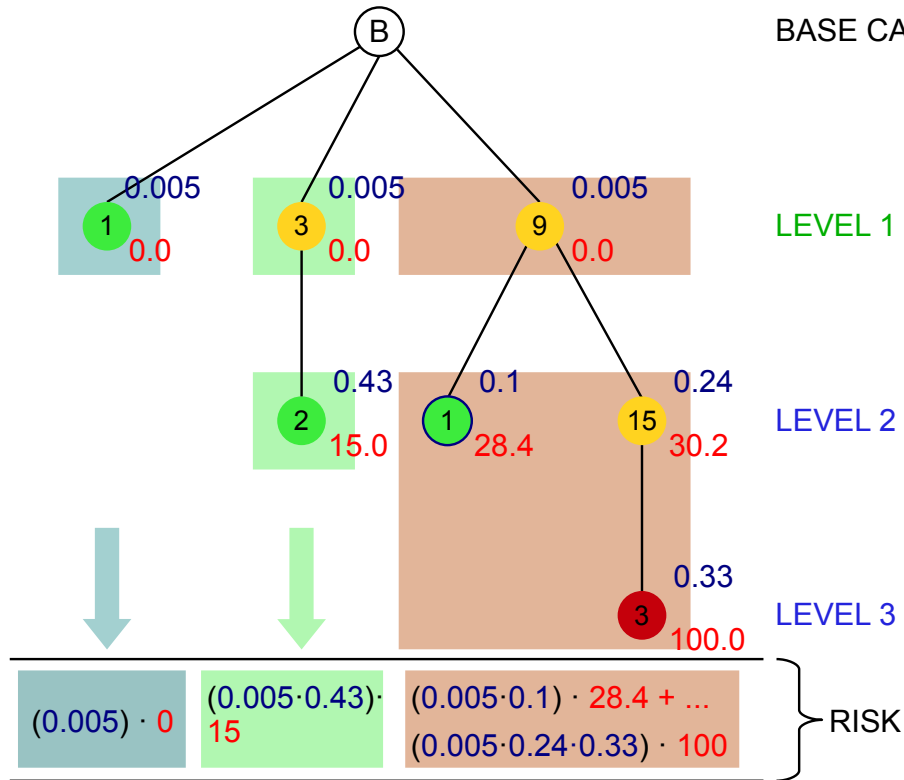


Figure 6.8.: Visualisation of the risk computation of an individual contingency. Each contingency has a ‘region of attraction’, which consists of the endpoints of that branch from that contingency.

## 6.4. Calibration of the Severity Functions

### 6.4.1. Concept

There is an obvious difference between the risk measure of McCalley and the tree-risk derived from the consequence trees. McCalley’s risk is based on the assumption that a network is in a less risky state if there are as little contingency flows in the penalty area as possible. His severity is based on the line flow. The method proposed in the last section on the other hand obtains a clear measure of the severity of a contingency by actually simulating its consequences. The tree-probability is based on the assumption that the failure rate increases with the flow.

However, these two approaches of computing the risk need to be this different as they are constructed for two distinct purposes.

- The **RBOPF risk** is greatly simplified in order to include the risk evaluation in the optimization problem. It is not possible to compute the whole tree in every step of the solving process of the already very complex optimization problem.
- The **tree-risk** is deliberately complex to derive, in order to capture the actual risk as precisely as possible. The quality of the tree-risk is defined by the accuracy of the simulation and the information provided about the operation procedures of the system.

Although these are two very different approaches to capture one and the same matter, it is possible to bring them together. Despite some uncertainty about the probabilities the tree-risk is a very good approximation of the real risk. The RBOPF – as well as the SCOPF – does not have any information about the involved dynamics but assumes that the system states jump discretely from one state to another. Clearly this is far from reality and leads to contradictions to the simulation results as well as a misjudgement of the severity of the contingencies. In order to compensate this blindness, attempts have been made to adjust the severity functions of the RBOPF. This “calibration” cannot be done in general. Instead it is a unique process for each individual network.

The simulation computes the load shed according to the physical principles of the involved components. The RBOPF severity functions on the other hand do not need to represent any underlying physical behaviour and therefore can be arbitrarily shaped so as to best approximate the real risk. This freedom enables the RBOPF to adapt the results of the tree-risk. If the severity functions of *all* variables (line flow, generation, voltages, etc.) were known it would be possible to capture the actual risk with this model. The derivation of all these relationships requires tremendous effort but brings tremendous reward. It would be possible to exactly predict the consequences of any contingency. Obviously, in practice it is not possible to know all the severity functions. The fewer is known about the functions, the greater the approximation obtained and the more uncertain is the prediction of the consequences.

### 6.4.2. Example

The idea of the calibration is illustrated using the first five line contingencies of the 39-bus network. In the beginning the RBOPF features the original severity functions. The severity functions are consequently altered to better predict the simulated consequences. The loads of the system are modelled as 30% constant PQ and 70% impedance. The optimization problem is formulated as in Section 5.3.

The under-frequency load shedding scheme was adapted from Machowski et al. [13]. For low voltage a reasonable threshold was set.

<i>Under-frequency</i>	
$f < 49.0$ Hz	10% of total load shed (global) <sup>1</sup>
$f < 48.7$ Hz	25% of total load shed (global)
$f < 48.4$ Hz	45% of total load shed (global)
$f < 47.5$ Hz	system shutdown
<i>Under-voltage</i>	
$v_B < 0.8$ p.u.	15% of load shed locally at the corresponding bus

Table 6.3.: The load shedding scheme adapted from Machowski et al. [13].

For this test the following settings have been chosen.

System	39-bus network
Set of contingencies	1,...,5
$\rho$	0.05
$\xi$	$5 \cdot 10^3$
Load model	30% PQ , 70% Z
$\eta$	1
$LoadShedCost_d$	500
$\omega_R$	$5 \cdot 10^3$
$Pr_c$	0.005

Table 6.4.: Parameters of the RBOPF model as used in the calibration.

Based on this data the RBOPF is solved for the original severity functions as depicted in Figure 6.9. A consequence tree is calculated on the basis of this solution and the risk of the five contingencies is calculated for both cases.

<sup>1</sup>If the network is islanded, global refers to the whole island but not the whole system.

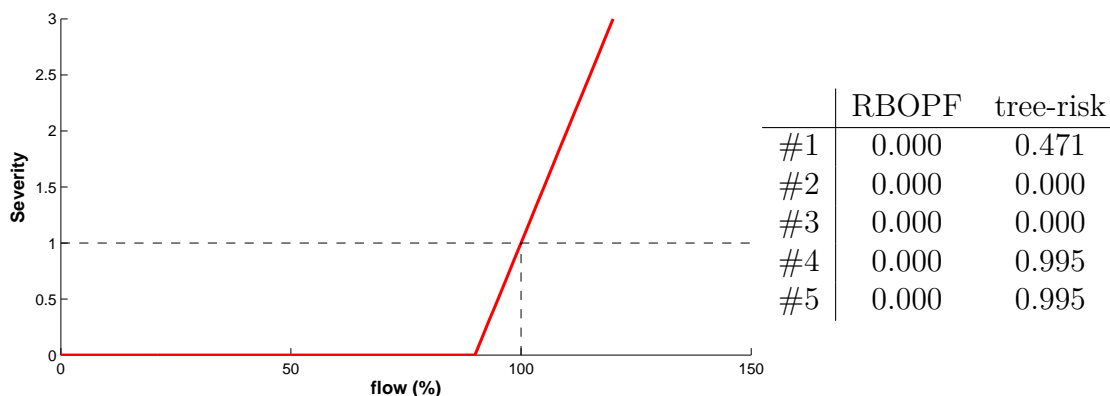


Figure 6.9.: The first step of the calibration. All contingencies have the same severity function, which is the original proposed by McCalley.

It is obvious that the RBOPF does not at all capture the severity of the contingencies. Although the RBOPF predicts that there is no risk attached to any of the contingencies, the system is actually put into a severe state for the contingencies #1, #4 and #5. To account for that, the severity functions of these contingencies are adjusted by shifting the functions to the left. The updated severity functions are depicted in Figure 6.10, together with the new solution of the RBOPF and the corresponding tree-risk.

It can be seen that the results changed but the RBOPF risk still does not match the tree-risk. Therefore the calibration process is repeated in a loop according to Figure 6.11. The idea is to gradually shift the severity functions until the ranking of the contingencies match in both approaches. Match of the ranking means that the most risky contingency in the tree is also listed as the most risky contingency

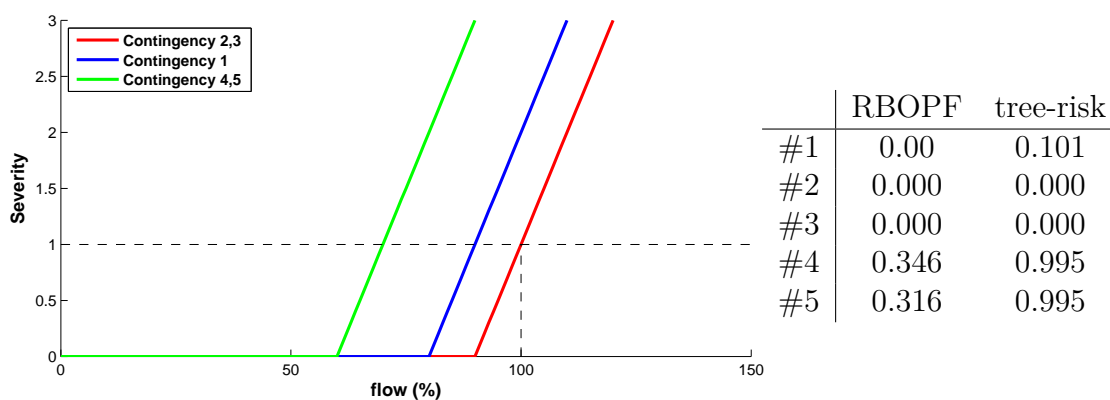


Figure 6.10.: The second step of the calibration process. The severity functions of the contingencies 1, 4 and 5 have been shifted to the left in order to account for their actual risk.

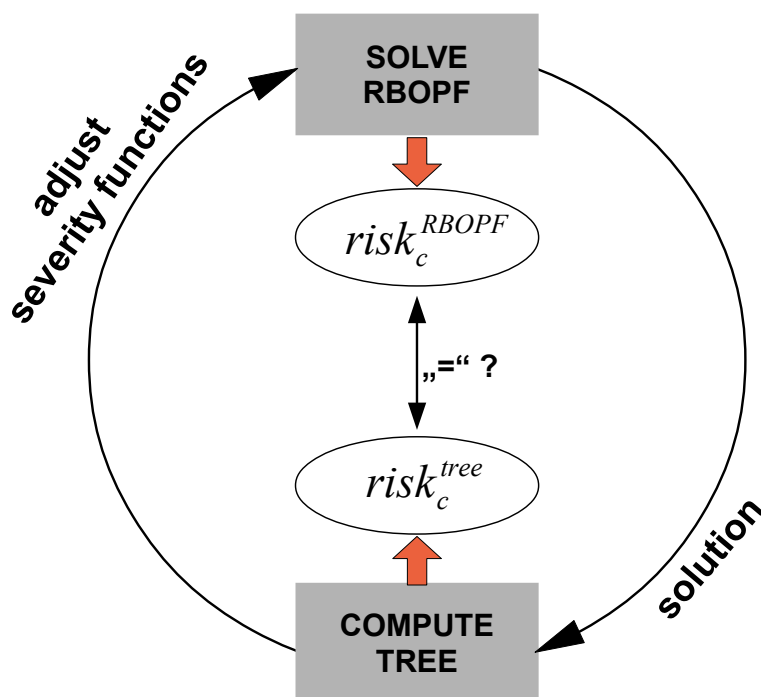


Figure 6.11.: The loop structure of the calibration process. The procedure starts at the top with solving the RBOPF with the original severity functions. A consequence tree is calculated based on this solution and the results are compared. If they do not match the severity functions are adjusted and the RBOPF is solved again. This is repeated until the risk measures are within the desired threshold.

in the RBOPF solution, the second most risky contingency is the same in the tree and in the RBOPF solution, etc. If this can be achieved the severity functions can be adjusted further, e.g. by changing the slope or by using different functions for different lines in one and the same contingency. This way, the severity functions can be adjusted until ultimately the relative differences of the contingencies match. In the above example the correct ranking could be achieved according to Figure 6.12.

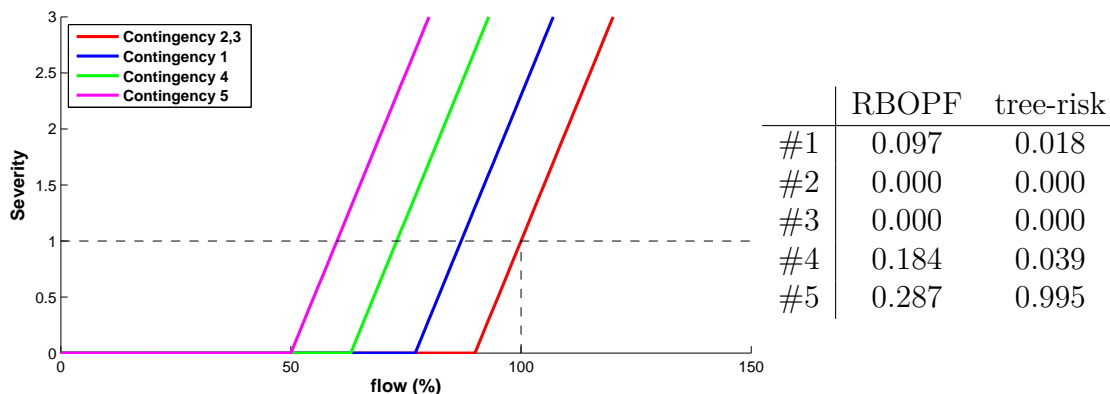


Figure 6.12.: With these severity functions the ranking of the contingency risks of the RBOPF could be matched with the tree-risks. The relative distances of the various contingencies are not adjusted.

The SCOPF, the uncalibrated RBOPF and the RBOPF calibrated according to Figure 6.12 are compared. The results can be seen in Table 6.5 and 6.6.

	SCOPF	RBOPF not calibrated	RBOPF calibrated
Contingencies	1–5	1–5	1–5
$\Delta t$	1 hr	1 hr	1 hr
reaction time	15 min	15 min	15 min
opt. risk	–	0	0.0567
GenCost	92,991	92,992	93,151
tree risk	2.5481	2.4615	1.0519

Table 6.5.: Comparison of the solutions for contingencies #1 – #5. The extra security that the calibrated RBOPF offers has to be paid by higher costs.

As the calibrated RBOPF is able to estimate the actual risk better, it can find a solution that is safer compared to the other two. However, this comes at additional cost. Table 6.6 reveals that the calibrated RBOPF matches the actual risk best.

Contingency	SCOPF	uncalibrated RBOPF		calibrated RBOPF	
	tree risk	opt. risk	tree risk	opt. risk	tree risk
#1	0.558	0	0.4714	0.0962	0.0183
#2	0	0	0	0	0
#3	0	0	0	0	0
#4	0.995	0	0.995	0.1837	0.0386
#5	0.995	0	0.995	0.2871	0.995

Table 6.6.: Comparing the tree-risk with the risk of the solution of the optimization problem. The calibrated RBOPF provides the best match.

## 7. Summary

A new approach of optimal power flow formulations was analysed and extended in this work, the risk-based OPF (RBOPF). This approach differs from other methods in that the likelihood as well as the severity of contingencies is taken into consideration. Thus, the RBOPF does not account for every imaginable event at all costs but tries to achieve a trade-off between the risk that a contingency holds and the contribution to the generation cost that is caused by considering this contingency. In the original version of the RBOPF this advantage of incorporating a risk measure is its main problem. There is no concept stated that describes how to derive the risk of a contingency such that its true regret is reflected in the optimization model. Also, there is no information about the price of that risk so that it can be balanced with the generation cost. Therefore, this study developed a procedure to address this issue connecting a full AC RBOPF formulation with the actual consequences of its computed operating state.

Key to this procedure is an exact simulation of the system's behaviour in order to be able to precisely detect the impact of a contingency. Therefore the open-source Matlab toolbox PSAT was used as a basis and upgraded with appropriate extensions. Beginning with very basic models various optimization problems were introduced. An established model that includes post-contingency situations was given by the security-constrained OPF (SCOPF). Following, the original RBOPF formulation was introduced, explained and discussed in detail.

The SCOPF and RBOPF try to make a network robust to contingency events based on their assumption of system security. Although the original RBOPF wants to achieve this robustness by predicting the impact of the contingency events, it just changes the assumption of security. This method might work better for some systems but worse for others and there is no guarantee that it is an improvement in general. However, the structure of the RBOPF allows calibration of the model in order to reveal the actual significance of a contingency event. In order to capture this actual significance, "consequence trees" have been developed, which enable very accurate

risk calculation. Using these tree structures the RBOPF model could be calibrated for a small set of line contingencies so that the true risk of the system could be better approximated.

In reality there are more influences than mentioned in this work, but in theory they can all be included in the RBOPF. There is still a lot of work to be done to find the real dependencies of the severity functions. The calibration process, which is unique to each individual system, needs to be tested on different, larger networks. Since the calibration is very time consuming but has to be executed every time a parameter of the system is changed, a more efficient and standardized method is desirable.

The huge benefit of the method proposed in this work is its ability to predict the true consequences and severity of a contingency event. The quality of the estimation can be tuned as desired since it is dependent on the effort that is invested in the calibration. In coastal regions, for example, the probability of line outages can be considered higher due to weather conditions than urban districts where underground cables are well protected. In hot areas overload can be penalized more than in cold areas as the line sag has a greater severity. For long distance lines or for lines with phase shifters on the other hand the voltage stability is to be treated with more caution than overload. These are only three examples and many more can be found. With the calibrated RBOPF a system operator has the flexibility to shape the risk measure so that it captures exactly the individual influences that are important to the network. At the moment no other optimization model provides such good approximations of the true risk of an operating state while simultaneously minimizing the economic cost. This circumstance makes the RBOPF a very promising approach in operating power systems. Since every power system is different, this flexibility of not only choosing what the important influences are but also obtaining an estimation of the risk that is caused by those influences is the great advantage of the RBOPF and makes it universally applicable.

## Bibliography

- [1] Final report of the investigation committee on the 28 september 2003 blackout in italy. UCTE, Final Report, April 2004.
- [2] Final report system disturbance on 4 november 2006. UCTE, Final Report, 2007.
- [3] F. Capitanescu, M. Glavic, D.Ernst, and L.Wehenkel. Applications of security-constrained optimal power flow. In *In Proceedings of Modern Electric Power Systems Symposium*, 2006.
- [4] Saikat Chakrabarti and Elias Kyriakides. Optimal placement of phasor measurement units for power system observability. *IEEE TRANSACTIONS ON POWER SYSTEMS*, Vol 23, No 3:1433 – 1440, 2008.
- [5] Valentin Crastan. *Elektrische Energieversorgung 1*. Springer, 2000.
- [6] Chris Dent. Lecture: Operational research in the energy industry, 2011.
- [7] U.S.-Canada Power System Outage Task Force. Final report on the august 14, 2003 blackout in the united states and canada: Causes and recommendations. Final Report, April 2004. Online Available: <https://reports.energy.gov/>.
- [8] Weihui Fu and James D. McCalley. Risk based optimal power flow. In *IEEE Porto Power Tech Conference*, 2001.
- [9] Klaus Heuck, Klaus-Dieter Dettmann, and Detlef Schulz. *Elektrische Energieversorgung: Erzeugung, Übertragung und Verteilung elektrischer Energie für Studium und Praxis, 7th Edition*. Vieweg, 2007.
- [10] M. Krasich. How to estimate and use mttf/mtbf would the real mtbf please stand up? In *Reliability and Maintainability Symposium*, 2009.
- [11] S. Larsson and A. Danell. The black-out in southern sweden and eastern denmark, september 23, 2003. In *IEEE Power Systems Conference and Exposition*, 2006.

- [12] Yuan Li and James D. McCalley. Risk-based optimal power flow and system operation state. In *Power & Energy Society General Meeting, 2009. IEEE*, 2009.
- [13] Jan Machowski, Janusz W. Bialek, and James R. Bumby. *Power Systems Dynamics: Stability and Control, 2nd Editon*. Wiley, 2008.
- [14] Tobias Matern. Die dunkle seite der macht. Online: sueddeutsche.de, 02.08 2012.
- [15] J. McCalley, S. Asgarpour, L. Bertling, R. Billinion, H. Chao, J. Chen, J. Endrenyi, R. Fletcher, A. Ford, C. Grigg, G. Hamoud, D. Logan, A.P. Meliopoulos, M. Ni, N. Rau, L. Salvaderi, M. Schilling, Y. Schlumberger, A. Schneider, and C. Singh. Probabilistic security assessment for power system operations. In *Power Engineering Society General Meeting, 2004. IEEE*, 2004.
- [16] J.D. McCalley, A.A. Fouad, V. Vittal, A.A. Irizarry-Rivera, B.L. Agrawal, and R.G. Farmer. A risk-based security index for determining operating limits in stability-limited electric power systems. *Power Systems, IEEE Transactions on*, Vol 12, No 3:1210 – 1219, 1997.
- [17] F Milano. *Documentation for PSAT version 2.0.0*. University of Castilla – La Mancha, February 2008.
- [18] F Milano. Continuous newton’s method for power flow analysis. *IEEE Transactions on Power Systems*, Vol 24 No 1:50–57, 2009.
- [19] Hadi Saadat. *Power System Analysis, 2nd edition*. Mcgraw, 2004.
- [20] Adolf J. Schwab. *Elektroenergiesysteme: Erzeugung, Transport, Übertragung und Verteilung elektrischer Energie, 3rd Edition*. Springer, 2011.
- [21] Betelehem T. Tessema. Strategies for electrical network expansion. Master’s thesis, Delft University of technology; Faculty of Electrical Engineering, Mathematics and Computer Science, 2011.
- [22] Fei Xiao and James D. McCalley. Power system risk assessment and control in a multiobjective framework. *IEEE Transactions on Power Systems*, Vol 24, No 1:78–85, 2009.

## A. 39-bus Network Data

### A.1. MATPOWER File Header

---

Data taken from [A1] with the following modifications/additions:

- renumbered gen buses consecutively (as in [A2] and [A4])
- added  $P_{\min} = 0$  for all gens
- added  $Q_{\min}$ ,  $Q_{\max}$  for gens at 31 & 39 (copied from gen at 35)
- added  $V_g$  based on  $V$  in bus data (missing for bus 39)
- added  $V_g$ ,  $P_g$ ,  $P_d$ ,  $Q_d$  at bus 39 from [A2] (same in [A4])
- added  $P_{\max}$  at bus 39:  $P_{\max} = P_g + 100$
- added line flow limits and area data from [A4]
- added voltage limits,  $V_{\max} = 1.06$ ,  $V_{\min} = 0.94$
- added identical quadratic generator costs
- increased  $P_{\max}$  for gen at bus 34 from 308 to 508 (assumed typo in [A1], makes initial solved case feasible)
- re-solved power flow
- changed generator cost data
- changed line emergency rating by at least 15%

Notes:

- Bus 39, its generator and 2 connecting lines were added (by authors of [A1]) to represent the interconnection with the rest of the eastern interconnect, and did not include  $V_g$ ,  $P_g$ ,  $Q_g$ ,  $P_d$ ,  $Q_d$ ,  $P_{\min}$ ,  $P_{\max}$ ,  $Q_{\min}$  or  $Q_{\max}$ .
- As the swing bus, bus 31 did not include and  $Q$  limits.
- The voltages, etc in [A1] appear to be quite close to the power flow solution of the case before adding bus 39 with its generator and connecting branches, though the solution is not exact.
- Explicit voltage setpoints for gen buses are not given, so they are taken from the bus data, however this results in two binding  $Q$  limits at buses 34 & 37, so the corresponding voltages have probably deviated from their original setpoints.
- The generator locations and types are as follows: 1 30 hydro 2 31 nuke01 3 32 nuke02 4 33 fossil02 5 34 fossil01 6 35 nuke03 7 36 fossil04 8 37 nuke04 9 38 nuke05 10 39 interconnection to rest of US/Canada
- This is a solved power flow case, but it includes the following violations:
  - $P_{\max}$  violated at bus 31:  $P_g = 677.87$ ,  $P_{\max} = 646$
  - $Q_{\min}$  violated at bus 37:  $Q_g = -1.37$ ,  $Q_{\min} = 0$

## References:

- [A1] G. W. Bills, et.al., "On-Line Stability Analysis Study" RP90-1 Report for the Edison Electric Institute, October 12, 1970, pp. 1-20 - 1-35. prepared by E. M. Gulachenski - New England Electric System, J. M. Undrill - General Electric Co."generally representative of the New England 345 KV system, but is not an exact or complete model of any past, present or projected configuration of the actual New England 345 KV system.
- [A2] M. A. Pai, Energy Function Analysis for Power System Stability, Kluwer Academic Publishers, Boston, 1989. (references [3] as source of data)
- [A3] Athay, T.; Podmore, R.; Virmani, S., "A Practical Method for the Direct Analysis of Transient Stability," IEEE Transactions on Power Apparatus and Systems , vol.PAS-98, no.2, pp.573-584, March 1979. URL: <http://ieeexplore.ieee.org/stamp/stamp.jsp?arnumber=4113518&isnumber=4113486> (references [1] as source of data)
- [A4] Data included with TC Calculator at <http://www.pserc.cornell.edu/tcc/> for 39-bus system.

MATPOWER \$Id: case39.m,v 1.14 2010/03/10 18:08:13 ray Exp \$

The reference notation was changed in order to prevent confusion.

## A.2. Bus Data

bus #	base [kV]	pf voltage [p.u.]	pf angle [rad]	bus #	base [kV]	pf voltage [p.u.]	pf angle [rad]
1	345	1.039	-0.2363	21	345	1.032	-0.1331
2	345	1.048	-0.1708	22	345	1.05	-0.05556
3	345	1.031	-0.2143	23	345	1.045	-0.05901
4	345	1.004	-0.2204	24	345	1.038	-0.173
5	345	1.006	-0.1953	25	345	1.058	-0.1461
6	345	1.008	-0.1817	26	345	1.053	-0.1647
7	345	0.9984	-0.2226	27	345	1.038	-0.1983
8	345	0.9979	-0.2328	28	345	1.05	-0.1035
9	345	1.038	-0.2475	29	345	1.05	-0.05532
10	345	1.018	-0.1426	30	345	1.05	-0.1286
11	345	1.013	-0.156	31	345	0.982	0
12	345	1.001	-0.1571	32	345	0.9841	-0.003289
13	345	1.015	-0.1559	33	345	0.9972	-0.003372
14	345	1.012	-0.187	34	345	1.012	-0.02847
15	345	1.016	-0.198	35	345	1.049	0.03101
16	345	1.033	-0.1751	36	345	1.064	0.07799
17	345	1.034	-0.194	37	345	1.028	-0.02763
18	345	1.032	-0.2092	38	345	1.026	0.06794
19	345	1.05	-0.09442	39	345	1.03	-0.2537
20	345	0.991	-0.1191				

Table A.1.: New England network bus data. The columns 'pf voltage' and 'pf angle' represent the power flow solution.

## A.3. Generator Data

### General data

Gen #	Bus #	type	power [MVA]	voltage [kV]	freq [Hz]	$P_{max}^G$ [MW]	$P_{min}^G$ [MW]	$Q_{max}^G$ [MVar]	$Q_{min}^G$ [MVar]
1	39	US/Can	100	345	60	1200	300	400	140
2	31	nuke	100	345	60	1624	156	300	-100
3	32	nuke	100	345	60	780	195	300	150
4	33	fossil	100	345	60	756	190	250	0
5	34	fossil	100	345	60	612	153	167	0
6	35	nuke	100	345	60	812	203	300	-100
7	36	fossil	100	345	60	672	168	240	0
8	37	nuke	100	345	60	650	163	250	0
9	38	nuke	100	345	60	998	250	300	-150
10	30	hydro	100	345	60	301	75	300	-100

Table A.2.: New England network generator data.

### Dynamic data

Gen #	Bus #	order	$x_l$ [p.u.]	$x_d$ [p.u.]	$x'_d$ [p.u.]	$T'_d$ [s]	$x_q$ [p.u.]	$x'_q$ [p.u.]	$T'_q$ [s]	M [kWs/kVA]
1	39	3	0.0030	0.0200	0.0060	7.00	0.019	0.0080	0.70	1000
2	31	4	0.0350	0.2950	0.0697	6.56	0.282	0.1700	1.50	61
3	32	4	0.0304	0.2495	0.0531	5.70	0.237	0.0531	1.50	71
4	33	4	0.0295	0.2620	0.0436	5.69	0.258	0.0436	1.50	57
5	34	4	0.0540	0.6700	0.1320	5.40	0.620	0.1320	0.44	52
6	35	4	0.0224	0.2540	0.0500	7.30	0.241	0.0500	0.40	70
7	36	4	0.0322	0.2950	0.0490	5.66	0.292	0.0490	1.50	53
8	37	4	0.0280	0.2900	0.0570	6.70	0.280	0.0570	0.41	49
9	38	4	0.0298	0.2106	0.0570	4.79	0.205	0.0570	1.96	69
10	30	4	0.0125	0.1000	0.0310	10.20	0.069	0.0310	1.50	84

Table A.3.: New England network generator dynamic data.  $x_l$  represents the leakage reactance,  $x_d$  the d-axis synchronous reactance,  $x'_d$  the d-axis transient reactance,  $T'_d$  the open circuit d-axis transient time constant,  $x_q$  the q-axis synchronous reactance,  $x'_q$  the d-axis transient reactance,  $T'_q$  the open circuit q-axis transient time constant and M the inertia constant.

## Turbine governor data

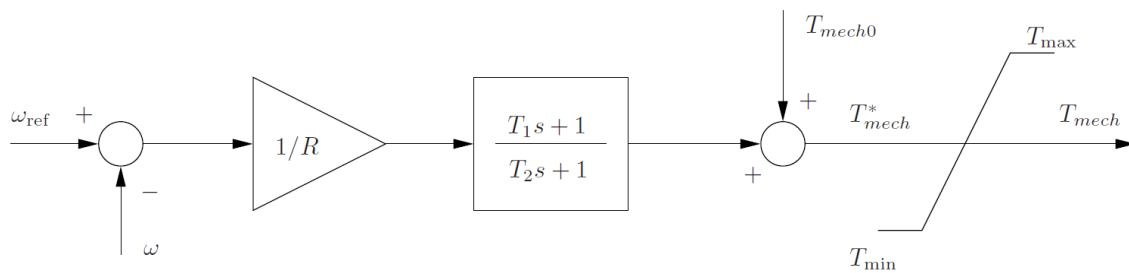


Figure A.1.: Turbine governor schematic

Gen #	Bus #	ref voltage [p.u.]	droop [p.u.]	$P_{max}^G$ [MW]	$P_{min}^G$ [MW]	$T_s$ [ $10^{-3}$ s]	$T_c$ [s]	$T_3$ [s]	$T_4$ [s]	$T_5$ [s]
1	1	1.0	0.02	1200	300	0.100	0.0200	0.006	0	7.00
2	2	1.0	0.02	1624	156	2.700	0.2950	0.070	0	6.56
3	3	1.0	0.02	780	195	0.386	0.2495	0.053	0	5.70
4	4	1.0	0.02	756	190	0.222	0.2620	0.044	0	5.69
5	5	1.0	0.02	612	153	0.140	0.6700	0.132	0	5.40
6	6	1.0	0.02	812	203	6.150	0.2540	0.050	0	7.30
7	7	1.0	0.02	672	168	0.268	0.2950	0.049	0	5.66
8	8	1.0	0.02	650	163	0.686	0.2900	0.057	0	6.70
9	9	1.0	0.02	998	250	0.300	0.2106	0.057	0	4.79
10	10	1.0	0.02	301	75	0.140	0.1000	0.031	0	10.20

Table A.4.: New England network turbine governor data.  $T_s$  represents the governor time constant,  $T_c$  the servo time constant,  $T_3$  the transient gain time constant,  $T_4$  the power fraction time constant and  $T_5$  the reheat time constant.

## Automatic voltage regulator data

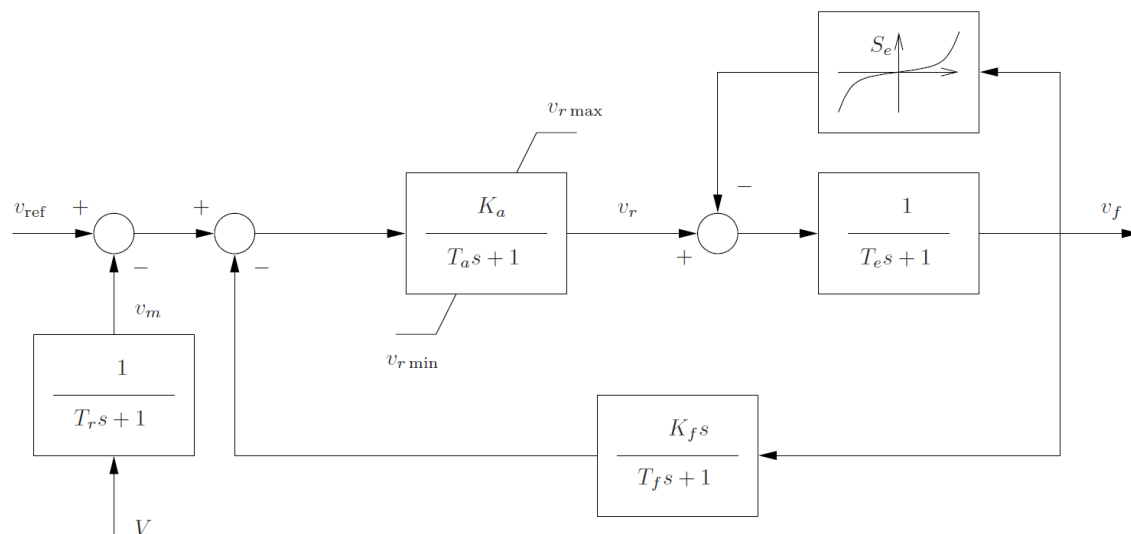


Figure A.2.: Automatic voltage regulator schematic

Gen #	Bus #	$V_r^{max}$ [p.u.]	$V_r^{min}$ [p.u.]	$K_a$	$T_a$ [s]	$K_f$	$T_f$ [s]	$T_e$ [s]	$T_r$ [s]	$A_e$	$B_e$
1	1	10.5	-10.5	40	0.02	0.03	0.100	1.400	0.001	0.0039	1.555
2	2	5.0	-5.0	6	0.05	0.06	0.050	0.410	0.001	0.0039	1.555
3	3	5.0	-5.0	5	0.06	0.08	0.100	0.500	0.001	0.0039	1.555
4	4	5.0	-5.0	5	0.06	0.08	0.100	0.500	0.001	0.0039	1.555
5	5	30.0	-10.0	40	0.02	0.03	0.100	0.785	0.001	0.0039	1.555
6	6	5.0	-5.0	5	0.02	0.08	0.125	0.471	0.001	0.0039	1.555
7	7	6.5	-6.5	40	0.02	0.03	0.100	0.730	0.001	0.0039	1.555
8	8	5.0	-5.0	5	0.02	0.09	0.126	0.528	0.001	0.0039	1.555
9	9	10.5	-10.5	5	0.02	0.03	0.100	0.500	0.001	0.0039	1.555
10	10	5.0	-5.0	5	0.06	0.04	0.100	0.250	0.001	0.0039	1.555

Table A.5.: New England network automatic voltage regulator data.  $V_r^{max}$  and  $V_r^{min}$  are regulator voltages,  $K_a$  is the amplifier gain,  $T_a$  the amplifier time constant,  $K_f$  the stabilizer gain,  $T_f$  the stabilizer time constant,  $T_e$  the field circuit time constant,  $T_r$  the measurement time constant and  $A_e$  and  $B_e$  are ceiling coefficients.

## A.4. Load Data

Load #	Bus #	$P^D$ [MW]	$Q^D$ [MVar]	$V_{max}$ [p.u.]	$V_{min}$ [p.u.]
1	1	97.6	44.2	1.06	0.94
2	3	322.0	2.4	1.06	0.94
3	4	500.0	184.0	1.06	0.94
4	7	233.8	84.0	1.06	0.94
5	8	522.0	176.6	1.06	0.94
6	9	6.5	-66.6	1.06	0.94
7	12	8.53	88.0	1.06	0.94
8	15	320.0	153.0	1.06	0.94
9	16	329.0	32.3	1.06	0.94
10	18	158.0	30.0	1.06	0.94
11	20	680.0	103.0	1.06	0.94
12	21	274.0	115.0	1.06	0.94
13	23	247.5	84.6	1.06	0.94
14	24	308.6	-92.2	1.06	0.94
15	25	224.0	47.2	1.06	0.94
16	26	139.0	17.0	1.06	0.94
17	27	281.0	75.5	1.06	0.94
18	28	206.0	27.6	1.06	0.94
19	29	283.5	26.9	1.06	0.94
20	31	9.2	4.6	1.06	0.94
21	39	1104	250.0	1.06	0.94

Table A.6.: New England network load data.  $P^D$  is the real power demand and  $Q^D$  the reactive power demand.

## A.5. Branch Data

<i>Line</i> #	<i>from</i> bus	<i>to</i> bus	<i>r</i> [p.u.]	<i>x</i> [p.u.]	<i>b</i> [p.u.]	$\tau$	$\theta^{shift}$ [rad]	rate A [MVA]	rate B [MVA]	rate C [MVA]
1	1	2	0.0035	0.0411	0.6987	0.000	0.0	600	600	600
2	1	39	0.0010	0.0250	0.7500	0.000	0.0	1000	1000	1000
3	2	3	0.0013	0.0151	0.2572	0.000	0.0	500	500	500
4	2	25	0.0070	0.0086	0.1460	0.000	0.0	500	500	500
5	2	30	0.0000	0.0181	0.0000	1.025	0.0	900	900	2500
6	3	4	0.0013	0.0213	0.2214	0.000	0.0	500	500	500
7	3	18	0.0011	0.0133	0.2138	0.000	0.0	500	500	500
8	4	5	0.0008	0.0128	0.1342	0.000	0.0	600	600	600
9	4	14	0.0008	0.0129	0.1382	0.000	0.0	500	500	500
10	5	6	0.0002	0.0026	0.0434	0.000	0.0	1200	1200	1200
11	5	8	0.0008	0.0112	0.1476	0.000	0.0	900	900	900
12	6	7	0.0006	0.0092	0.1130	0.000	0.0	900	900	900
13	6	11	0.0007	0.0082	0.1389	0.000	0.0	480	480	480
14	6	31	0.0000	0.0250	0.0000	1.070	0.0	1800	1800	1800
15	7	8	0.0004	0.0046	0.0780	0.000	0.0	900	900	900
16	8	9	0.0023	0.0363	0.3804	0.000	0.0	900	900	900
17	9	39	0.0010	0.0250	1.2000	0.000	0.0	900	900	900
18	10	11	0.0004	0.0043	0.0729	0.000	0.0	600	600	600
19	10	13	0.0004	0.0043	0.0729	0.000	0.0	600	600	600
20	10	32	0.0000	0.0200	0.0000	1.070	0.0	900	900	2500
21	12	11	0.0016	0.0435	0.0000	1.006	0.0	500	500	500
22	12	13	0.0016	0.0435	0.0000	1.006	0.0	500	500	500
23	13	14	0.0009	0.0101	0.1723	0.000	0.0	600	600	600
24	14	15	0.0018	0.0217	0.3660	0.000	0.0	600	600	600
25	15	16	0.0009	0.0094	0.1710	0.000	0.0	600	600	600
26	16	17	0.0007	0.0089	0.1342	0.000	0.0	600	600	600
27	16	19	0.0016	0.0195	0.3040	0.000	0.0	600	600	2500
28	16	21	0.0008	0.0135	0.2548	0.000	0.0	600	600	600
29	16	24	0.0003	0.0059	0.0680	0.000	0.0	600	600	600
30	17	18	0.0007	0.0082	0.1319	0.000	0.0	600	600	600
31	17	27	0.0013	0.0173	0.3216	0.000	0.0	600	600	600
32	19	20	0.0007	0.0138	0.0000	1.060	0.0	900	900	2500
33	19	33	0.0007	0.0142	0.0000	1.070	0.0	900	900	2500
34	20	34	0.0009	0.0180	0.0000	1.009	0.0	900	900	2500
35	21	22	0.0008	0.0140	0.2565	0.000	0.0	900	900	900

<i>Line</i> #	<i>from</i> bus	<i>to</i> bus	<i>r</i> [p.u.]	<i>x</i> [p.u.]	<i>b</i> [p.u.]	$\tau$	$\theta^{shift}$ [rad]	rate A [MVA]	rate B [MVA]	rate C [MVA]
36	22	23	0.0006	0.0096	0.1846	0.000	0.0	600	600	600
37	22	35	0.0000	0.0143	0.0000	1.025	0.0	900	900	2500
38	23	24	0.0022	0.0350	0.3610	0.000	0.0	600	600	600
39	23	36	0.0005	0.0272	0.0000	1.000	0.0	900	900	2500
40	25	26	0.0032	0.0323	0.5310	0.000	0.0	600	600	600
41	25	37	0.0006	0.0232	0.0000	1.025	0.0	900	900	2500
42	26	27	0.0014	0.0147	0.2396	0.000	0.0	600	600	600
43	26	28	0.0043	0.0474	0.7802	0.000	0.0	600	600	600
44	26	29	0.0057	0.0625	1.0290	0.000	0.0	600	600	600
45	28	29	0.0014	0.0151	0.2490	0.000	0.0	600	600	600
46	29	38	0.0008	0.0156	0.0000	1.025	0.0	1200	1200	2500

Table A.7.: New England network branch data. The three apparent power ratings, rate A, rate B and rate C correspond to a long-term limit, a 24-hour limit and an emergency 15-minute limit.

## B. Nomenclature

### Chapter 2

$P_{Loss}$	Real power loss
$R$	Resistance
$I$	Current
$c$	Speed of light
$f$	Frequency
$\lambda$	Wavelength
$\underline{Y}_L$	Line series admittance
$\underline{Y}_C$	Line shunt admittance
$\underline{Y}$	Admittance matrix
$\underline{V}$	Complex voltage
$\underline{I}$	Complex current
$\underline{S}$	Apparent power
$P$	Real power
$Q$	Reactive power
$y$	Admittance
$g$	Conductance
$b$	Susceptance
$\delta$	Voltage phase angle
$\theta$	Admittance phase angle
$\tau_l$	Tap ratio of line $l$

$\theta_l^{shift}$	Phase shift of line $l$
$\epsilon$	Maximum convergency error for the Newton-Raphson algorithm

### Chapter 3

$\sigma^{break}$	Limit that state vectors must be below in order to break the simulation
$t^{break}$	Time that state vectors must be below $\sigma^{break}$ in order to break the simulation
$\alpha$	ZIP load constant parameter
$\beta$	ZIP load linear parameter
$\gamma$	ZIP load quadratic parameter

### Chapter 4 and 5

$\mathcal{B}$	Set of Buses
$\mathcal{G}$	Set of generators
$\mathcal{D}$	Set of demands
$\mathcal{L}$	Set of lines
$\mathcal{C}$	Set of contingencies
$p_g^G$	Generated real power of unit $g$
$q_g^G$	Generated reactive power of unit $g$
$p_d^D$	Real power demand of load $d$
$q_d^D$	Reactive power demand of load $d$
$p_l^L$	Real power flow in line $l$
$q_l^L$	Reactive power flow in line $l$
$s_l^L$	Apparent power flow in line $l$
$v_b$	Bus voltage magnitude

$\delta$	Bus voltage phase angle
$\delta_0$	Bus voltage reference phase angle
$p_{g,c}^G$	Generated real power of unit $g$ in contingency $c$
$q_{g,c}^G$	Generated reactive power of unit $g$ in contingency $c$
$p_{d,c}^D$	Real power demand of load $d$ in contingency $c$
$q_{d,c}^D$	Reactive power demand of load $d$ in contingency $c$
$p_{l,c}^L$	Real power flow in line $l$ in contingency $c$
$q_{l,c}^L$	Reactive power flow in line $l$ in contingency $c$
$s_{l,c}^L$	Apparent power flow in line $l$ in contingency $c$
$v_{b,c}$	Bus voltage magnitude in contingency $c$
$\delta_c$	Bus voltage phase angle in contingency $c$
$\delta_{0,c}$	Bus voltage reference phase angle in contingency $c$
$P_{g\pm}^G$	Upper and lower real power generation limit of unit $g$
$Q_{g\pm}^G$	Upper and lower reactive power generation limit of unit $g$
$V_{b\pm}$	Upper and lower voltage limit of bus $b$
$S_{l,max}^L$	Thermal limit for apparent power of line $l$
$P_{l,max}^L$	Thermal limit for real power of line $l$
$\mathbf{g}^{KCL}(\mathbf{x})$	Constraints incorporating Kirchhoff's current law equations
$\mathbf{g}^{KVL}(\mathbf{x})$	Constraints incorporating Kirchhoff's voltage law equations
$\mathbf{g}^{base}(\mathbf{x})$	Base case equality constraints
$\mathbf{h}^{base}(\mathbf{x})$	Base case inequality constraints
$\mathbf{g}^{con}(\mathbf{x}_c)$	Contingency case equality constraints
$\mathbf{h}^{con}(\mathbf{x}_c)$	Contingency case inequality constraints
$\mathbf{r}(\mathbf{x})$	Risk constraints

$\omega_R$	Weight assigned to the risk
$\eta$	Weight assigned to load shedding
$\xi$	Auxiliary weight for generator contingencies
$Pr_c$	Probability of a contingency c
$Sev_l^{base}$	Severity of line l in the base case
$Sev_c^{con}$	Severity of contingency c
$Sev_{l,c}^{line}$	Severity of line l in contingency c
$Z_{c,l}^1$	Severity function index 1
$Z_{c,l}^0$	Severity function index 0
$ShedCost$	Total cost of applied load shed
$ShedCost_c^{con}$	Cost of applied load shed for each contingency
$LSC_d$	Cost to shed on unit of load d

## Chapter 6

$p$	Probability
$\lambda$	Failure rate
$\Delta t$	Time slot

## Chapter A

$P_{max}^G$	Generation maximum limit for real power
$P_{min}^G$	Generation minimum limit for real power
$Q_{max}^G$	Generation maximum limit for reactive power
$Q_{min}^G$	Generation minimum limit for reactive power
$x_l$	Leakage reactance

$x_d$	d-axis synchronous reactance
$x'_d$	d-axis transient reactance
$T'_d$	Open circuit d-axis transient time constant
$x_q$	q-axis synchronous reactance
$x'_q$	d-axis transient reactance
$T'_q$	Open circuit q-axis transient time constant
M	Inertia constant
$T_s$	Governor time constant
$T_c$	Servo time constant
$T_3$	Transient gain time constant
$T_4$	Power fraction time constant
$T_5$	Reheat time constant
$V_r^{max}$	Maximum regulator voltage
$V_r^{min}$	Minimum regulator voltage
$K_a$	Amplifier gain
$T_a$	Amplifier time constant
$K_f$	Stabilizer gain
$T_f$	Stabilizer time constant
$T_e$	Field circuit time constant
$T_r$	Measurement time constant
$A_e$	1 <sup>st</sup> ceiling coefficient
$B_e$	2 <sup>nd</sup> ceiling coefficient